A MESOSCALE DATA ASSIMILATION SYSTEM FOR REAL-TIME USE IN THE McIDAS ENVIRONMENT

G. A. Mills
G. M. Callan
B. M. Goodman

Introduction

The McIDAS interactive data access and analysis system (Suomi et al. 1983) has extensive capability to access conventional surface and upper air meteorological data, as well as satellite-derived data which can be processed and edited in the McIDAS environment. These satellite data routinely consist of temperature and moisture profiles from both orbiting (Smith et al. 1979) or geostationary (Smith 1983) satellites, as well as cloud drift and water vapor winds derived from geostationary satellite imagery (Mosher 1979, Stewart et al. 1985), and winds estimated from VAS temperature soundings (Hayden 1985). These data may either be those gathered routinely or as part of special measurement programs such as SESAME-AVE (e.g. Hill et al. 1979) or the proposed GALE and STORM experiments, in which enhanced spatial and temporal resolution data sets are obtained.

While a large amount of applications software exists to analyze and process these data for specific applications and case studies, including advanced objective analysis and numerical weather prediction models (see Mills and Hayden 1983, LeMarshall et al. 1985), no formal mechanism has hitherto existed to perform routine assimilation of these mixed data types, with the aim of producing temporally and spatially consistent three-dimensional gridded data sets of the primary atmospheric variables.

It is the purpose of this report to describe a mesoscale data assimilation system which has been developed for use on the McIDAS computer. The system has been designed to have a variable grid spacing in the range of 50-150 km (i.e., the meso-alpha scale), a time resolution (that is, analysis update frequency) of 3-12 hours, to have a variable domain, and to have the ability to merge data from all sources available at SSEC. Potential envisaged uses of the system are to provide gridded fields of primary atmospheric variables for diagnostic

studies, particularly during special effort field experiments such as GALE and STORM, to provide initial state specification for NWP studies of significant weather events, to provide guess fields for satellite retrieval processing during the assimilation, and to provide a vehicle for further investigation of the problem of assimilation of data from mixed sources at mesoscale resolution.

The first part of this report describes in some detail the design philosophy of the system, the method by which the data are assimilated, and the various options under which the system can be operated. The second part contains results from two assimilation sequences which have been carried out--one using a series of data from March 6, 1982, and a second during a nine-day period of October 1985. Also in this section will be presented examples of data-impact case studies using the system. In the third part (the Appendices), detailed descriptions of the operation of the system are given. As the analyses prepared using this system will be available to the McIDAS user community, it is intended that the first and second parts of the report will provide some understanding of the processes which the data and the fields undergo in the analysis process so that results obtained by calculating diagnostic fields from these data can be correctly interpreted. The third section should allow a user to operate the data assimilation system himself if it is desired to change program options, or, indeed, to interact with the source code itself.

PART I

THE DATA ASSIMILATION SYSTEM

1.1 INTRODUCTION

The First Garp Global Experiment (FGGE) provided a considerable impetus to the development of so-called four-dimensional data assimilation systems in which a forecast model is integrated forward in time and is periodically updated (or corrected) by the insertion of data observed at or near that time. The method has chiefly been applied to global or hemispheric forecast systems (see, for example, Bengtsson et al. 1982, Ploshay et al. 1983, Dey and Morone 1985, and Bourke et al. 1982).

While most national weather centers use these global products to provide the first guess for the analyses used to initialize their limited area forecast models, there is no reason why an equivalent data assimilation system should not be operated on a limited area domain, provided care is taken in the specification of the lateral boundary conditions. Indeed, Mills, 1981, demonstrated a stable analysis/forecast cycling system using FGGE data sets over a limited area domain in the Australian region. The essential phases of a data assimilation scheme are a model forecast to the data insertion time, the correction of the forecast fields to fit the observed data (the analysis phase), and an initialization phase to balance the adjusted fields prior to the next forecast stage. Lorenc (1984) lists the following desirable principles of such a scheme:

(1) The analysis must fit the observations to within their estimated observational errors.

(2) The analyzed fields must be internally consistent, matching the structure, scale and balance of the atmosphere.

(3) The analysis must be near the forecast based on earlier observations, unless current observations indicate otherwise.

It was decided to base the first generation of this system on existing analysis and forecast modules, with which some experience and expertise was

available, and to modify these pre-existing components to improve their suitability as assimilation vehicles. Each component is maintained as a self-contained module so that further development can take place in the future.

Two further requirements were made: first, the system should be computationally efficient and geographically portable. To this end the grid dimensions have been parameterized as to number of rows and columns, and number of levels in the model part of the code, and the domain and grid resolution can be varied to suit the data base and intended use of the output fields by means of the projection parameter routine which is accessed by each of the job steps. These projection parameters are also carried, along with the date/time, in the header records of the input and output files of each job step, and are thus passed through each cycle of the assimilation. Second, the system should be as robust as possible, without excessively compromising the quality of the output product. That is, minimal manual intervention should be needed in the operation of the system. However, this is at the expense, to some extent, of always obtaining maximum detail in the analysis, and a variety of options exist to relax these constraints in development and testing of this system.

The basic modules which are used in the scheme are the three-dimensional variational analysis scheme of R. S. Seaman (see, for example, Mills 1981), and the new Australian Region Primitive Equation (ARPE) model which has been extensively described by Leslie et al. (1985). The interface programs have been extensively modified so that the system should approach satisfying Lorenc's condition (3) above. The analysis scheme, the forecast model and the interface codes are now discussed in detail, followed by a description of how they would be linked together to perform an assimilation sequence in the McIDAS environment, and the combination of options which are available.

1.2 THE OBJECTIVE ANALYSIS SCHEME

The three-dimensional objective analysis scheme used is an evolution of the scheme developed in the Australian Numerical Meteorology Research Centre (ANMRC) by R. S. Seaman for limited area analysis over the Australian Region, and adapted to the U.S. region by Mills et al. 1980. Examples of its use in the U.S. Region can be found in Mills and Hayden, 1983 and LeMarshall et al., 1985. The scheme combines the successive correction (SCM) method of Cressman (1959) and the variational blending techniques of Sasaki (1958, 1970).

The analysis system differs from the earlier incorporation of variational techniques into Australian limited area objective analysis (Seaman et al. 1977) in that is based upon major levels at 1000 and 250 mb, and the calculus of variations is used in an explicitly three-dimensional manner. Estimates of the geopotential ϕ and the geopotential gradient in each coordinate direction are combined at each grid-point in the three-dimensional analysis domain. The basic observational ingredients combined in this blending are wind components to define the geopotenial gradients, geopotential thickness of each layer, and a lower reference level. The reliability weights for the independently analyzed geopotential thickness and gradient fields are determined on the basis of data density fields, produced during the SCM analyses. These data density fields are used with latitude- and level-varying standard deviation parameters and externally specified tuning parameters to generate the final reliability weights used in the variational blending. In this way, the blended geopotential fields reflect a greater weight to the wind data in low latitudes, and to the thicknesses at higher latitudes. Once the three-dimensional geopotential structure has been defined, then the temperature, dewpoint depression, and wind fields are defined.

Three versions of this analysis scheme are available for use in the McIDAS environment. The first is basically the version used in Mills and Hayden, 1983, augmented with additional levels at 400 and at 150 mb by J. C. Derber (unpublished), and its structure will be described in detail in the following section. Particular emphasis will be placed on the way in which mass and wind data are blended to define the geopotential fields, since this is general to all three versions, and has crucial implications to the problem of mixing satellite and conventional data.

The second version includes several modifications made in the interests of efficiency or meteorological utility, while the third incorporates an incremental wind analysis, and is intended to be the assimilation analysis vehicle. The second and third versions will be described in the subsequent sections of this report. All three versions have ten analysis pressure levels (1000, 850, 700, 500, 400, 300, 250, 200, 150, and 100 mb) and output fields of geopotential (HGHT), temperature (TEMP), dewpoint (TDPT), divergent and non-divergent wind components (UDIV, VDIV and UCMP, VCMP respectively), and total wind (WIND) at all levels, as well as mean sea-level pressure (MSLP).

1.2 BASIC ANALYSIS VERSION

1.2.1 The analysis sytem is highly modular, and has six components; the specification of lower reference level and gross (i.e. 1000-250 mb) atmospheric thickness, the specification of individual geopotential layer thicknesses below 250 mb, the specification of individual geopotential layer thickness above 250 mb, the specification of temperature fields at all analysis levels, the specification of dewpoint fields at all analysis levels up to and including 400 mb, and the specification of the wind fields.

The influence radii for each pass of the SCM analyses are defined by parameter cards, and influence functions are circular except for wind component analyses, where the influence area is elongated along the direction of the wind once the total wind speed exceeds 60 kts. The degree of elongation then depends on the wind speed.

At each pass of the SCM analysis, the data are tested against calculated tolerances, and are accepted or rejected based on whether the difference between the datum and the interpolated value of the background field and the datum point is greater or lesser than the tolerance. This tolerance decreases with successive passes of the correction phase from 3 times a pre-set value to 1.75 times that value on the last (fifth) pass. As the necessary tolerances will vary depending on the accuracy of the guess field, which will vary according to the source and the prognosis interval of the guess field, a multiplicative factor has been included in the data cards for the analysis module, allowing some tuning of the pre-set tolerances for different applications of the system (see Appendix 4).

No spatial variation of the rejection tolerances across the grid has yet been instituted, however some effort should be made in the near future to refine this aspect of the code. In addition, of course, data may be manually flagged

using the editing facilities of the McIDAS system, and will not then be read into the analysis system.

The six modules of the analysis scheme will now be described in detail.

1.2.2 Reference Level and Gross Thickness Specification

A MSLP analysis is prepared using observed pressure data. The first guess is the predicted MSLP field. The 1000 mb geopotential field is then defined by an SCM analysis using observations of geopotential and a guess field derived hydrostatically from the MSL pressure analysis, the predicted 1000 mb temperature and an assumed lapse rate.

The 1000-250 mb thickness analysis is performed in two stages. First, a 1000-500 mb thickness analysis is done, followed by a 500-250 mb thickness analysis. Each is an SCM analysis using observed data, with the guess fields being the predicted thicknesses. The two analyses are separated to facilitate the Australian Bureau of Meteorology operational practice of manual interaction with the 1000-500 mb thickness analysis through the use of bogus observations.

The analyses of geopotential gradient in the grid coordinates, $\frac{\partial \phi}{\partial x}$ and $\frac{\partial \phi}{\partial y}$ are obtained by performing an SCM analysis of observed wind components, with the guess fields obtained by centered differences of the 250 mb geopotential field, as defined by the 1000 mb geopotential and the 1000-250 mb thickness. The fields of geopotential gradient are geostrophic at this point, since observed wind and geopotential gradient have been related via that assumption. Following the SCM analyses, the $\frac{\partial \phi}{\partial x}$, $\frac{\partial \phi}{\partial y}$ fields are adjusted to allow for curvature effects using the gradient wind law, with the amount of correction being linearly related to the density of observed wind data at that gridpoint. That is, the geopotential gradient field is unchanged in areas where there is no wind data, but is changed to conform to the wind law in areas affected by wind data. (The

wind law used is actually a weighted mean of the geostrophic and gradient wind laws, but in practice it has been found best to give full weight to the gradient wind, although this can be changed by varying the weighting parameter on a data card (see Appendix 4)).

From these preceding steps, there are now availabe estimates of ϕ, $\frac{\partial\phi}{\partial x}$, $\frac{\partial\phi}{\partial y}$ at 1000 mb, $\frac{\partial\phi}{\partial p}$ for the 1000-250 mb layer, and $\frac{\partial\phi}{\partial x}$, $\frac{\partial\phi}{\partial y}$ at 250 mb. These independently analyzed fields are then combined according to estimates of their reliability derived from observational data density using the calculus of variations. The variational blending algorithm is the three-dimensional analogue of that used in the two-dimensional blending version (see Seaman et al. 1977). The blended fields of geopotential at 1000 mb and 250 mb derived in this step provide the framework for all subsequent layers.

1.2.3 Specification of Geopotential Fields Between 1000 and 250 mb

For each standard layer between 1000 and 250 mb, an SCM analysis of thickness is performed, using observed thicknesses. The guess fields are derived from the 1000-250 mb blended thickness, while preserving the fractional thickness of that layer to the 1000-250 mb layer thickness of the forecast field. At each analysis level, the $\frac{\partial\phi}{\partial x}$ and $\frac{\partial\phi}{\partial y}$ fields are analyzed using observed wind components, where the guess fields are derived from centered differences of the geopotential field calculated by adding the SCM analyzed layer thicknesses to the 1000 mb geopotential field defined during the preceding step. As before, after the SCM analyses of $\frac{\partial\phi}{\partial x}$, $\frac{\partial\phi}{\partial y}$, these fields are adjusted toward gradient rather than geostrophic balance in data areas, using curvatures calculated from the analyzed gradient fields, and a data density field.

A three-dimensional blending is then carried out to define the individual layer thicknesses. For each level, the variational blending algorithm uses the

SCM analysis estimates of geopotential thickness above and below the level in question, and the geopotential gradients at that level to define the geopotential thickness fields. This procedure is carried out iteratively in the vertical, with fixed 1000 and 250 mb geopotentials from the preceding step as lower and upper boundary conditions. This defines the geopotential height fields, and thus also the thickness fields, for each level or layer between 1000 and 250 mb.

1.2.4 Specification of Geopotential Fields Above 250 mb

The procedure of step 1.2.3 is carried out for levels above 250 mb, with the exception that only the lower boundary (the 250 mb height) is fixed.

1.2.5 Specification of Analysis Level Temperatures

SCM analyses of temperature are performed at each level, using observed temperatures. The guess field for any particular analysis is derived from the blended geopotentials at the level (L) and the levels immediately below (L-1) and above (L+1) and stability parameters STL and STU which relate to the layers below and above the analysis level. The stability parameters STL and STU are derived from the forecast fields and are the ratio of the predicted temperature at the level to the predicted thickness of the layer below (above) that level. The form of the relation then becomes

$$T_{GUESS} = \ln\left(\frac{PL-1}{P}\right) * \Delta\phi_B * STL + \ln\left(\frac{PL}{PL+1}\right) * \Delta\phi_A * STU,$$

where $\Delta\phi_B$, $\Delta\phi_A$ refer to the layer thicknesses below and above the analysis level, and thus reduce to changing the forecast temperature of the layer by the amount implied hydrostatically by the changes made during the analysis to the predicted thicknesses of the layers above and below the analysis level.

1.2.6 Specification of Level Dewpoint

SCM analyses of dewpoint depression are performed at each level up to 400 mb, using observed temperatures and dewpoints. The guess field is a prediction, and the final analysis is constrained not to allow super-saturation.

It should be noted that, while dewpoint depression is the analyzed variable, the output variable is dewpoint, which is thus simply the difference of the analyzed temperature and the dewpoint depression at that level.

1.2.7 Specification of Wind Component Fields

The purpose of this step is to provide wind component fields for numerical prediction model initiation, and is thus a crucial stage of the analysis, particularly as the situation of having large volumes of mass data from satellite profile measurements, but lesser quantities of wind vector information is a frequent occurrence, and information regarding the wind field must be diagnosed from the mass field.

First, SCM analyses of wind components are prepared, using observed wind components. The guess fields are derived from the blended geopotentials using the gradient wind equation. The facility exists to use a weighted average of the geostrophic and gradient winds, as has long been the Australian operational practice; however, Mills and Hayden, 1983, in a case study of the April 10, 1979 case found that the gradient wind equation produced wind components derived from an analyses of satellite geopotential thickness data which much better fit the radiosonde data of the SESAME special observing network. In addition, Mills and McGregor, 1983, found in a limited area assimilation experiment that the gradient winds were more in balance with the ARPE model dynamics than were winds from the geostrophic-gradient combination. Williamson et al. (1981) have also demonstrated this in a separate context.

It has also been found empirically that in areas of dense satellite data coverage, the curvatures calculated from the blended geopotentials tend to be somewhat noisy, and result in locally highly variable curvature corrections being made to the geostrophic winds. To alleviate this, the curvatures are subjected to (an empirically selected) five passes of a 1:2:1 filter in each grid direction prior to making the gradient wind corrections. In addition, a further empirical constraint is placed as these gradient winds that

$$0.5Vg \leq Vgr \leq 1.2\ Vg$$

where Vg is the geostrophic wind and Vgr is the gradient wind.

A stream function is then derived, using as a first guess the blended geopotential for that level, scaled by $g/\overline{f}$, where $\overline{f}$ is the domain averaged coriolis parameter, and the analyzed wind components and a vorticity field derived from these wind components as forcing functions, using the variational approach detailed in Seaman et al. 1977, with the exception that a velocity potential is not derived. The wind components UCMP and VCMP output are non-divergent winds derived from the stream function field, and the WIND field is calculated from these non-divergent components. While this may not well reflect the observed data, this version of the analysis scheme was designed to initialize the ARPE model with non-divergent wind fields, and thus a display of these diagnosed winds shows the input to the numerical weather prediction model.

In principle, options exist for either geostrophic correction of forecast wind fields, or addition of forecast divergent wind components to the stream-function winds, however, these options have not been exhaustively tested in this version.

1.3 UPDATED ANALYSIS VERSION

1.3.1 This analysis version is essentially the same as the basic version, but has some changes made to it to improve its efficiency and/or meteorological verisimillitude. The changes are:

(1) Incorporation of a dynamically calculated variable pass radius within the model code, so that the pass radii are reduced in data-dense areas. This is essentially an efficiency modification.

(2) Incorporation of an elongated influence function for the SCM analyses of dewpoint depression, to better depict strong gradients of moisture.

(3) Output of the SCM u- and v-component wind analyses--i.e. wind analyses which include the divergent component.

(4) Addition of surface temperature and dewpoint depression analyses for ultimate use in initializing the surface parameters of the prognosis model's boundary layer parameterization.

1.3.2 Variable Pass Radius Code

There are five passes through the data for each SCM analysis, with the radii of influence decreasing an successive passes, and being specified in the "basic" analysis version by parameter cards. However, in order to allow for sparse data areas, the initial pass radius is quite large, and this can mean that a huge number of observations may be used to influence a single gridpoint if that point happens to be within a satellite orbit data swathe. Stephens and Stitt, 1970, concluded that a radius of influence to average station separation ratio of 1 to 2 gave best accuracy for the first pass of an SCM analysis, which would result in an extremely small pass radius in areas of dense satellite data, and would also result in a considerable savings in computer time in accumulating corrections at each gridpoint. However, at the edge of a dense swathe of

satellite data, such a small pass radius could potentially result in anomalous gradients in the final analysis field should the guess field and the data not be well matched.

The code has been modified such that, prior to each SCM analysis, the data is scanned, and in each quadrant around each observation, that radius which contains n_s observations is determined, subject to upper and lower radius bounds. These four radii are then averaged to provide the radius of the influence area for the first pass of the SCM analysis. In the 125 km grid resolution version of the analysis system, in which most of the testing has been done, a lower bound of three grid units and an upper bound of eight grid units, with $n_s = 4$ has been found to produce satisfactory results, and in the case of the VAS sounding data set of March 6, 1982, reduced the CPU time necessary to perform an analysis of these data to some 35% of that required using fixed pass radii.

For each of the five passes of the SCM analysis, the pass radius is determined from this base radius by multiplying it by a pass-number-dependent factor P(k), where P(1)...P(5) = 1.0, 0.7, 0.5, 0.3, 0.2, subject to the pass radius not being less than one grid-length.

There is obviously scope for a great deal of tuning of the various empirically selected constants, and, indeed, there is unlikely to be a single combination which is ideal for all applications. To provide some flexibility, the minimum pass radius has been specified for each field on a parameter card, and it would be expected that an inspection of data-density distribution for the different data types would allow some interaction with this part of the code. (N.B. The characteristics of the Cressman distance weighting function should be born in mind when the minimum distance is specified.)

1.3.3 Elongated Influence Function for Dewpoint Analyses

Atkins (1974) demonstrated that analyzed moisture fields are improved both subjectively and by showing positive impact on NWP model rainfall forecasts if a non-isotropic influence region is used in the analysis, with a greater weight being given to moisture data in the direction along closely packed isopleths than in the transverse direction.

The standard Cressman weighting scheme used in this analysis scheme is isotropic. It is desired to modify this weighting so that weight given to a particular datum is greater in directions parallel to the isopleths of the guess field than it is in the transverse direction, with the degree of anisotropy being greater in regions of strong gradient in the background field, such as on the edge of moist tongues or cloud bands. Such a system has been implemented in the analysis code, in the following way:

If D is the dewpoint depression, let

$\bar{D}_G$ be the averaged value of $|\underset{\sim}{\nabla} D|$ in the analysis domain

$\underset{\sim}{\nabla} D$ be the local value at a gridpoint

$\underset{\sim}{r}$ be the radius vector from the observation to the gridpoint being corrected

d be the pass radius determined by the data density dependent pass radius code.

Then a parameter AI is determined where

$$AI = |\underset{\sim}{\nabla} D| \; / \; \bar{D}_G$$

and determines the relative strength of the local gradient of D compared to the array averaged value. The parameter AI determines the degree of anisotropy of the influence function, and a lower limit of unity is set, so that the influence area will be circular in regions of low gradient. An upper bound may also be set, if desired.

Then set

$$d_A = d \; / \; (1 + AI \cos \theta)$$

where θ is the angle between $\underset{\sim}{r}$ and $\underset{\sim}{\nabla}D$, and calculate the weight using the normal Cressman formula

$$W = \frac{d_A^2 - r^2}{d_A^2 + r^2}, \quad W = o \text{ if } d_A^2 < r^2 .$$

This has the effect of sharply reducing the weight given to observations in a direction transverse to the isopleths of the balckground field. Currently, an upper limit of two is set for AI, which means that d_A can be as little as one-third of d in the regions of strongest gradient. After each successive pass of the correction scheme, the direction and degree of elongation of the influence region is redefined.

1.3.4 Output of Full Wind Components

If it is intended to use the output of the analysis for diagnostic purposes, then it is desirable that the winds output contain both the rotational and divergent wind components. To this end fields, the menomics of which are UDIV and VDIV, are output immediately following the SCM analyses of the wind components. Thus, these fields will consist of a gradient wind calculated from the analyzed geopotentials, corrected to fit the observed data where those data exist. The output isotach field (WIND) is calculated from these two wind components at each level.

1.3.5 Surface Temperature and Dewpoint Analyses

The prognosis model includes in its physical parameterization package predictive equations for surface temperature and mixing ratio. A desirable option for studying model sensitivity to boundary layer processes is to be able

to initialize the model with observed surface values. Thus, SCM analyses of surface temperature and dewpoint depression have been included in the temperature and moisture analysis modules, respectively. The guess fields come from the forecast, and the data are the screen-level observations from the radiosonde and/or SVCA networks.

1.4 INCREMENTAL WIND ANALYSIS VERSION

1.4.1 This version includes those modifications made to the basic version which were described in section 1.3, but differs in the manner in which the wind analysis is performed. The purpose of this method was to provide the model with an "incremented" set of fields, so that the model fields would only be altered in data regions, as required by Lorenc's principle #3, and has the aim of leaving the model's wind field unchanged if there is no information to the contrary, but equally, to allow changes in the mass fields to produce changes to the wind fields in those areas where there are mass, but not vector wind data.

The procedure is similar to that used in the previously described versions of this analysis scheme, but treated incrementally, as follows: the incremental data are the differences between the observed winds and the forecast wind fields, interpolated vertically from the model's sigma surfaces to pressure surfaces using cubic spline interpolation, and interpolated horizontally to the observation point using a bi-directional Bessell interpolation. If this analysis was uni-variate, then the appropriate background (guess) field would be zero. However, in practice a considerable degree of mass data are available, and it is desirable that this mass data be available to the wind analysis. Accordingly, the guess field is derived from the difference between a weighted average of the geostrophic and gradient winds obtained from the analyzed and the forecast geopotentials. In the case of zero weight being given to the gradient wind law, this reduces to a "geostrophic correction" first guess which is a simple linear process. However, it has been shown that the gradient wind law provides a better estimate of model winds, when derived from model geopotentials, and a better fit to observed winds when derived from analyzed geopotential fields, and it seems desirable to incorporate some of this information if possible, in spite of the non-linearity of the differencing in this case.

Accordingly, the relative weights given to the geostrophic and gradient wind estimates may be varied via a parameter card.

Following the SCM analysis of wind increments, the stream function blending process is again used (an option) to derive non-divergent wind component increments. The first guess to this blending process is the scaled geopotential difference between the analyzed and the forecast geopotential fields. On output, the wind component increments are added to the prognosis wind fields to facilitate display. Thus, the UCMP and VCMP fields contain the full model winds plus a non-divergent increment, and so retain the model's divergence field, while the UDIV and VDIV fields contain divergence both from the model and from the analysis process. In this respect, the output wind component information differs in this version of the analysis from that described in the preceding section.

1.5 THE PROGNOSIS MODEL

The forecast model used is the "new" Australian Region Primitive Equation (ARPE) model. This model is a development of the original ARPE model (see McGregor et al. 1978) which was implemented at CIMSS by Mills et al. 1980. The formulation and physical parameterizations of the new model have been extensively described by Leslie et al. 1985. The chief changes to the old model have been a re-coding such that all model variables are stored in core, with the only input-output of data being at specified forecast intervals, and the inclusion of an extensive parameterization of the so-called physical processes; i.e., an adequate representation of the planetary boundary layer, a diurnal thermal cycle, and the simulation of large-scale and convective precipitation.

The model is formulated in terms of the primitive equations for momentum, mass, moisture, and thermal energy. These equations can be written in either flux form or advective form, but are in flux form in the version used here. The integrations are carried out on the staggered Arakawa C-grid using a semi-implicit time differencing scheme.

The model domain is variable, the grid dimensions being set via a parameter statement, while the resolution and geographical area selected are defined using a set of projection parameters appropriate to the Lambert Conformal Conic projection used. In addition, as will be described in more detail below, a salient feature of the model is that it can be "nested" within itself to provide higher resolution forecasts on a selected area of interest. The number of levels in the vertical is parameterized, and is typically 10 to 15, depending on the application.

The vertical mode initialization scheme of Bourke and McGregor (1983) is then used on option, and with a choice of filtering conditions.

The values of variables at the lateral boundaries of the coarse mesh are specified in two possible ways. The simplest method is to hold all variables constant, and to control the effects of this over-specification by applying a filter at the penultimate boundary points. An alternative, and the preferred method, uses the boundary relaxation technique of Kallberg (1977) to nest the model within an externally specified model forecast, with the outermost grid rows being defined by a weighted mean of the internal and external tendencies of the forecast variables. The profile of the weighting function changes from unity on the outermost row to zero a specified number of grid rows from the boundary. The prediction of precipitation consists of two successive adjustment procedures: a cumulus convection scheme based on a modified version of Kuo (1965), followed by a large-scale saturation adjustment.

(1) Cumulus convection

The cumulus convection scheme closely follows Kuo's original scheme in that it models the consequences of a simultaneous occurrence of large-scale moisture convergence and conditional instability. However, certain changes have been made on the basis of suggestions by Hammarstrand (1977) who showed that the unrealistically low precipitation rates produced by the Kuo (1965) scheme could be improved by increasing the partitioning of the large-scale moisture convergence into the release of latent heat in the cloud and decreasing the proportion that goes into the moistening of the model cloud.

(2) Large scale condensation

Large scale condensation is allowed to occur where at any model level the mixing ratio exceeds 95% of the saturation value. The excess is treated as precipitation and an adjustment is made to reduce the mixing ratio to its saturated value and increase the temperature such that moist

static energy is conserved. The surface turbulent fluxes of momentum, heat and moisture are calculated in a manner similar to that proposed by Louis et al. (1981) for the ECMWF model. In this approach it is assumed that the turbulent fluxes may be computed from an eddy diffusivity formulation in which the eddy diffusivities are functions of the stability of the layer. In the surface layer, the similarity theory of Monin and Obukhov (1954) is used to suggest the form of the functional dependence on stability, while above the surface layer the mixing length theory of Blackadar (1962) is employed. To ensure continuity with the surface fluxes, the dependence of the eddy diffusivity with stability is assumed to be the same as for the surface fluxes.

There is no horizontal diffusion code incorporated in the model, however there is available, on option, a horizontal diffusion of the convective heating and moistening. This does ameliorate the positive feedback of the convective parameterization which sometimes occurs with the Kuo scheme, but at the expense of loss of detail and spreading of the forecast precipitation areas.

The surface temperature and moisture are specified following Bhumralkar, 1975. The predictive equations for these parameters are only applied over land. Over the oceans the sea-surface temperature T_s is held at the climatological (initial state) value.

Topography is generated from high resolution data sets held on McIDAS, and may be as "realistic" as desired. A degree of smoothing or damping of the topography can be applied during the pre-processor (see next section) stage, depending on the application and the grid resolution used.

The vertical mode initialization scheme of Bourke and McGregor, 1983 is included as an option in the model, with either "free" initialization or "surface pressure constrained" initialization options available. These correspond

to their filter condition A and B. It is also possible to have uninitialized forecasts.

Full details of the model formulation and its method of solution can be found in the Appendixes of Leslie et al. 1985, while examples of forecasts obtained from the model can be found in that paper and in Mills and Leslie, 1985.

1.6 THE INTERFACE MODULES

The interface modules are those which interpolate from the sigma to pressure coordinate systems, or vice versa, and the modules which prepare the boundary tendency data sets for nesting purposes. As in each assimilation cycle, there must be an interpolation from pressure to sigma coordinates and back; this part of the assimilation system is of considerable importance.

1.6.1 The Pre-Processor

This is the code which interpolates atmospheric variables from the pressure surfaces of the analysis system to the sigma surfaces of the prognosis model, computes surface pressure and transforms the units of the variables to be model-compatible. Sigma level disposition is specified by a parameter card.

The surface pressure is calculated from the analyzed mean sea-level pressure, the analyzed 850 mb temperature, the model topographic height, and an assumed lapse rate of 6.5° Km^{-1} between the model surface and 850 mb.

Analysis variables are interpolated in the vertical using cubic spline interpolation. If upward extrapolation is necessary, the thermal wind equation is used to extrapolate the wind components, based on the temperature gradients at the 100 mb analysis surface. While this is not perfect, it does provide a better balanced upper state for the model than independent spline extrapolation of the temperature and the two wind components. In addition, the wind components are staggered in the horizontal to the Arakawa C-grid. An option switch exists to select either divergent or non-divergent winds from the analysis.

Surface temperatures and moistures can be either those specified by the surface temperature and dewpoint analyses, or derived from the free atmosphere variables, after interpolation to sigma coordinates. In either case, the

surface boundary layer is constrained to neutrality at the start of the integration. Future applications could investigate the possibility of either carrying the model-predicted surface stability forward in an assimilation mode, or specifying the stability using remotely sensed parameters (e.g. Diak et al. 1986).

In this code, the unsmoothed topography which is input is smoothed by two passes of a 1:2:1 filter, and can also be damped or enhanced by an externally specified multiplicative factor.

This version of the pre-processor is that which would be used for cold start prognosis, for individual case studies, and to commence an assimilation sequence. While the version of the pre-processor which is to be described below is the one designed for use in the assimilation system, it is essentially this code which was used by Mills, 1981, and Mills and McGregor, 1983, in their successful assimilation of FGGE data in the Australian region.

1.6.2 The Incremental Pre-Processor

This version is a close derivative of the preceding pre-processor version. However, it has been designed to be used in the assimilation mode, and should be used in conjunction with analyses prepared using the incremental wind analysis code (see I.4).

The difference in this version is that only analysis increments are interpolated to sigma surfaces, and once on those surfaces, are added to the primary forecast fields from the model integration up to analysis time. The analysis increments are the difference between the prognosis fields on pressure surfaces and the analyzed fields, and thus in the case of the winds, when used in conjunction with the incremental wind analysis, reduce to the analyzed/ derived wind component from I.4. Adding these interpolated increments to the model

forecast fields, in part, satisfies Lorenc's condition (3), and allows the model's divergent wind components to be preserved unchanged in the subsequent forecast. The option exists to interpolate either divergent or non-divergent wind increments.

Small adjustments of the forecast parameters on the model's sigma surfaces are then made to account for the changes made in surface pressure during the analysis, as both wind components and mixing ratios are carried in the model scaled by surface pressure, and also as all model variables are functions of σ in the vertical, and σ is a function of surface pressure. Each of these adjustments requires a small interpolation in the vertical. In addition a light smoother is applied to these adjusted fields to remove two grid-length waves prior to the addition of the analysis increments. This was found to substantially improve the stability of the system.

The disposition of σ-levels is maintained internally via directory information on the model's output data set, and is thus not changed during an assimilation sequence.

1.6.3 The Nesting Code

This code takes a series of pressure surface fields on the map projection and grid resolution being used and calculates time tendencies of surface pressure and temperature, wind components and mixing ratio on the model's sigma surfaces for specification of the boundary tendency values. Appropriate unit conversion, scaling and grid staggering is performed in this stage. The sigma surface disposition is specified via a parameter card, but MUST be the same as that used in the model formulation. The time interval between the base data sets, and number of data sets available for computing these tendencies is specifiable via parameter cards, however the time interval is usually 12 hours

when the external boundary condition are specified by the LFM or NMC global forecast fields.

1.6.4 The Post-Processor

The post-processor is the jobstep which outputs the model prediction file to field storage arrays, interpolating from sigma to pressure surfaces as well. Fields may be output to both sigma surfaces and also pressure surface fields, and thus can be used for diagnostic, display, and guess field for subsequent analysis purposes.

Fields output on sigma surfaces are the primary model parameters of u- and v-component of wind, temperature, mixing ratio, $\frac{\partial \sigma}{\partial t}$, surface pressure and precipitation, all subject to appropriate unit conversion and scaling. No spatial filtering is applied to these fields.

On pressure surfaces, u- and v-components of wind, temperature, mixing ratio, dewpoint, vertical motion ($\frac{\partial p}{\partial t}$) and isotachs are output at each of ten pressure levels, together with surface pressure, mean sea-level pressure, and precipitation, once again subject to appropriate unit conversion and scaling. These fields are optionally subjected to a light spatial filter designed to eliminate the two-grid length waves. The values of precipitation and vertical motion are set to zero on the outer two rows of the grid.

Interpolation from sigma to pressure coordinates is done using a cubic spline interpolation formula. Where extrapolation is necessary below the lowest sigma level, a lapse rate of 6.5° Km^{-1} is assumed for temperature and geopotential height from the lowest sigma level. The u- and v-compoments of the wind are derived assuming the thermal wind law applies below the lowest sigma level, with the temprature gradients being calculated from the previously interpolated 850 mb temperature field. While it may be more realistic to make these fields

zero, this approach facilitates the behavior of the incremental wind analysis system. Mixing ratio is set equal to the value on the lowest sigma surface, while vertical motion is set to zero at pressure levels below the lowest sigma surface.

The number and disposition of pressure levels to which the fields are interpolated are specified on a parameter card, as are the switches for filtering and for output of sigma surface fields.

Code exists to derive a large number of other fields, such as advective, gradient, cloud cover, cloud top, geostrophic frontogenesis functions, boundary layer parameters, etc., as well as vorticity, divergence, etc., all of which have relevance in certain diagnostic circumstances, examples of which are given by Mills and Leslie, 1985. In order to minimize use of disc storage space, however, these fields are not routinely output by the post-processor, but are computed using McIDAS key-in commands (see Appendix 5) and are designed specifically for use with the Lambert grid projections of the analysis and forecast models.

1.7 ANCILLARY MODULES

There are various other job steps used to interface grid files to the field-storage data sets used by the model and analysis systems, to pre-format direct access data sets (not possible in the FORTRAN-77 compiler), and to interface the MD files of the McIDAS system to the data-table structure used by the analysis scheme, and data fitting programs used for diagnostic purposes. These programs and their functions are listed in the Appendices.

1.8 THE CONCEPTUAL OPERATION OF THE SYSTEM

The system can be operated in either a case study mode or in a continuous quasi-real-time mode. One would feel that a more conservative approach to the selection of the combination of options would be taken in a real-time mode, to maximize stability of the system, with the possible overhead of some loss of fine detail, while in a case study mode, where a limited number of assimilation cycles are to be performed, the option combinations could be varied.

It should be repeated that Mills, 1981, and Mills and McGregor, 1983, have used what are essentially these analysis and prognosis modules to assimilate data for nine days of FGGE SOP II data, with good stability of the system, and a system with that configuration could be expected to continue its stable performance in most circumstances. However, in the opinion of this author, it is not reasonable to expect any assimilation system to operate indefinitely completely without human intervention, unless such a system is unreasonably heavily constrained. Only extensive operation will reveal what combinations of previously unencountered circumstances can require human intervention, and define how much constraint must be placed on the system.

Having said this, however, it is equally the belief of this author that the system being offered has been shown to be sufficiently stable to perform its designed function, (see Part 2 of this report) and will also provide a vehicle for extensive testing of many aspects of the process of assimilation of mesoscale data sets of mixed origins.

Thus, the system would operate in the following way:

(1) Select grid resolution and domain over which the assimilation will be carried out. This will define a set of projection parameters for the Lambert Conformal Conic projection on which the system operates (see HELP LAMM on McIDAS). These projection parameters are carried in the directory

records of the data sets, and are passed from stage to stage of the system in this way. The exception is in the subroutine which actually does the coordinate transformation from latitude/longitude to grid coordinates, where the projection parameters must be hard-wired.

Depending on the grid dimensions selected, the parameter statements in all stages of the code may need to be changed (see Appendix 2).

(2) Obtain a guess field from NMC's global or LFM analyses and forecasts. This guess field is then transferred from a latitude/longitude grid to the Lambert Conformal grid, and is then used as first guess for the initial analysis which commences the assimilation sequence.

If it is desired that the prognosis stage of the sequence should be nested--that is, have updated boundary conditions, then a second (or more) global or LFM data set at a later time must be also interpolated to the Lambert grid. These data sets are then used to calculate the boundary time-tendencies for the model's prognostic variables, and must be equally spaced in time.

(3) Select which data sources are to be combined in the analysis. Data sources which have been routinely accessed are routine R/S, special network R/S, SVCA reports, VAS and TIROS temperature retrievals, VAS gradient winds, cloud and water vapor drift winds and drifting buoy data.

(4) Use analysis version #2 to prepare the initial analysis. The only real option here is to adjust the weight of the geotrophic to gradient wind, other than setting the minimum pass radius and data rejection tolerance factor for each analysis variable.

(5) Use the basic pre-processor package to interpolate the analysis fields to the model sigma coordinates. It is in this stage that the sigma surface values and number of levels are set via a parameter card, the option of

initializing with divergent or non-divergent wind fields is exercised, and an option can be exercised to proportionally reduce the model topography at each grid point.

(6) Do a prognosis forward in time. Initialization options, physical parameterization options, timestep and boundary condition options are exercised here.

(7) Post-process the model forecast to pressure surfaces. This data set becomes the first guess field for the subsequent analysis.

Steps (3) to (6) constitute a cold-start analysis/forecast run, and it is this form which would be used for data impact studies, etc., or for initializing an assimilation sequence. The sequence is shown schematically in Figure 1.1. In addition, of course, the forecast field could provide the guess field for a subsequent analysis, in which case this module would form one assimilation cycle of the form used by Mills, 1981.

After this initial forecast step, a series of incremental assimilation cycles can be performed, with the previous model forecast on both sigma and on pressure surfaces providing feedback to the incremental preprocessor of the next sequence. This sequence is shown schematically in Figure 1.2, and the range of available options is summarized in Table 1.1, while details of how to exercise these options via data cards and data sets are described in Appendix 4.

Examples of the use of the system in a case study mode, in a limited period assimilation mode, and in a more extended quasi-real time mode are given in Part 2 of this report.

Table 1.1

Options to Be Selected

Data mix:	Radiosonde	
	Special network	
	Satellite temperature retrievals/gradient winds (either/or)	
	Cloud and water vapor drift winds	
	SVCA/buoys	
Assimilation type:	Basic	
	Incremental	
Analysis:	Weight of geostrophic/gradient wind	
	Rejection tolerance	
	Minimum pass radii for first pass	
Pre-processor:	Sigma level disposition	
	Divergent or non-divergent winds	
	Topography enhancement factor	
Model:	Timestep	
	Boundary conditions	- fixed
		- updated
	Initialization	- none
		- free VMI
		- pressure constrained VMI
	Physics options	- surface T, T_D prediction
		- convective pptn
		- large scale pptn
		- vertical diffusion

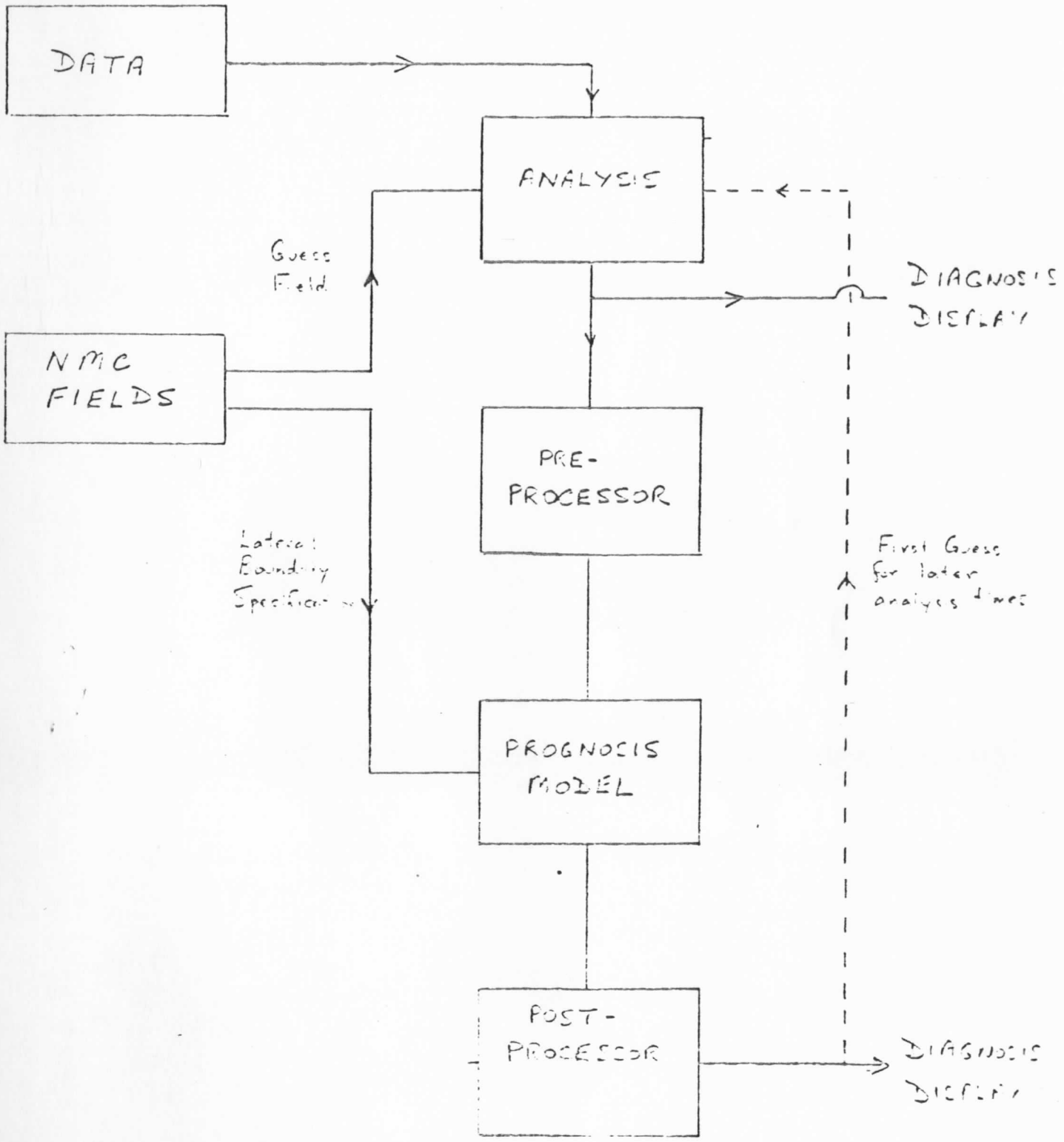

FIGURE 1.1 : COLD-START CASE STUDY CONFIGURATION

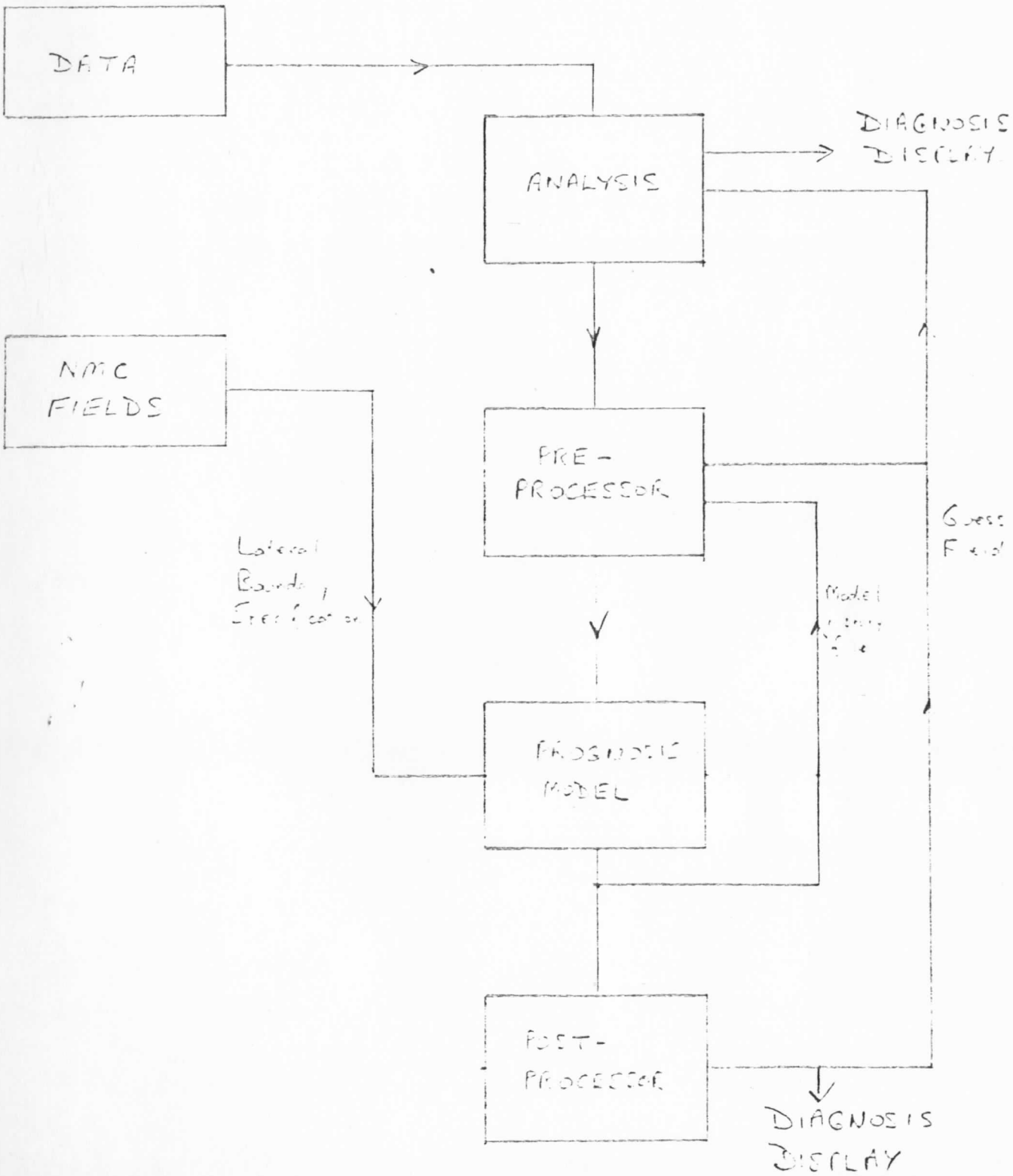

FIGURE 1.2 : INCRE[illegible] ASSIMILATION CONFIGURATION

ACKNOWLEDGEMENTS

Many people have contributed in diverse ways to the analysis and forecast systems implemented on McIDAS, as demonstrated by the recurring names in the reference list. However, there are several contributions which must be acknowledged. First, Mr. R. S. Seaman's contribution in writing the original three-dimensional blending analysis system must always be acknowledged, and parts of section 1.2 drew on his unpublished description of his methodology.

Others, whose use of the "basic" analysis system on McIDAS, produced or suggested improvements to the scheme, are J. C. Derber, J. LeMarshall and G. Diak. It is hoped that anyone whose contribution has been inadvertently or inadequately acknowledged will have the grace to "not ascribe to a conspiracy that which could be put down to a cock-up".

Finally those people who generated data sets which were used during the development of the system, notably Tony Schreiner and Tod Stewart, must be acknowledged, for without data there would be no point to using the system.

Kit Hayden and Bill Smith's ongoing interests were also greatly appreciated.

REFERENCES

Atkins, M. J., 1974: The objective analysis of relative humidity. Tellus, 26, 663-671.

Bengtsson, L., M. Kanamitsu, P. Kallberg, and S. Uppala, 1982: FGGE four-dimensional data assimilation at ECMWF. Bull. Amer. Meteor. Soc., 63, 29-43.

Blackadar, A. K., 1962: The vertical distribution of wind and turbulent exchange in a neutral atmosphere. J. Geophys. Res., 67, 3095-3102.

Bhumralkar, C. M., 1975: Numerical experiments on the computation of ground surface temperature in an atmospheric general circulation model. J. Appl. Met., 14, 1246-1258.

Bourke, W., K. Puri, R. Seaman, B. McAvaney and J. LeMarshall, 1982: ANMRC data assimilation for the southern hemisphere. Mon. Wea. Rev., 110, 1749-1771.

Bourke, W. P. and J. L. McGregor, 1983: A non-linear vertical mode initialization scheme for a limited area prediction model. Mon. Wea. Rev., 111, 228-2297.

Cressman, G., 1959: An operational objective analysis system. Mon. Wea. Rev., 87, 367-374.

Dey, C. H. and L. L. Morone, 1985: Evolution of the National Meteorological Center global data assimilation system: January 1982-December 1983. Mon. Wea. Rev., 113, 304-318.

Diak, G., S. Heikkinen and J. Bates, 1986: The influence of variations in surface treatment on 24-hour forecast with a limited area model, including a comparison of modelled and satellite-measured surface temperatures. Accepted by Mon. Wea. Rev.

Hammarstrand, U., 1977: On the parameterization of convection for large scale numerical forecasts at mid-latitudes. Contrib. Atmos. Phys., 50, 78-88.

Hayden, C. M., 1985: Estimating the wind field from VAS temperature soundings. Submitted to J. Climate Appl. Meteor.

Hill, K., G. S. Wilson and R. E. Turner, 1979: NASA's participation in the AVE-SESAME '79 program. Bull. Amer. Meteor. Soc., 60, 1323-1329.

Kallberg, P., 1977: Test of a lateral boundary relaxation scheme in a barotropic model. ECMWF Internal Report No. 3, Shinfield Park, Reading, Berkshire, England.

Kuo, H. L., 1965: On the formation and intensification of tropical cyclones through latent heat release by cumulus convection. J. Atmos. Sci., 22, 40-63.

LeMarshall, J. F., W. L. Smith and G. M. Callan, 1985: Hurricane Debby - An illustration of the complementary nature of VAS soundings and cloud and water vapor motion winds. Bull. Amer. Meteor. Soc., 66, 258-263.

Leslie, L. M., G. A. Mills, L. W. Logan, D. J. Gauntlett, G. A. Kelly, J. L. McGregor and M. J. Manton, 1985. A high resolution primitive equations NWP model for operations and research. Aust. Meteor. Mag., March 1985.

Lorenc, A. C., 1984: Data assimilation by repeated insertion into a forecast model - principles, practice, problems and plans. ECMWF Seminar/Workshop. Data assimilation systems and observing system experiments with particular emphasis on FGGE. Vol. 2, pp. 181-214.

Louis, J. F., M. Tiedtke and J. F. Geleyn, 1981: A short history of the PBL parameterization at ECMWF. Workshop on Planetary Boundary Layer Parameterization, ECMWF, Shinfield Park, Reading, Berkshire, England. 260 pp.

McGregor, J. L., L. M. Leslie and D. J. Gauntlett, 1978: The ANMRC limited area model: consolidated formulation and operational results. Mon. Wea. Rev., 106, 427-438.

Mills, G. A., 1981: An objective limited area analysis/prognosis experiment using FGGE data in the Australian region. Mon. Wea. Rev., 109, 1898-1913.

Mills, G. A., L. M. Leslie, J. L. McGregor and G. A. M. Kelly, 1980: A high resolution numerical analysis/forecast system for short-term prediction over the North American region. Unpublished ANMRC report, available from the author at BMRC, Box 1289K, Melbourne 3001, Australia.

Mills, G. A. and C. M. Hayden, 1983: The use of high horizontal resoution satellite temperature and moisture profiles to initialize a mesoscale numerical weather prodiction model - a severe weather event case study. J. Climate Appl. Meteor., 22, 649-663.

Mills, G. A. and J. L. McGregor, 1983: Vertical mode initialization in a limited area data assimilation experiment. Mon. Wea. Rev., 111, 2110-2121.

Mills, G. A. and L. M. Leslie, 1985: The use of NWP model output in the prediction of significant weather events. Aust. Meteor. Mag., Sept. 1985.

Monin, A. S. and Obukhov, 1954: Basic laws of turbulent mixing in the ground layer of the atmosphere. Akad. Nauk. SSSR Geofiz. Inst. Tr., 151, 163-187.

Mosher, F. R., 1979: Cloud drift winds from geostationary satellites. Atmos. Tech. 10, 53-60.

Ploshay, J., R. White and K. Miyakoda, 1983: FGGE IIIb daily global analyses - part I. NOAA Data Report, ERL GFDL-1. GFDL, Princeton, NJ, 150 pp.

Sasaki, Y., 1958: An objective analysis based on the variational method. J. Meteor. Soc. Japan, 36, 77-88.

Sasaki, Y., 1970: Some basic formalisms in numerical variational analysis. Mon. Wea. Rev., 98, 875-910.

Seaman, R. S., R. L. Falconer and J. Brown, 1977: Application of a variational blending technique to numerical analysis in the Autralian region. Aust. Meteor. Mag., 25, 3-23.

Smith, W. L., 1983: The retrieval of atmospheric profiles from VAS geostationary radiance observations. J. Atmos. Sci., 40, 2025-2035.

Smith, W. L., H. M. Woolf, C. M. Hayden, D. Q. Wark, and L. M. McMillin, 1979: The TIROS-N operational vertical sounder. Bull. Amer. Meteor. Soc., 60, 1177-1187.

Stephens, J. J. and J. M. Stitt, 1970: Optimum influence radii for interpolation with the method of successive corrections. Mon. Wea. Rev., 98, 680-687.

Stewart, T. R., C. M. Hayden and W. L. Smith, 1985: A note on water vapour wind tracking using VAS data on McIDAS. Bull. Amer. Meteor. Soc., 66, 1111-1115.

Suomi, V. E., R. Fox, S. S. Limaye and W. L. Smith, 1983: McIDAS III: A modern interactive data access and analysis system. J. Climate Appl. Meteor., 22, 766-778.

Williamson, D. L., R. Daley and T. W. Schlatter, 1981: The balance between mass and wind fields resulting from ultivariate optimal interpolation. Mon. Wea. Rev., 109, 2357-2376.

PART 2

APPLICATIONS OF THE MESOSCALE ANALYSIS/PROGNOSIS SYSTEM TO VARIED DATA SET ASSIMILATION AND CASE STUDIES IN THE MCIDAS ENVIRONMENT

2.1 INTRODUCTION

The suite of analysis and prognosis software has been tested extensively, using different data sets, in both a case study and a data assimilation mode, and at a variety of resolutions and over varied geographic locations. It is the purpose of this section of the report to describe some of the results obtained using these data sets, and to demonstrate different aspects of the cases. The results fall into three sub-sections. The first describes the results of assimilating a mixture of VAS sounding and special network radiosonde data at 1430 and 1730 GMT on 6 March 1982, and concentrates on the accuracy of short term forecasts based on different assimilation configurations and data mixes, with emphasis on the comparison between assimilating VAS temperatures or gradients. In the second part, a report on a quasi-real-time assimilation of VAS soundings, cloud and water-vapour drift winds, radiosonde and buoy data at 12-hour intervals over a period of 10 days in October 1985 are reported, and examples of the diagnostics package output are presented there. In the third section, some results of using the analysis/forecast model in a near real-time case-study mode to assess the impact of satellite data on the numerical prediction of the environmental flow around hurricanes are described. In addition the system has been used with TIROS-N data sets over the ALPEX region (see Menzel et al. 1985), and is at the time of writing this report (December, 1985) being used to assess the impact of VAS data sets over the East Pacific on numerical forecasts.

the control forecast as first guess. This sequence is shown diagramatically in Figure 2.3.

While a large number of option combinations were explored, only the following combinations will be discussed here. First, two basic data mixes were considered. In the first, the VAS height, temperature and moisture profiles were merged with the corresponding special network data sets, and MSLP from the SVCA hourly network. These became the VAST data sets at 1500 and 1800 GMT. A second set in which gradient winds (see Hayden, 1985) derived from the VAS soundings, and VAS dewpoint profiles, were merged with the special network radiosonde data and SVCA surface pressure data to form the VASG data set. The distribution of VAS-derived gradient wind data for 1500 and 1800 GMT are shown in Figure 2.4 (note larger scale). One further data mix was explored, suggested by the characteristics of the analysis scheme. In this set, VAS gradient winds and temperature and dewpoint profiles were merged with the special network and SVCA data, but the VAS geopotential heights were excluded to preclude the "wind from mass" nature of the analysis scheme producing spurious wind fields on the edges of the VAS data swathe. This will be known as the VASG4 sequence. In all cases, the analysis code used was the incremental wind analysis version described in Part I, section 4 of this report, together with the incremental preprocessor. For each data mix, the forecast model was run both without vertical mode initialization (hereafter referred to as the VAST2 and VASG2 sequences) and with free (see Bourke and McGregor, 1983) vertical mode initialization (VAST3 and VASG3 sequences). Table 2.1 summarizes the characteristics of these five sequences. While both gradient and geostrophic wind increments were tested, and interpolation of both divergent and nondivergent wind increments, only gradient wind, non-divergent increment cases will be addressed here.

Table 2.1 Data/initialization combinations for the assimilation sequences referred to in the text.

Experiment	VAS				Special Network Radiosonde	SVCA MSLP Data	Vertical Mode Initialization
	Height	Temperature	Dewpoint	Gradient Winds			
VAST2	Yes	Yes	Yes	--	Yes	Yes	--
VASG2	--	--	Yes	Yes	Yes	Yes	--
VAST3	Yes	Yes	Yes	--	Yes	Yes	Yes
VASG3	--	--	Yes	Yes	Yes	Yes	Yes
VASG4	--	Yes	Yes	Yes	Yes	Yes	Yes

2.2 THE MARCH 6, 1982 CASE

2.2.1 The Experiment

This was one of the NASA-AVE observing days (Hill and Turner, 1983), and aspects of the situation have been discussed by Lewis and Derber, 1985, Earl, 1985, and by Hayden, 1985. Special network radiosonde data were available at 3-hour intervals over the Texas/Oklahoma area, as well as the routine radiosonde data at 0000 and 1200 GMT, and VAS temperature and dewpoint profiles in a dense area surrounding and east of the special network area at 1430 GMT and 1730 GMT. The domain chosen is shown in Figure 2.1, with the special network radiosonde data at 15 GMT and 18 GMT superimposed, while the location of the VAS temperature profiles at 1430 GMT and 1730 GMT are shown in Figure 2.2. The grid resolution selected was 125 km, on a 26x31 mesh. This relatively coarse mesh was chosen to reduce computational expense during the development phase, but past experience indicates that the system should work reliably if the grid spacing is reduced by at least a factor of 2. The basis of the experiment was an assimilation sequence as follows: an analysis of the 1200 GMT routine and special network radiosonde data was prepared, using the interpolated NMC global analysis as first guess. A 12-hour forecast was then made, with the output file being written every three hours. This forecast is termed the control forecast. A series of assimilations were then carried out, using different combinations of the options listed in Table 1.1, and with data being inserted at 1500 GMT at 1800 GMT. At 1500 GMT the control 3-hour forecast provided the first guess for that analysis, and a 3-hour forecast from this 1500 GMT forecast became the first guess for the 1800 GMT analysis. From each 1800 GMT analysis a 6-hour forecast was prepared, and these forecasts were verified against an 00 GMT analysis of radiosonde data, which used

2.2.2 Results and Discussion

Given the large number of fields and variations available for assessment from this experiment, points will be made in the following order. First, the effect of the different data mixes on the fit of the special network data to the analyses will be addressed, by means of data fitting statistics, and in this will also be included the effects of VMI where applicable; some contour charts will be presented here as well. Second, the changes made to the fit of the special network data through the initialization process will be documented. Third, the accuracy of the 6-hour forecasts based on the 1800 GMT analyses from the various assimilation sequences will be discussed, by comparison with both the 0000 GMT radiosonde data, and also by comparing the forecast fields with the verifying analysis.

(i) Effect of data mixes on analyses

Table 2.2 presents statistics of root-mean-square (RMS) difference between the special network radiosonde data and the analyses from the different sequences. It demonstrates, not unexpectedly, that the fit of the analyses of thickness to the data is better if the VAS data are presented as gradients rather than as heights/temperatures, where the volume of the VAS soundings swamps the radiosonde data, particularly in this case where the height/temperature data from the VAS retrievals are biased relative to the radiosonde data. The improvement of the fit of the mass data to the analyses is, of course, at the expense of a deterioration of the fit of the wind data. By comparing the statistics at 1500 GMT and 1800 GMT, it can also be seen that the effect of differing guess fields at 1800 GMT between the three VASG sequences is having some effect on the fit of the data, even after the analysis phase.

Table 2.2 Root-mean-square difference between special network radiosonde data and analyses from the different sequences.

Time Sequence	1500 GMT VAST2	VASG2	VAST3	VASG3	VASG4
Field					
1000-500 mb THIK (m)	26.9	18.3	26.9	18.3	18.3
700 mb TEMP (°K)	1.49	0.43	1.49	0.43	1.49
300 mb TEMP (°K)	1.44	0.63	1.44	0.63	1.44
500 mb WIND ($msec^{-1}$)	2.74	7.36	2.74	7.36	7.36
250 mb WIND ($msec^{-1}$)	3.12	7.01	3.12	7.01	7.01
Time					
1000-500 mb THIK (m)	32.7	17.9	30.5	17.4	22.8
700 mb TEMP (°K)	1.37	0.38	1.36	0.38	1.36
300 mb TEMP (°K)	2.00	0.70	2.00	0.70	2.00
500 mb WIND ($msec^{-1}$)	3.91	8.12	3.78	8.32	6.53
250 mb WIND ($msec^{-1}$)	1.93	7.63	1.95	7.71	6.79

A sequence of charts is now presented. Fields discussed will be the 1000-500 mb thickness and the 250 mb isotach patterns for 1500 and 1800 GMT for the five sequences. Figure 2.5 shows the initial 1200 GMT radiosonde analyses of 1000-500 thickness and 250 mb isotach, and Figures 2.6 and 2.7 show the 1500 and 1800 GMT 1000-500 mb thickness analyses from the VAST2 and VASG2 sequences. While both analyses show an eastward progression of the thickness trough, the VAST sequence shows considerably lower values on the axis of the trough, and there is a much sharper transition from the 1200 GMT radiosonde analysis to the 1500 GMT VAST2 analysis than to the 1500 GMT VASG2 analysis. Another consequence of the differing data mixes is the "bumpier" patterns in the Florida area and northward just out of the VAS data area in the VAST sequence. (N.B. No gradient wind data were output in this area, although some temperature retrievals over and east of Florida were produced.) This is more evident in the 250 mb isotach analyses of Figures 2.8 (VAST2) and 2.9 (VASG2) where the VAST analyses produce a much noisier isotach pattern from Florida northwestwards to the Mississippi Valley, and also extrapolate to a noisier pattern outside the data area in the north-eastern sector of the analysis domain. The VASG2 isotach analyses again produce a smoother and more consistent progression from the 1200 GMT initial conditions.

Figures 2.10, 2.11 and 2.12 show the 1000-500 mb thicknesses and 250 mb isotachs at 1800 GMT from the VAST3, VASG3, and VASG4 sequences. The visual differences between these analyses and their counterparts in Figure 2.6-2.9 are quite subtle, although the VASG4 analyses do show a somewhat sharper thickness trough in Oklahoma and slightly enhanced strength of the jet stream through Tennessee and Kentucky, and also off the Texas coast.

(ii) Effect of initialization on data fit

It is desirable that an initialization process does not detract too much from the fit of the analysis to the data: that is, the initialization should not reject the data which has been inserted through the analysis phase. However, it is unavoidable that the fit of the data to initialized fields be worse than that to analysis fields, by the very fact that fields are adjusted to approximate model balance during the initialization. Table 2.3 shows the RMS fit of special network radiosonde data at selected levels to the analyses, and to the initialized forecast fields.

In all sequences, there is considerable degradation of the fit to the data for at least some data types and levels, although the changes seem to be greater in the VAST3 and VAS4G sequences than in the VAS3G sequence. It should be remembered that when assessing the RMS fit of the wind data to the analyses, some contribution to the RMS error comes from the removal of the divergent component of the wind analysis increment, and these values are thus higher than if the divergent wind increments were used to initialize the forecast model.

Table 2.3 Root-mean-square difference between special network radiosonde data and analyses and initialized fields for the VAST3, VASG3, and VASG4 sequences.

Time	1500 GMT					
Sequence	VAST3		VASG3		VASG4	
Anal/Init	A	I	A	I	A	I
Field						
1000-500 THIK (m)	26.9	40.6	18.3	12.5	18.3	39.8
700 T (°K)	1.49	1.64	0.43	1.74	1.49	1.71
300 T (°K)	1.44	1.28	0.63	1.36	1.44	1.35
500 WIND ($msec^{-1}$)	2.74	5.16	7.36	8.36	7.36	7.40
250 WIND ($msec^{-1}$)	3.12	8.08	7.01	9.11	7.01	10.77
Time	1800 GMT					
1000-500 THIK (m)	30.5	43.4	17.4	20.3	22.8	39.6
700 T (°K)	1.36	2.26	0.38	1.61	1.36	2.46
300 T (°K)	2.00	1.77	0.70	1.53	2.00	1.86
500 WIND ($msec^{-1}$)	3.88	6.59	8,32	8.05	6.53	8.27
250 WIND ($msec^{-1}$)	1.99	8.01	7.71	8.87	6.79	9.48

(iii) Accuracy of 6-hour prognoses based on these assimilated analyses

The statistics and the analyses presented in the preceding two subsections suggest that the analyses based on a combination of radiosondes and VAS gradient winds are both subjectively and objectively superior to those which used the VAS temperatures and heights. However the objective statistics are based on the fit of the analyses to the special network radiosondes, which have only a very limited geographic coverage (see Figure 2.1), while the subjective impressions lack independent verification.

In order to provide another measure of the quality of the different analyses, six hour forecasts to 0000 GMT 7 March 1982 were prepared, based on the 1800 GMT analyses from each of the five sequences under discussion. These will be verified against radiosonde data at 0000 GMT, against the 0000 GMT verification analysis, and will also be compared with the control 12-hour prognosis.

Table 2.4 lists RMS difference between radiosonde data at 0000 GMT 7 March and the five 6-hour prognoses, and the 12-hour control forecast for selected levels and fields. Of the 6-hour forecasts from the assimilation sequence, the VASG3 or VASG4 forecasts are the most accurate, and are also generally more accurate than the control forecast in the mass fields, particularly mean-sea-level pressure and in the upper troposphere, but are slightly less accurate than the control forecast of wind.

Charts of 1000-500 mb thickness forecast error for the VAST3 and VASG3 forecasts are shown in Figure 2.13, and for comparison the same charts for the VASG4 and control forecasts in Figure 2.14. The error patterns are very similar for each of the assimilation prognoses, with error maxima over the Gulf of Mexico, and extending southward from North Dakota/Iowa, and with negative errors in the north-east and northwest of the domain. Encouragingly,

Table 2.4 Root-mean-square difference between radiosonde data at 0000 GMT 7 March, 1982, and various prognoses valid at that time.

Field	Prognosis					
	Control	VAST2	VASG2	VAST3	VASG3	VASG4
MSLP (mb)	6.55	5.09	4.44	4.10	3.15	3.34
1000-500 (m)	34.2	42.2	32.3	42.3	32.4	33.9
700 T (°K)	1.65	1.82	1.75	1.84	1.79	2.01
500 T (°K)	2.12	1.82	1.99	1.92	1.93	1.82
300 T (°K)	2.45	2.34	2.16	2.36	1.98	1.86
700 WIND ($msec^{-1}$)	6.84	8.32	8.43	8.51	8.40	8.27
500 WIND ($msec^{-1}$)	7.95	8.70	8.72	9.06	8.25	8.73
250 WIND ($msec^{-1}$)	12.25	14.87	12.88	15.33	13.45	13.17
700 T_D (°K)	6.29	6.39	6.22	6.52	6.13	6.57

however the VASG3 forecast has eliminated the large area of negative error over the southern Texas border. Another encouraging feature is the greatly reduced magnitude of the error outside the data areas in the VASG3 forecast when compared to the VAST3 forecast. This suggests that the use of the VASG data set leads to a lesser extrapolation of errors outside the data area.

It has been shown by Mills and Leslie, 1985, that the field of the magnitude of the gradient of the temperature or dewpoint field provides a visually striking display of regions of strong thermal contrast, such as occur at frontal zones. Figures 2.15 and 2.16 show the fields of $|\Delta T|$ at 700 mb for the 1500 and 1800 GMT analyses and the 6 hour forecast to 0000 GMT for the VAST3 and VASG3 sequences, while Figure 2.17 shows the control forecast and verification analysis valid 00 GMT 7 March. The VAST sequence, where the temperatures from the VAS soundings were explicitly included in the analysis, show stronger temperature gradients than do the VASG sequence. However, all show a region of strong temperature gradient extending from Texas to the northeastern U.S., and with this region of strong gradient tending to move southeastwards, particularly over Texas. The location of the axis of maximum gradient is in very close to the same position in both the VAST and VASG forecasts, and is just a little inland from the position of this region along the Texas coastline in the verification analysis.

2.2.3 Summary

The results of the experiments in assimilation of data from the March 6, 1982 data sets are not a definitive study of the effects of different methodologies for merging VAS and radiosonde data, or of determining the optimum configuration of the CIMSS assimulation system to merge these data, and indeed neither of these aims was the intention. However, it has been shown that

(1) the assimilation system described in Part 1 of this report can successfully operate in a limited-period case study mode, merge data from differing observing systems, and produce analyses which contain both useful diagnostic information, and which also can provide the initial state from which useful short-period numerical forecasts can be based.

(2) for this particular case, and for the analysis method used, there appears to be some advantages to using the VAS data as geopotential gradient data rather than as temperature and geopotential height.

2.3 THE-QUASI-REAL-TIME ASSIMILATION

2.3.1 Introduction

It was desired to test the assimilation system using data from a longer period than are available from special observing periods such as that described in section 2.2. In spite of the obvious attractions of three-hourly radiosondes, extremely dense satellite retrieval data sets, and interesting synoptic situations, the special observing periods do not operate for a sufficiently long time to adequately test an assimilation system which is intended to operate for extended periods. Accordingly, the advantage was taken of CIMSS support of the National Hurricane Centre (see for example, Velden et al. 1984) to assimilate radiosonde, buoy, VAS temperature and dewpoint (see Smith, 1983), and gradient wind data (Hayden, 1985), and cloud and water vapour motion winds (Stewart et al. 1985). The assimilation interval was 12-hours, and data were assimilated from 12 GMT on 8 October 1985 to 12 GMT on 18 October 1985. No VAS or cloud drift wind data were available during the weekend. The domain chosen was the same as that used for the March 6 assimilation, for the simple convenience of not having to change software modules. While the original intention was to operate the system in delayed real-time, the practicalities of operating in a background mode on MCIDAS, and the development work necessary to ensure a stable configuration of the assimilation model compromised this ambition. However, once a stable configuration was established, the 10 days of assimilation was completed in less than 10 days elapsed time, with each 12-hour analysis/forecast cycle consuming approximately 15 mins CPU time. The final configuration arrived at for this assimilation is listed in Table 2.3.1.

As can be seen from this table, some compromises from the intended configuration have been made while a stable configuration was being

Table 2.3.1: Configuration of quasi-time assimilation vehicle.

Data mix	:	Radiosonde Buoy VAS temperature and dewpoint profiles VAS gradient winds Cloud drift and water vapour winds
Analysis	:	Incremental wind analysis Geostrophic wind law "Nested" analysis
Preprocessor	:	"Basic" preprocessor
Model	:	Timestep 600 secs Vertical Mode Initialization (Free) Physics - Large scale precipitation Kuo convective parameterization Vertical diffusion Updated boundary conditions provided by global 12 hour forecast.

established. The chief of these was the replacement of the incremental preprocessor with the basic version, and the revision to the use of the geostrophic wind law from the gradient wind law. Both these changes came about while the cause of a positive feedback to the low-level wind fields in the southern corners of the domain was being sought, and it was ultimately found that neither of these features was the cause. Thus the system could now be returned to its full incremental form.

The cause of the positive feedback was in interaction of the lateral boundary tendencies from the global forecasts with the incremental wind analysis. For four consecutive analysis/prognosis assimilation cycles, the global forecast 1000 mb wind tendencies showed some 10 m sec^{-1} increase over the 12-hour prognosis interval (but the absolute values remained much the same from cycle to cycle). This lead the prognosis model to increase these wind strengths from cycle to cycle (in spite of a degree of moderation in the analysis), ultimately leading to numerical instability in the sixth assimilation prognosis. The pragmatic solution to this problem was to, prior to the forecast step, nest the analysis inside the interpolated global analysis using the same weighted average on the outer five rows of the grid which is used for the tendencies from the outer and inner forecast meshes in the prognosis model (see Leslie et al. 1985). This means that the absolute values of the outermost rows of the input fields to the forecast model are matched to the externally specified fields, as well as the tendencies. This was found to make the system quite stable, and no further need for intervention was found while assimilating these 10 days of data. Intuitively, one would expect that the prognosis will reflect more of the externally specified fields using this procedure, and thus, with the relatively small grid dimensions used, may not show as much fine mesh detail in the forecast as could be expected. However,

this procedure is no different to matching the external row values in the prognosis to the outer forecast, and it should be stressed that the analysis fields archived are those prior to this nesting procedure, and thus the fields fully reflect the mix of guess field and data. Having established, by the fact that the system operated successfully for this 10-day period, a stable assimilation configuration, the remainder of this section of the report will describe some features of the assimilation vehicle. First the fit of the radiosonde data to the analysis, 12-hour prognosis, and to the initialized fields will be shown as time sequences to provide some measure of the accuracy of the forecasts and the amount of degradation of the fit of the data to the initial fields by the vertical mode initialization scheme. Second, a full sequence of 500 mb height/wind fields will be presented to demonstrate the temporal continuity of the analyses. Third, the vertical motion patterns from the 12-hour forecast and after analysis/initialization will be shown for selected cases to demonstrate that information from the preceding prognosis is being carried through the subsequent cycles, and fourth, some diagnostic fields will be presented, showing some of the uses of the analysis output.

2.3.2 Data Fitting Statistics

Figures 2.18-2.20 show time series of root-mean-square difference between radiosonde data and analyses, initialized fields and 12-hour forecasts for MSLP, 1000-500 mb thickness, 850, 500 and 250 mb temperatures and 500 and 250 mb vector wind for each analysis time through the assimilation sequence. In general the desired pattern is followed, with the analysis fitting the data best, and the initialized fields not fitting the data as well as the analysis, but still better than the prognosis to that time. That is, the initialization is not, in general, rejecting the data.

There is, however, a great deal of case to case fluctuation, and some interesting situations occur. For example, at 12 GMT on day 283, the initialization makes very large changes to almost all fields, and clearly there was considerable imbalance in the initial state, and this was followed by the largest 1000-500 mb thickness errors in any of the 12-hour forecasts. It was encouraging, however, at this stage of development of the system, to find that this did not destabilize the system. When looking at the 1000-500 mb thickness statistics, there is a considerable degree of oscillation in the skill of the forecasts based at 12 GMT and those based at 00 GMT. The cause of this may be due to the differing mixes of satellite and conventional data at the different times, or may be due to more subtle factors needing further investigation.

It is also notable that possibly the greatest rejection of any of the data types during initialization occurs in the mean-sea-level field. This is a consequence of using the "free" form of the vertical mode initialization, where both surface pressure and tropospheric variables are adjusted. If it is desired to retain more of the surface information, then the "surface pressure constrained" option could be exercised, but at the consequence of greater adjustment of the lower tropospheric fields. When looking at the RMS vector errors of Fig. 2.20 it must be remembered that the wind fields input to the prognosis model are non-divergent increments (see section 1.4) added to the model forecast wind fields, and thus the RMSVE statistics have a greater magnitude than would be expected from a scalar analysis of wind components. Indeed, these fields are also output from the analysis, and the RMSVE of the radiosonde data to these wind fields are also included for comparison, and are substantially lower than the statistics for the winds used for model initiation. The later examples of diagnostic fields computed from the analysis will use these latter wind component fields.

2.3.3 Prognosis Feedback

Lorenc's condition (3) (see section 1.1) stated that the analysis must be near the forecast based on earlier observations, unless current observations indicate otherwise. To a large extent this condition is met by correcting the first guess forecast in the analysis. However, equally it is desirable that information from the prognosis model which is not resolved by the observations or the analysis scheme be preserved through the analysis (correction) and initialization phases of the assimilation. One such field is the vertical motion structure. To examine the way in which the vertical motion patterns are preserved through analysis/initialization, the 500 mb omega field ($\partial p/\partial t$) was compared before the analysis and after initialization at each data insertion time. In general the preservation of major features, and indeed structure, was highly encouraging. Two examples are shown in Figures 2.21 and 2.22. These show the 12-hour forecast vertical motion and the after initialization vertical motion at 00 GMT 10 October and 00 GMT 16 October 1985. In each case it is clear that substantial continuity of these fields has been preserved, even though there has been, as shown by Figures 2.18 to 2.20, significant changes to the prognosis fields during the analysis. These patterns are quite typical of the synoptic sequence during this period, with an area of upward vertical motion towards the north west of the grid, associated with an advancing trough, and another weaker, elongated SW-NE area of upward motion which has propagated southeastwards in association with the eastward passage of the preceding middle latitude trough.

2.3.4 Field Continuity

A demonstration of the coherence of the synoptic pattern through this assimilation sequence is shown in Figure 2.23, where the entire sequence of

500 mb height and isotach analyses are shown. This period was not particularly synoptically active, with a powerful anticyclonic circulation covering the southeastern part of the U.S. during the entire period. However the sequence of advancing troughs can be seen entering the analysis domain from the west and northwest and then being forced northward by the anticylone as they move eastwards. The sequence demonstrates a synoptic continuity through the assimilation period, as would be expected from a robust analysis/prognosis system.

2.3.5 Diagnostic Quantities

2.3.6 Summary

2.4 APPLICATIONS TO TROPICAL CYCLONE STEERING FLOW FORECASTS

2.4.1 Introduction

For the past three years, CIMSS has generated data daily from geostationary satellites to support National Hurricane Center (NHC) forecasting operations, as described by Velden et al. 1984. Several approaches have been taken to assess the utility of these data, such as the quasi-operational VASTRA forecasts described by Velden et al. 1984, and the limited modelling studies of LeMarshall et al. 1985 and of Lewis et al., 1985. One of the highly encouraging products is the VASTRA forecast, which is a trajectory forecast based on a deep-layer-mean wind vector field which is derived from analyses of radiosonde, VAS gradient winds, and cloud drift and water vapour winds, and this has produced some highly encouraging forecasts of hurricane movement. However, such an approach does not allow for any evolution of the steering flow with time through the forecast period, and thus must be expected to be most successful in those cases where the environmental flow does not change rapidly throughout the forecast period.

A limited study is presented here, where a coarse mesh limited area forecast model is, for three cases, initialized with conventional, and with conventional and satellite data, and integrated in one case for 48 hours, and in the other two cases for 36 hours. The aim of this exercise was to attempt to demonstrate the utility of the satellite products for initializing a NWP model forecast of the environmental flow around a hurricane and to show that useful forecast guidance could be gained in the 24 hour timeframe and beyond using this technique. Thus a relatively coarse mesh size was selected to take advantage of the broad geographical spread of the satellite data, and to allow synoptic patterns to evolve within the grid during the time of the forecast. Thus the hurricane vortex itself was inadequately resolved by the forecasts,

so assessment of the impact of the satellite products was made by computing a forecast deep-layer-mean wind field each 6 hours of the forecast model run, and trajectories were calculated, the deep-layer-means used being updated each 6-hours from the forecast.

The three cases selected were Hurricane Elena with a 48-hour prognosis, grid spacing 150 km, based at 12 GMT 29 August 1985, and a 36-hour forecast based at 00 GMT 30 August, and Hurricane Bob, with a 36-hour forecast, grid spacing 100 km, based at 1200 GMT 23 July 1985. The domains and grid resolutions were selected based largely on data density of the satellite products, and by consideration of the prevailing synoptic situation. All forecasts were nested within the global forecast fields from NMC, and the analysis version used was that described in part 1.3. The deep layer means and the trajectory forecasts were calculated in the manner of Velden et al., 1984, but without their insertion of current storm motion at the initial time.

2.4.2 The Forecasts

Figures $2.n_1$, to $2.n_3$ show the trajectory forecasts computed using the forecast deep-layer-mean for the two Elena forecasts and the Bob forecast at 12-hour intervals, together with the observed positions. For both the Elena forecasts, the predicted track was better from the forecast with satellite data than that without, particularly towards the end of the forecast period in each case. While neither of the SAT forecasts predicted the curvature to the east that Elena actually took (see Velden, 1985 for a discussion) each of the SAT forecasts did predict a trend towards the north or north-northeast during the forecast, and also showed significant slowing of the storm speed, and did not predict that the storm would cross the coastline, as did the prognosis based on coonventional data only. Perhaps more visually impressive

are the time sequences of DLM forecast charts. Figure n_4 shows the upper level wind distribution at the initial time of the 1200 GMT 29 August Elena forecasts, and a sequence of forecast deep layer mean wind fields at 12-hour intervals form both the SAT and the NOSAT forecasts. The much stronger southerly steering flow which develops in the southern Gulf of Mexico in the NOSAT forecast, and then extends northward to cross the coast near the Alabama-Mississippi border is clearly seen, while the flow in the SAT forecast is weakening until the last few hours of the integrations. Figure n_5 shows the sequence of forecast deep-layer-mean wind flows at 6-hour intervals for the 36-hour forecast based at 0000 GMT 30 August 1985 from the SAT forecast based at this time. The weakening and turning of the initially strong south-easterly steering flow west of the Florida peninsula as the trough in the westerlies extends southwards is quite striking.

The forecast of the track of Hurricane Bob (Figure n_3) was rather less successful. Both the SAT and the NOSAT forecasts were very good to 12-hours, and did show the subsequent curvature to the northward. However beyond this point the centre of the circulation associated with the hurricane moved close to this point, and only marginal movement was forecast in the final 24 hours of the forecast period. Any impact from the satellite data was, however, positive and again the sequence of 6-hour deep-layer-mean forecasts (not presented for reasons of space) did show some useful information content out to approximately 24 hours, as ridging in the Atlantic Ocean turns the steering flow from west-south-west to southeasterly immediately to the east of the Florida peninsula. After 24 hours into the forecast though, northeasterlies extend from the north southward into the Carolinas, effectively stalling the vortex.

2.4.3 Discussion

This brief study asks more questions than it answers. The subjective impression of looking at the evolution of the steering flow vectors is perhaps more positive than the trajectories forecast using these steering flows. This perhaps suggests that, as the best deep layer mean wind has been determined statistically using radiosonde data, then the statistics may not be strictly applicable to output from the NWP model. The study has demonstrated though, that (1) the use of VAS temperature, dewpoint and gradient wind data and cloud drift and water vapour wind data do positively impact on a NWP forecast of the environmental flow surrounding hurricanes in the 24-48 hour time frame, (2) using an updated deep-layer-mean steering flow from a NWP model forecast does provide a better trajectory forecast of hurricane movement than does a simple trajectory forecast based only on he analysis at base time.

The obvious next step in such a study will be to use forecasts which have been produced here incorporating both satellite and conventional data products to provide the lateral boundary conditions for a fine mark internally nested model integration in which the hurricane vortex is explicitly resolved, in the manner of the MFM model of Hovermale and Livezey, 1977, or the pocket MFM model (Marks, 1985). This would enable the hurricane/environment interactions to be modelled, and the forecast track would then be that of the model vortex, producing a less ambiguous track forecast. In such a scenario the satellite derived data produced at CIMSS should provide a better specified initial state for the broad-scale forecast than has hitherto been available over the oceans.

2.5 SUMMARY

A data assimilation system has been developed for use at mesoscale resolution in both a real-time and a case-study mode on the McIDAS computer system, and is capable of using all data types, both satellite and ground-based, which are accessed by or produced on that system.

It has been demonstrated that the system is stable and robust in time during an assimilation sequence lasting 10 days, and that during these 10 days the analyzed fields showed a close fit to the observational data, a realistic evolution of the synoptic fields, that the fields analyzed contained useful diagnostic information, and that there is information being retained from the guess field through the analysis, in accordance with the general design aims of an assimilation system. Other examples of the use of the system have been presented here. It has been shown that, in tests of assimilating mixes of special network radiosonde data and VAS temperatures/heights or of special network radiosonde data and VAS-derived gradient winds, that the VAS gradient winds mix produced subjectively better analyses and objectively measured improved prognoses. A third application of the system shown here has been the case studies of data impact of satellite data on the numerical prediction of the environmental flow around hurricanes.

These studies and examples of use suggest many further applications of the system. It is intended that the system be used to assimilate the data from the impending GALE and forthcoming STORM regional experiments, and to be further used to investigate methodologies of merging data of differing types. Already it has been used to assimilate TIROS-N retrievals over the ALPEX region of Europe, and is being used in a case study mode to assess the impact of VAS data over the East Pacific during the winter of 1985/86. In the future, the system will be further applied to the problems of assessing the

best ways of mixing data from different sources, and also to replace the successive correction analysis code with a univariate optimum interpolation analysis to assess the interactions between these different analysis methodologies and the different data mixes which can be expected to become available in the next few years.

CAPTIONS TO FIGURES

Figure 2.1: Location of 1500 and 1800 GMT March 6, 1982 special network radiosonde data on the assimilation grid.

Figure 2.2: Location of VAS temperature and dewpoint retrieval profiles at 1430 and 1730 GMT March 6, 1982.

Figure 2.3: Basic configuration of the March 6 assimilation experiments.

Figure 2.4: VAS derived gradient winds at 1430 and 1730 GMT, March 6, 1982. Full barbs 10 $msec^{-1}$. Note the reduced geographical area, selected to improve clarity of the wind plots.

Figure 2.5: 1000-500 mb thickness and 250 mb isotach patterns from the radiosonde analysis at 1200 GMT March 6, 1982.

Figure 2.6: 1000-500 mb thickness analyses at 1500 and 1800 GMT March 6, 1982 from the VAST2 sequence.

Figure 2.7: As Figure 2.6 from the VASG2 sequence.

Figure 2.8: 250 mb isotach analyses at 1500 and 1800 GMT March 6, 1982 from the VAST2 sequence.

Figure 2.9: As Figure 2.8 from the VASG2 sequence.

Figure 2.10: 1000-500 mb thickness analyses at 1800 GMT March 6 1982 from the VAST3 and VASG3 sequences.

Figure 2.11: 250 mb isotach analyses at 1800 GMT March 6, 1982 from the VAST3 and VASG3 sequences.

Figure 2.12: 1000-500 mb thickness and 250 mb isotach analyses at 1800 GMT March 6, 1982 from the VASG4 sequence.

Figure 2.13: 1000-500 mb thickness 6-hour forecast errors at 0000 GMT March 7, 1982 from the VAST3 and VASG3 sequences.

Figure 2.14: 1000-500 mb thickness forecast errors at 0000 GMT March 7, 1982 from the 12-hour control prognosis and the 6-hour VASG4 prognosis.

Figure 2.15: Temperature gradient fields-analyses at 1500 and 1800 GMT 6 March 1982 and 6-hour forecast valid 0000 GMT 7 March 1982 from VAST3 sequence (units are 1/10th of °K for 100 km).

Figure 2.16: As Figure 2.15 for the VASG3 sequence.

Figure 2.17: Temperature gradient fields at 0000 GMT 7 March 1982 for the 12-hour control forecast and the verifying analysis (units are 1/10 of °K for 100 km).

Figure 2.18: Root-mean-square fit of radiosonde data mean-sea-level pressure and 1000-500 mb thickness to analyses, initialized fields, and 12-hour prognoses at 12-hour intervals from 00 GMT 9 October 1985 (day 282) to 12 GMT 18 October 1985 (day 291).

Figure 2.19: Root-mean-square fit of radiosonde temperature data at 850, 500 and 250 mb to analyses, initalized fields and 12-hour prognoses at 12-hour intervals from 00 GMT 9 October 1985 (day 282) to 12 GMT 18 October 1985 (day 291).

Figure 2.20: Root-mean-square vector error at 500 mb and 250 mb of 12-hour prognoses, analyses with non-divergent wind increments, analyses with divergent wind increments (triangles), initialized fields and 12-hour prognoses at 12-hour intervals from 00 GMT 9 October 1985 (day 282) to 12 GMT 18 October 1985 (day 291).

Figure 2.21: Before analysis and after initialization 500 mb vertical motion ($\partial p/\partial t$) fields at 0000 GMT 10 October 1985. (units mb/hr)

Figure 2.22: Before analysis and after initialization 500 mb vertical motion ($\partial p/\partial t$) fields at 0000 GMT 16 October 1985. (units mb/hr)

Figure 2.23: 500 mb geopotential height/isotach patterns from 0000 GMT 9 October 1985 to 1200 GMT 18 October 1985.

Figure 2.n1: Track positions at 12-hour intervals for Hurricane Elena, for the 48-hour forecast based at 1200 GMT 29 August 1985 (circles, observed position, crosses SAT forecast, squares NOSAT forecast).

Figure 2.n2: As Figure 2.n1 for the Hurricane Elena 36-hour forecast based at 0000 GMT 30 August 1985.

Figure 2.n3: As Figure 2.n1 for the Hurricane Bob 36-hour forecast based at 1200 GMT 23 July 1985.

Figure 2.n4: 200 mb VAS and cloud drift winds (top, right) and 200 mb radiosonde winds (top, left) at 1200 GMT 28 August 1985. Then deep layer mean wind fields analyzed and then forecast at 12-hour intervals from the SAT (left) and NOSAT (right) forecasts. The length of the wind vectors is proportional to the strength of the steering flow.

Figure 2.n5: Deep layer mean forecast steering flow at 6-hour intervals from 00 GMT 30 August for Hurricane Elena.

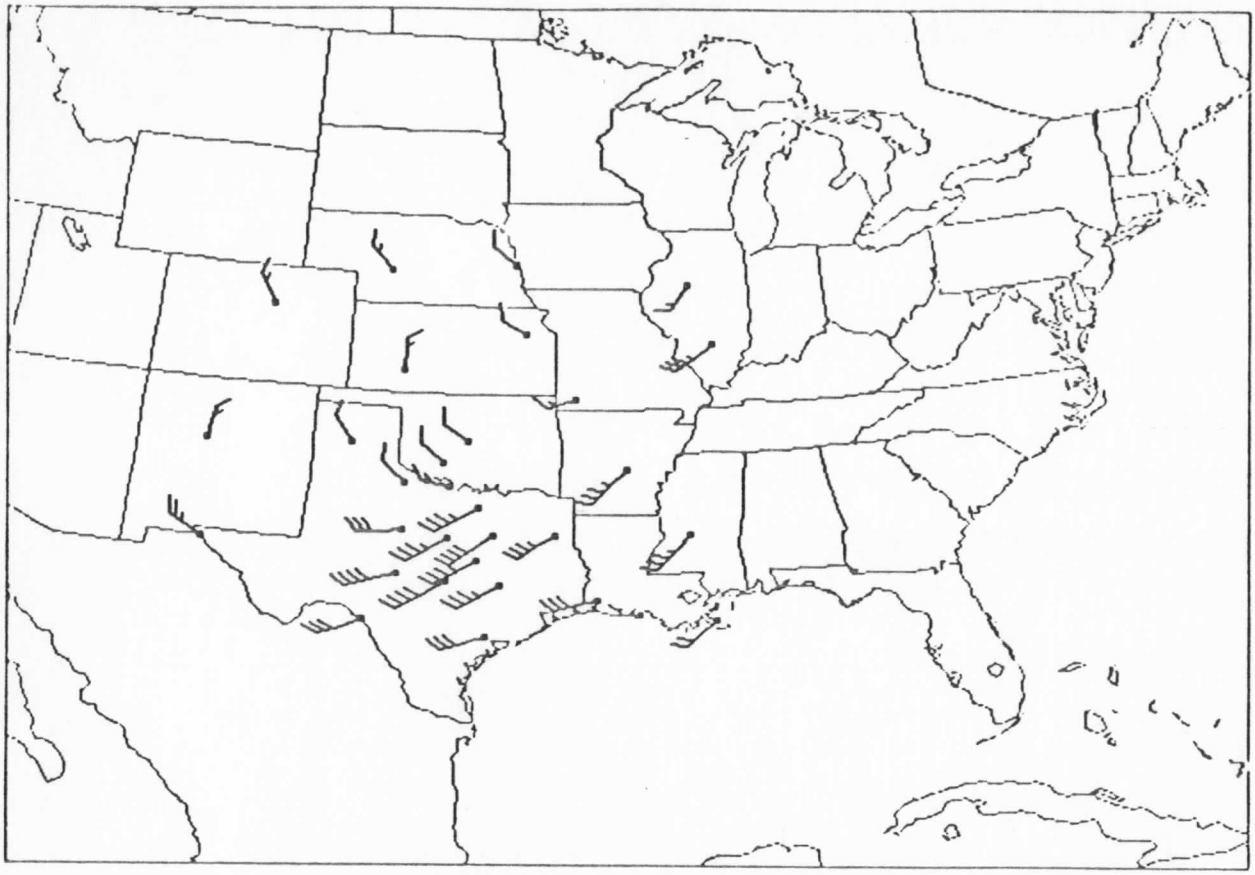

MARCH 6 15Z SNET RAOBS 500MB

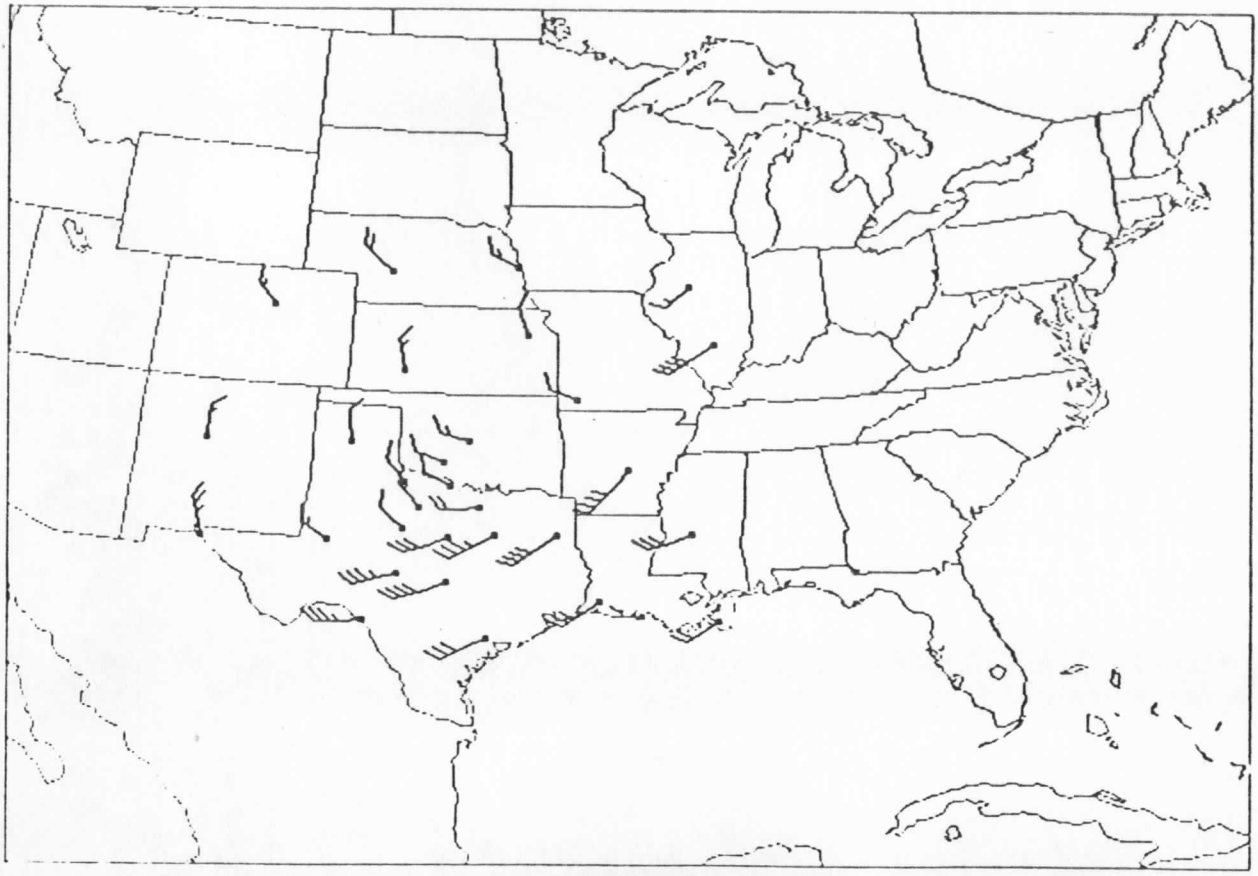

MARCH 6 18Z SNET RAOBS 500MB

Fig 2

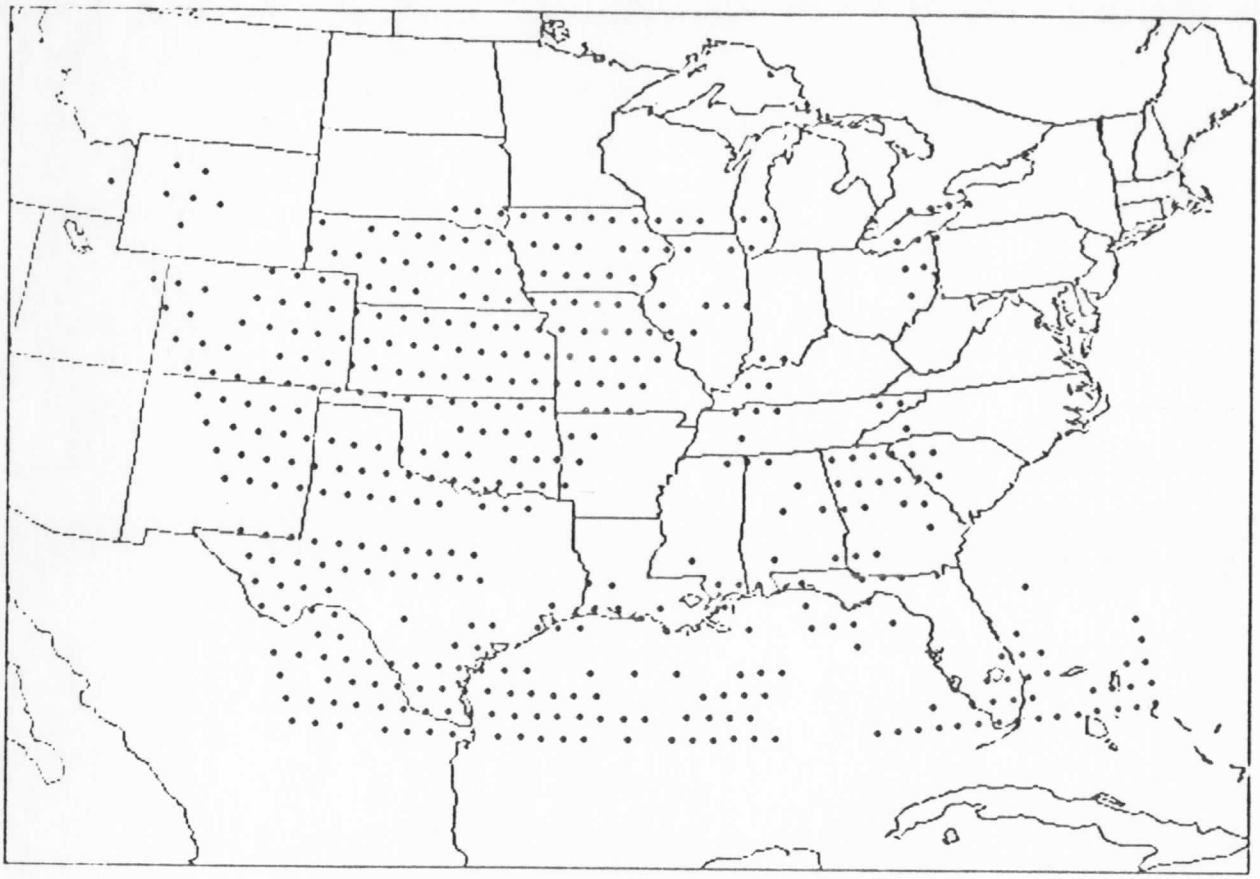

MARCH 6 1430 RETRIEVAL LOCATIONS

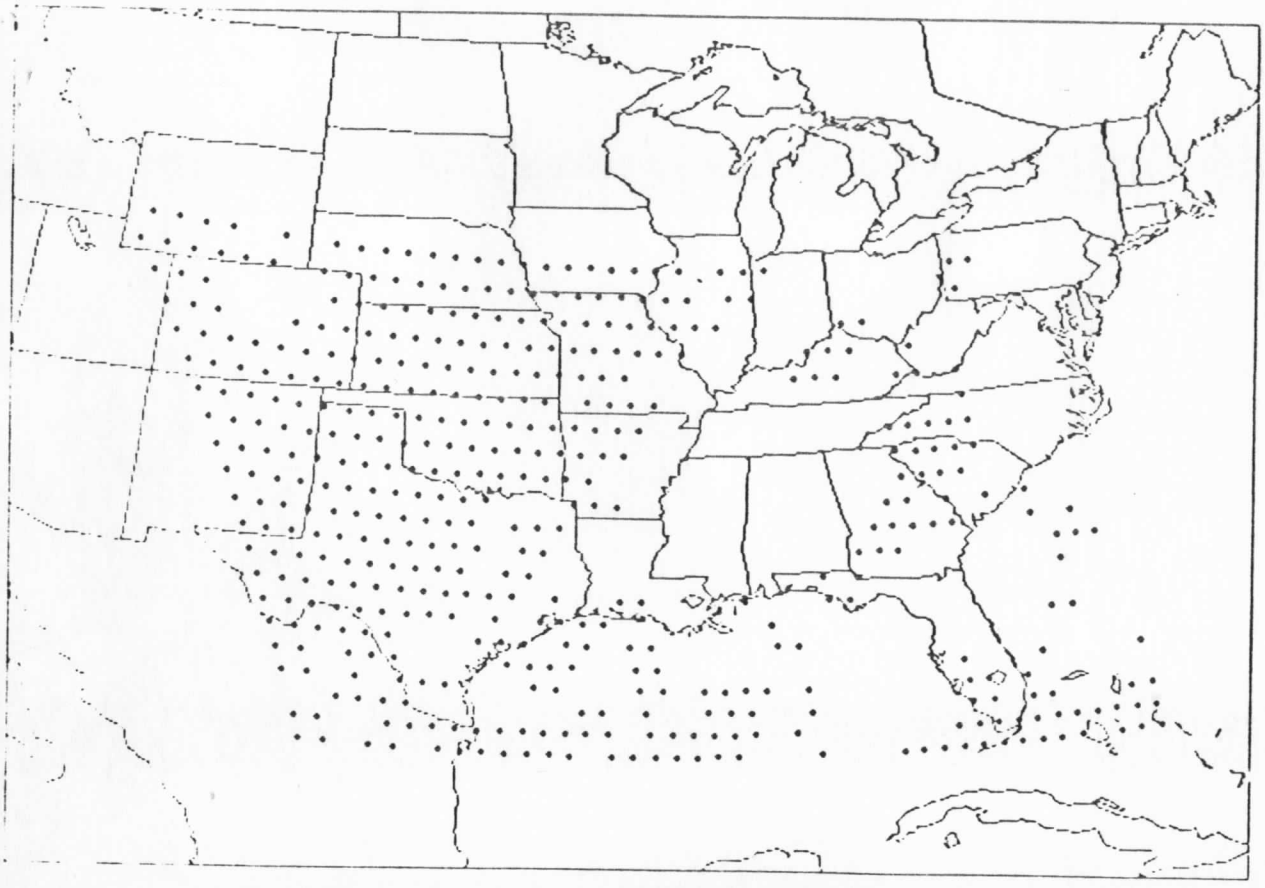

MARCH 6 1730 RETRIEVAL LOCATIONS

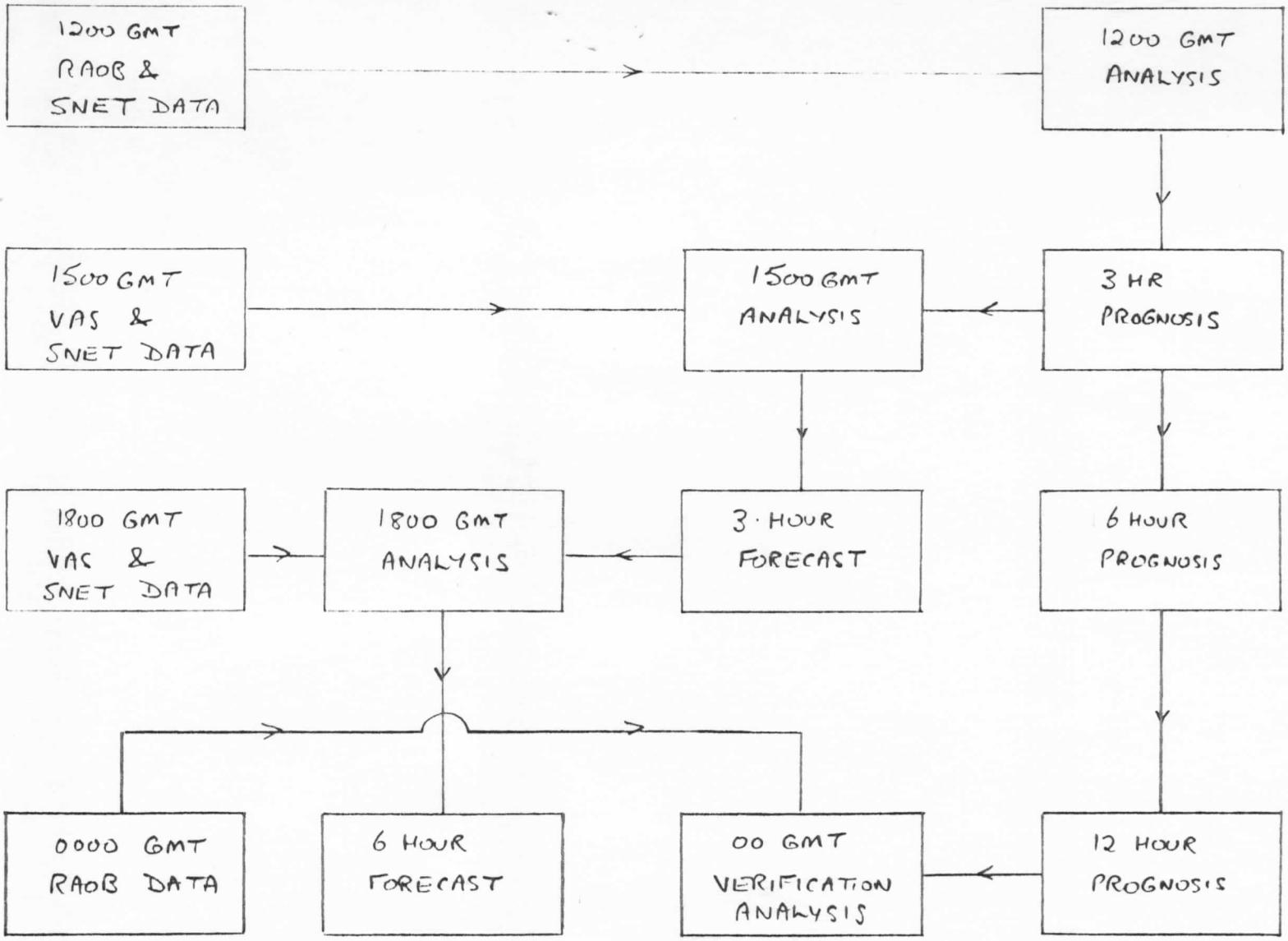

FIGURE 2.3 BASIC CONFIGURATION OF THE MARCH 6 ASSIMILATION EXPERIMENTS

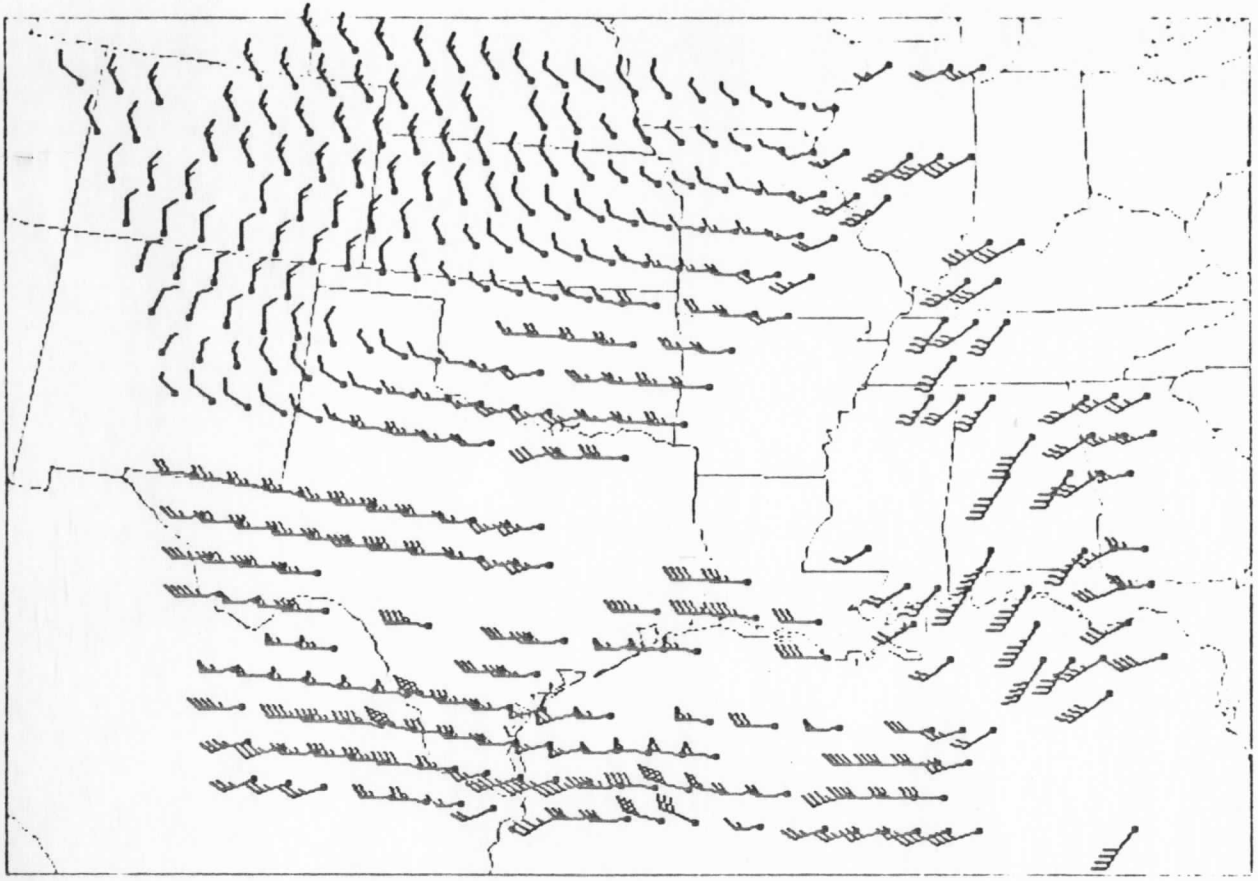

1430 500MB VASGR

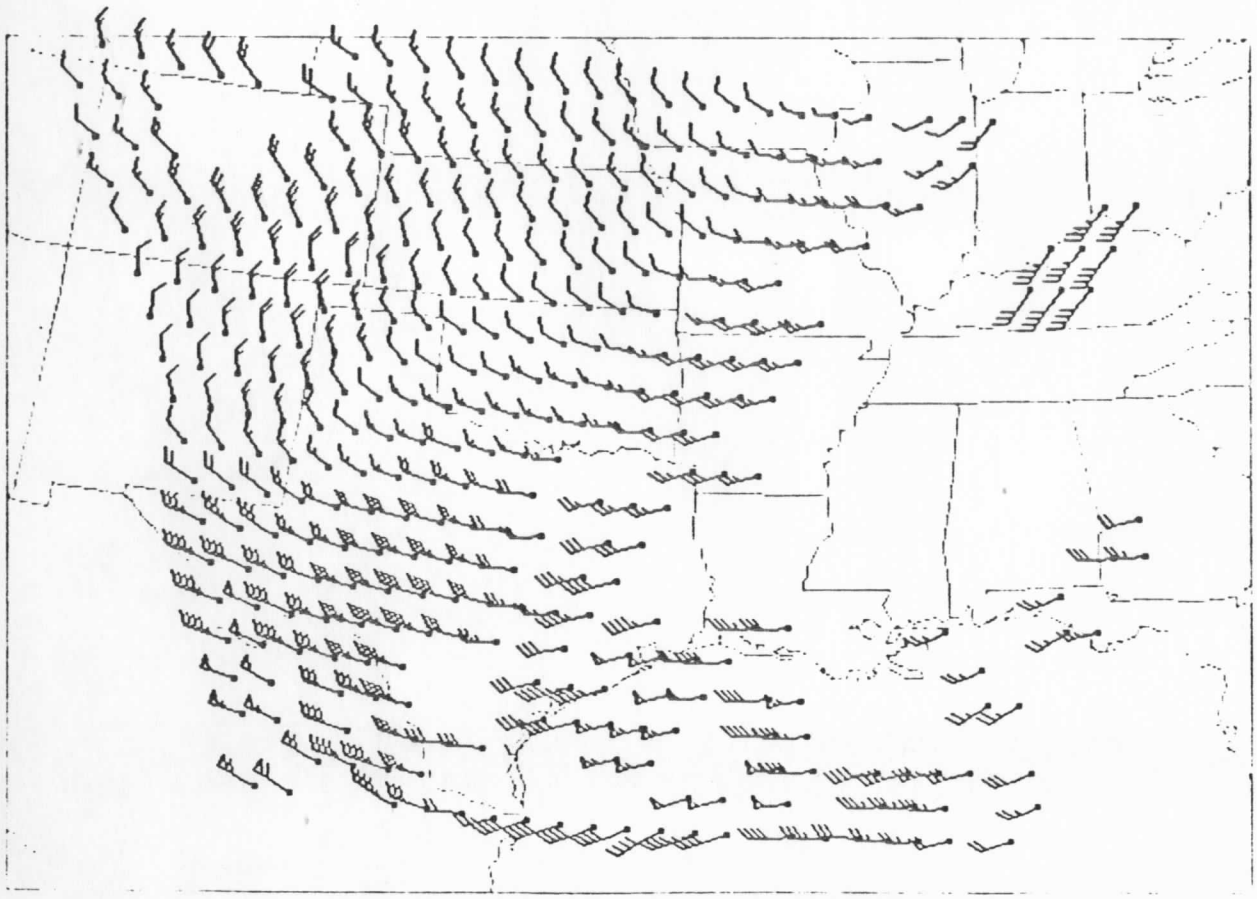

1730 VASGR 500MB

FIG 2.4

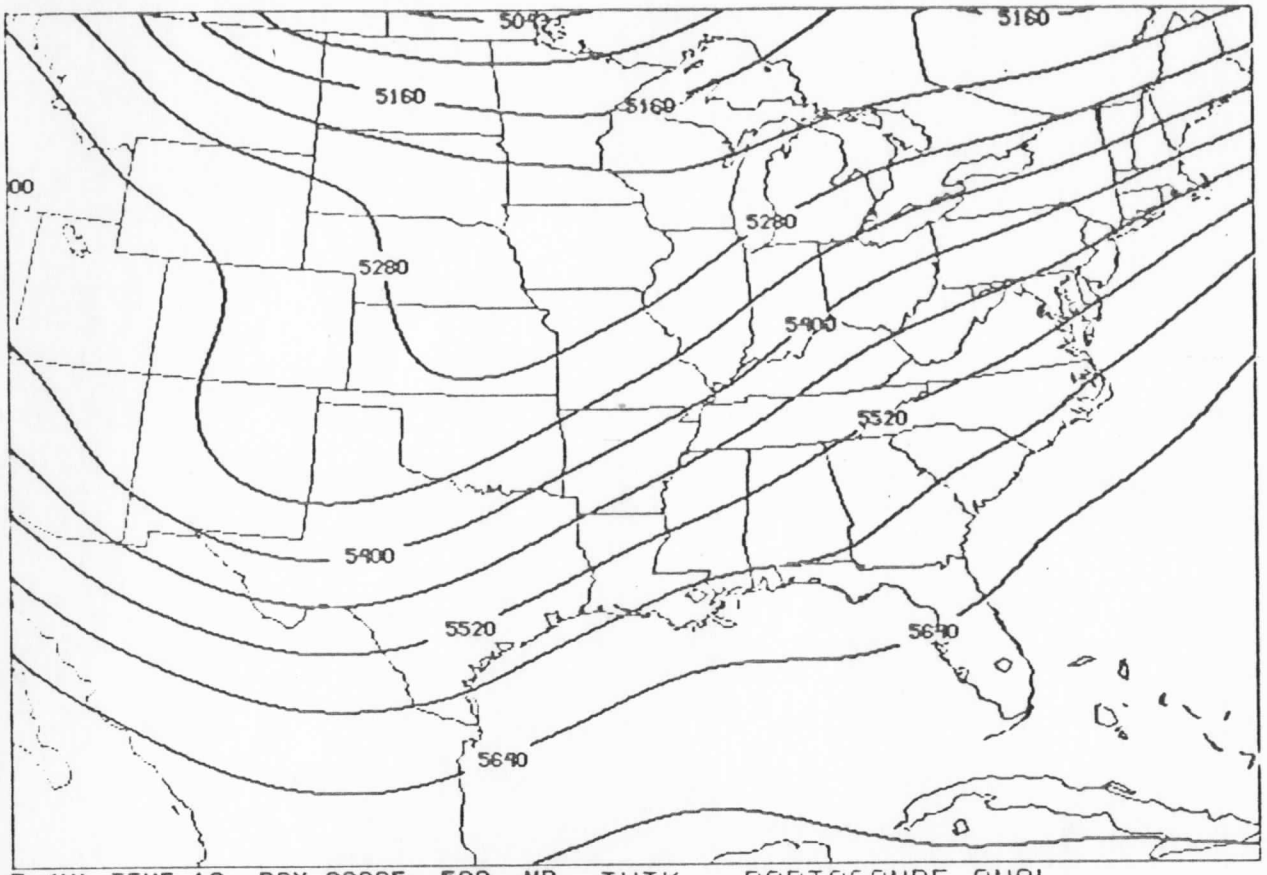

Z (M) TIME 12. DAY 82065. 500. MB THIK RADIOSONDE ANAL

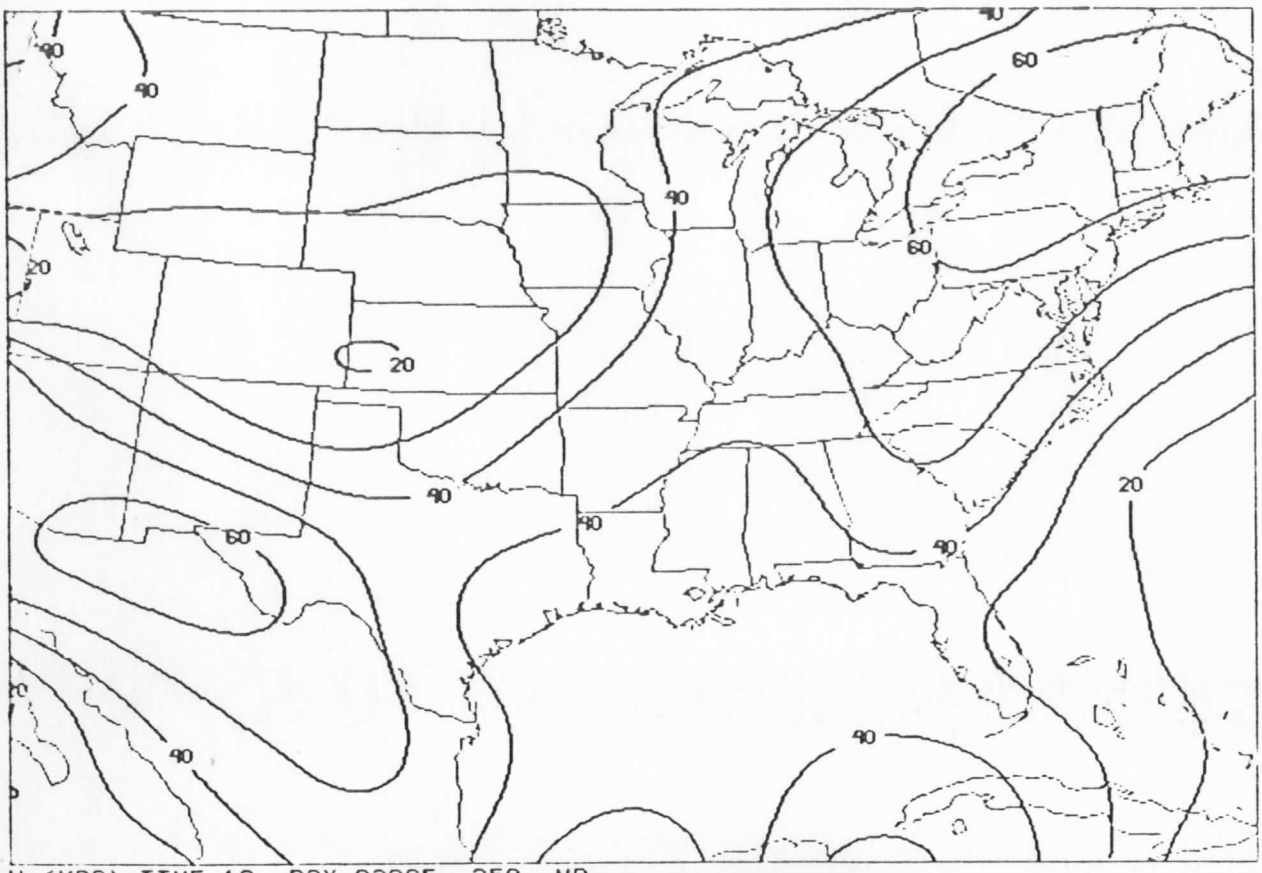

W (MPS) TIME 12. DAY 82065. 250. MB RADIOSONDE ANAL

Fig 2.5

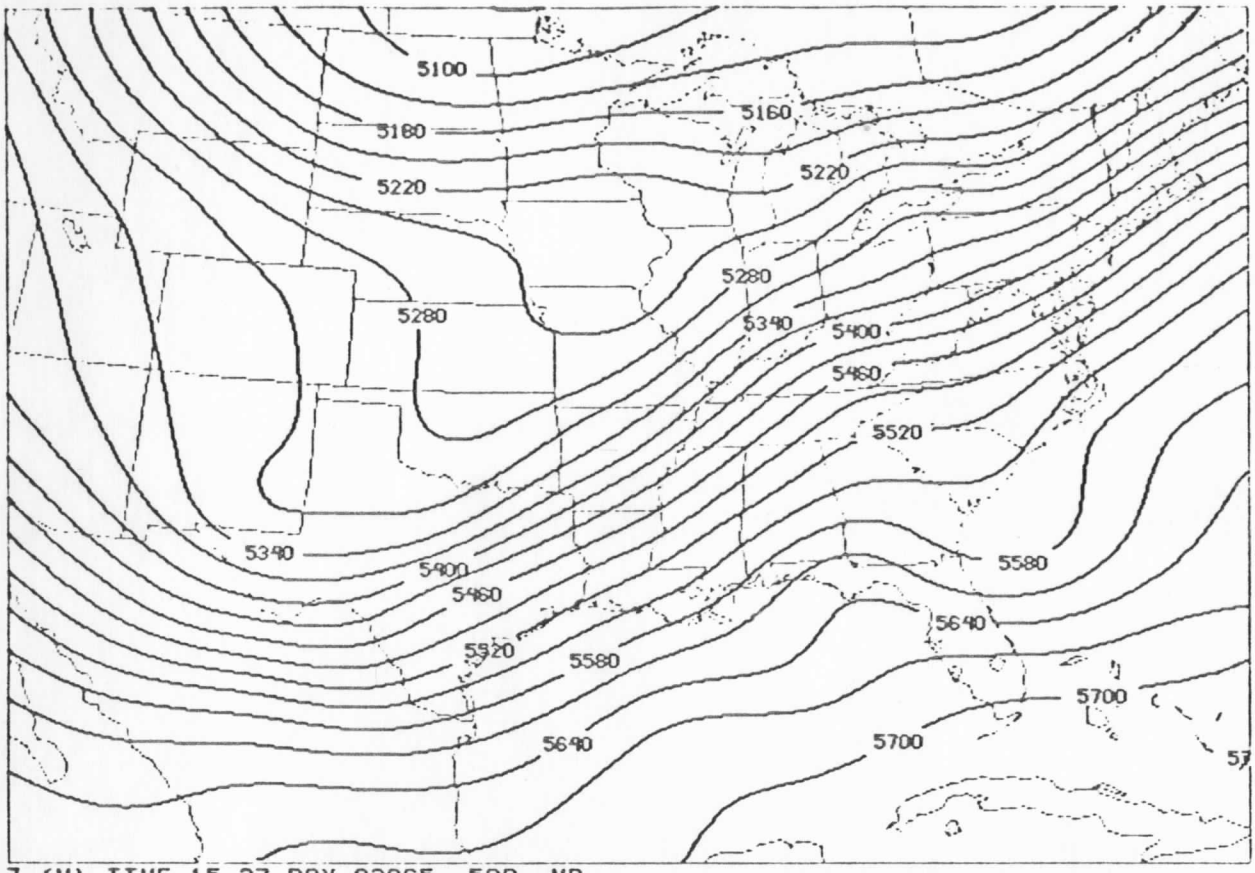

Z (M) TIME 15.27 DAY 82065. 500. MB

THIK VAST ANAL SEQ2

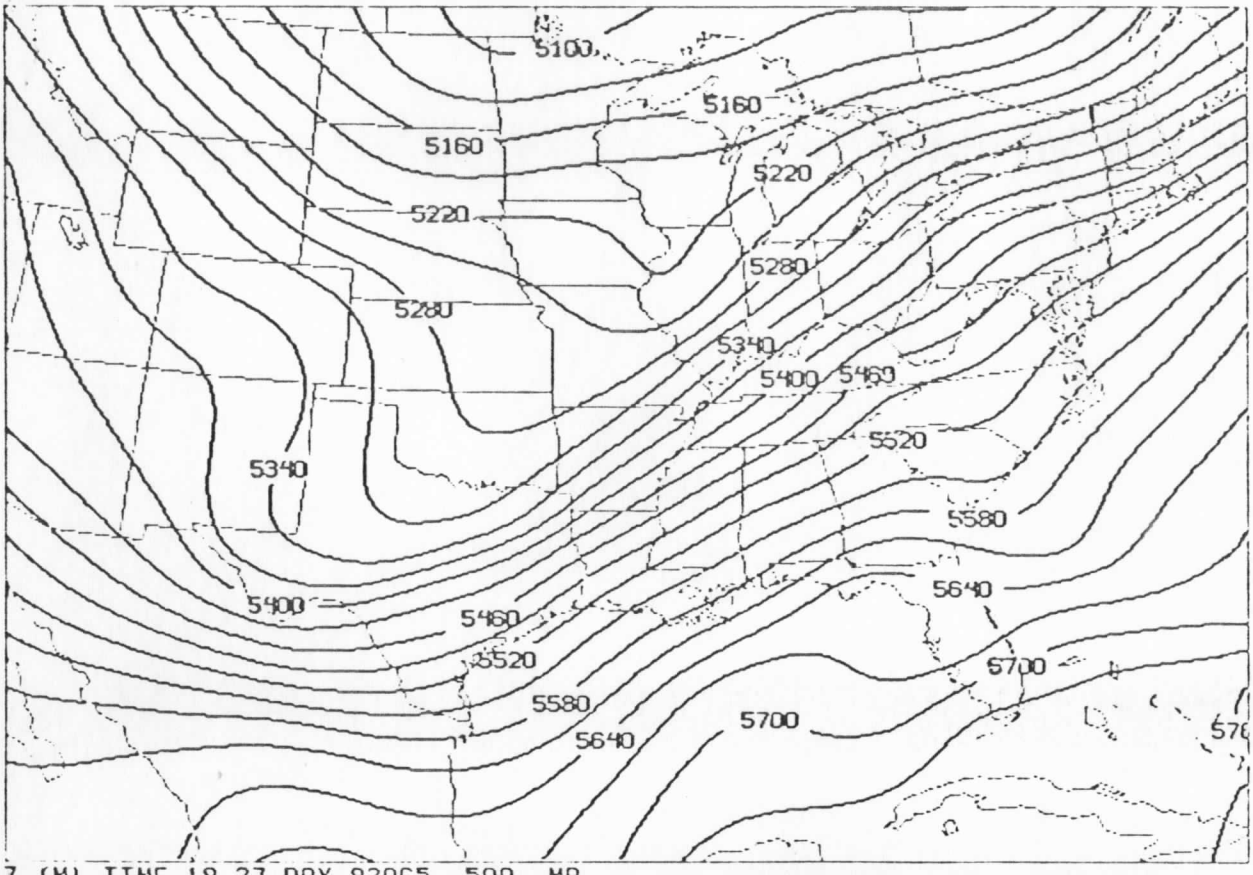

Z (M) TIME 18.27 DAY 82065. 500. MB

THIK VAST ANAL SEQ2

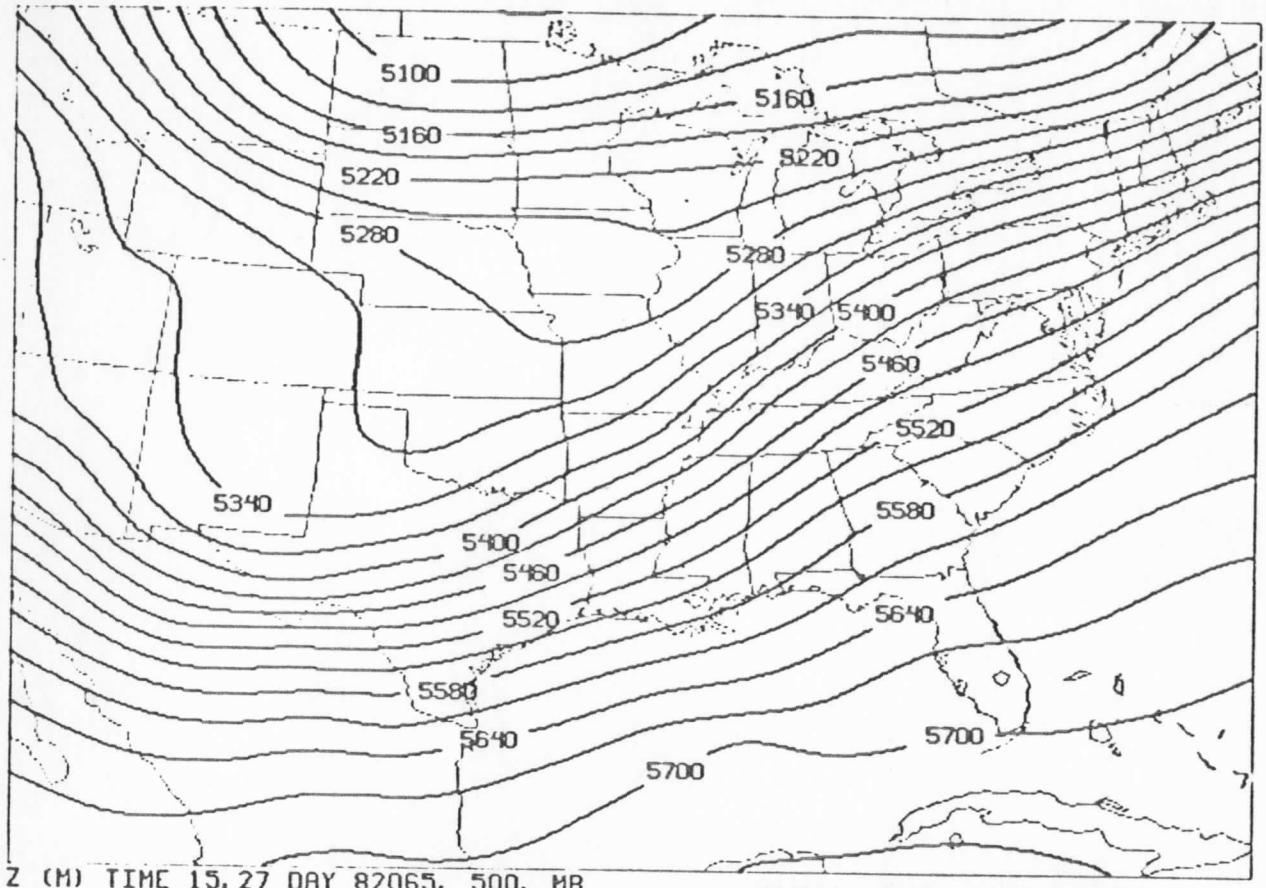
5100
5160
5160
5220
5220
5280
5280
5340
5340
5400
5400
5460
5460
5520
5520
5580
5580
5640
5640
5700
5700
Z (M) TIME 15.27 DAY 82065. 500. MB
THIK VASG ANAL SEQ2

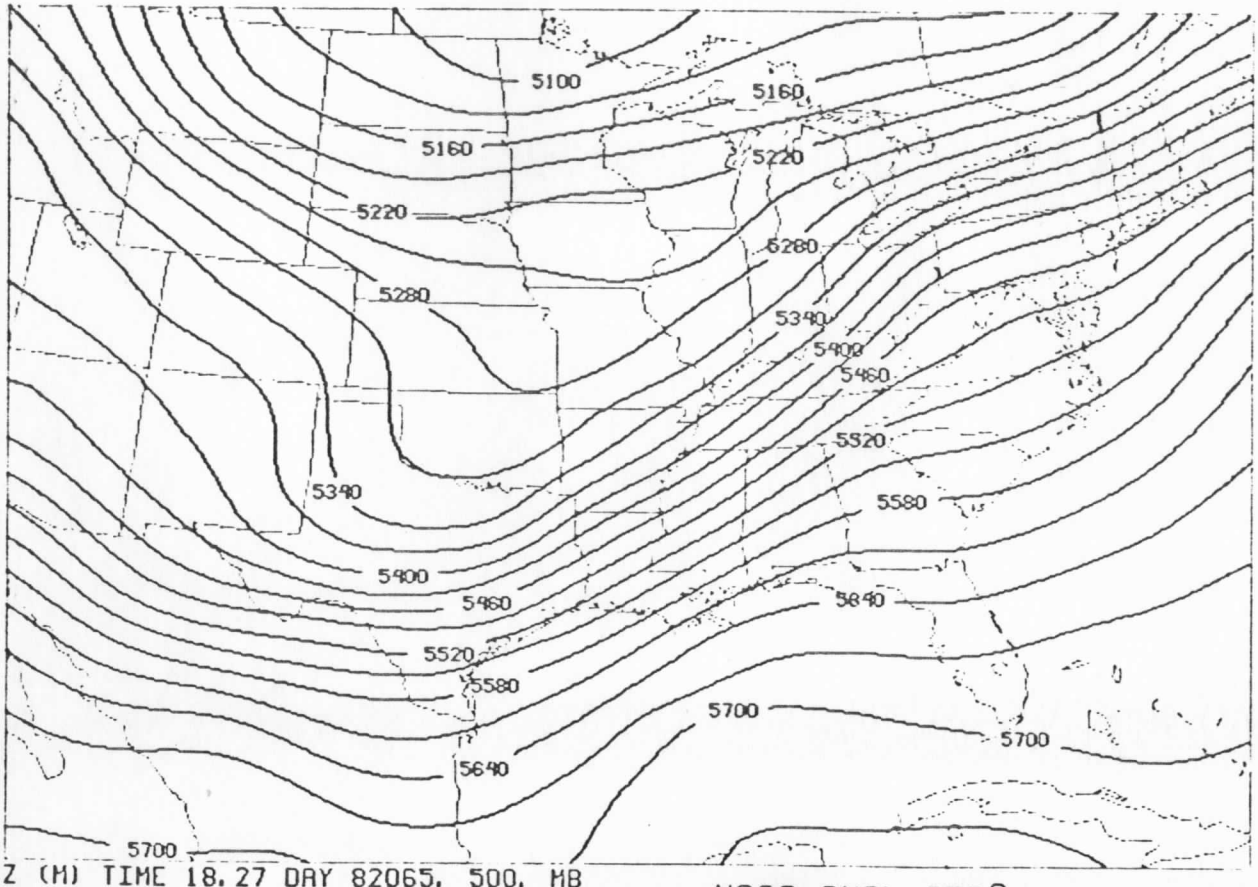
5100
5160
5160
5220
5220
5280
5280
5340
5340
5400
5400
5460
5460
5520
5520
5580
5580
5640
5640
5700
5700
5700
Z (M) TIME 18.27 DAY 82065. 500. MB
VASG ANAL SEQ2

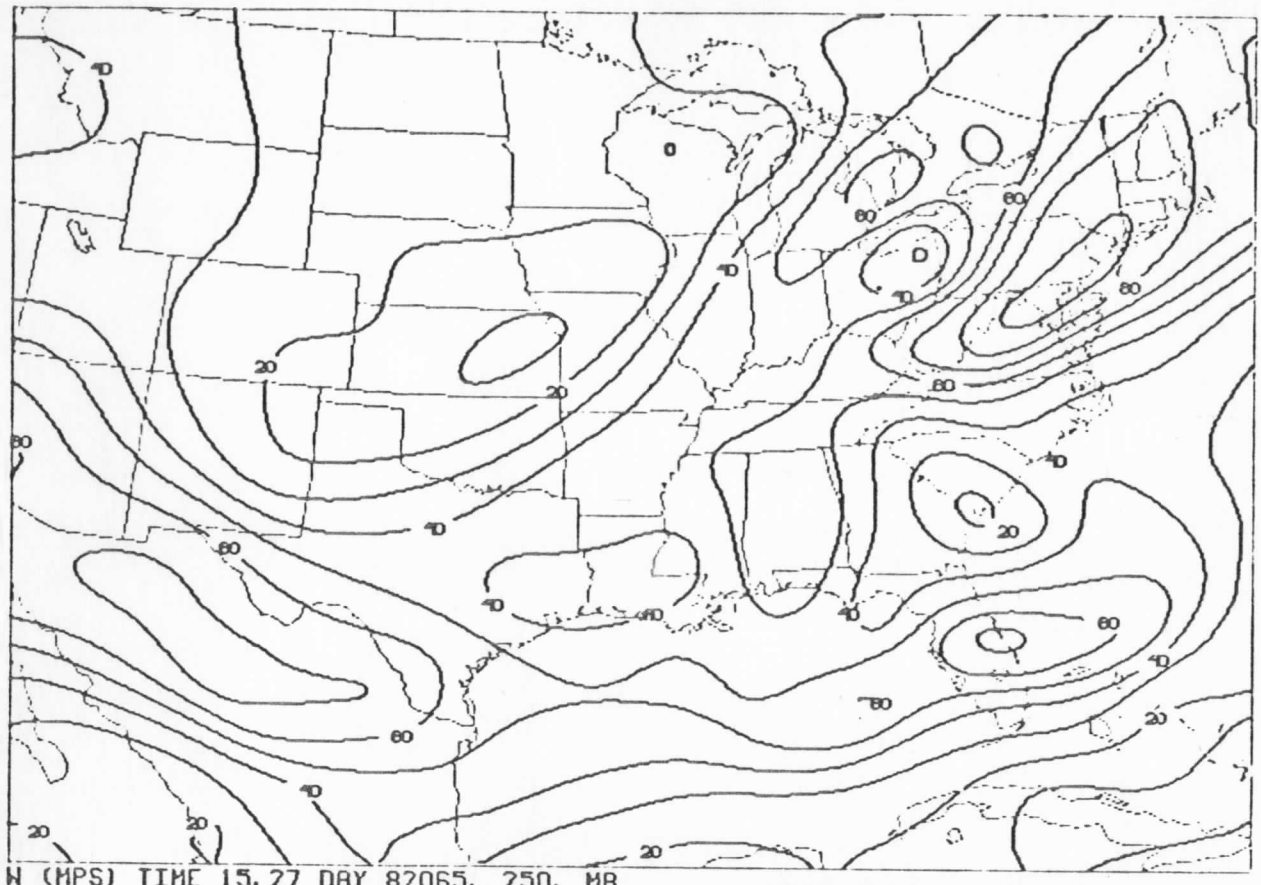
W (MPS) TIME 15.27 DAY 82065. 250. MB
VAST ANAL SEQ2


W (MPS) TIME 18.27 DAY 82065. 250. MB
VAST ANAL SEQ2

Fig 2.8

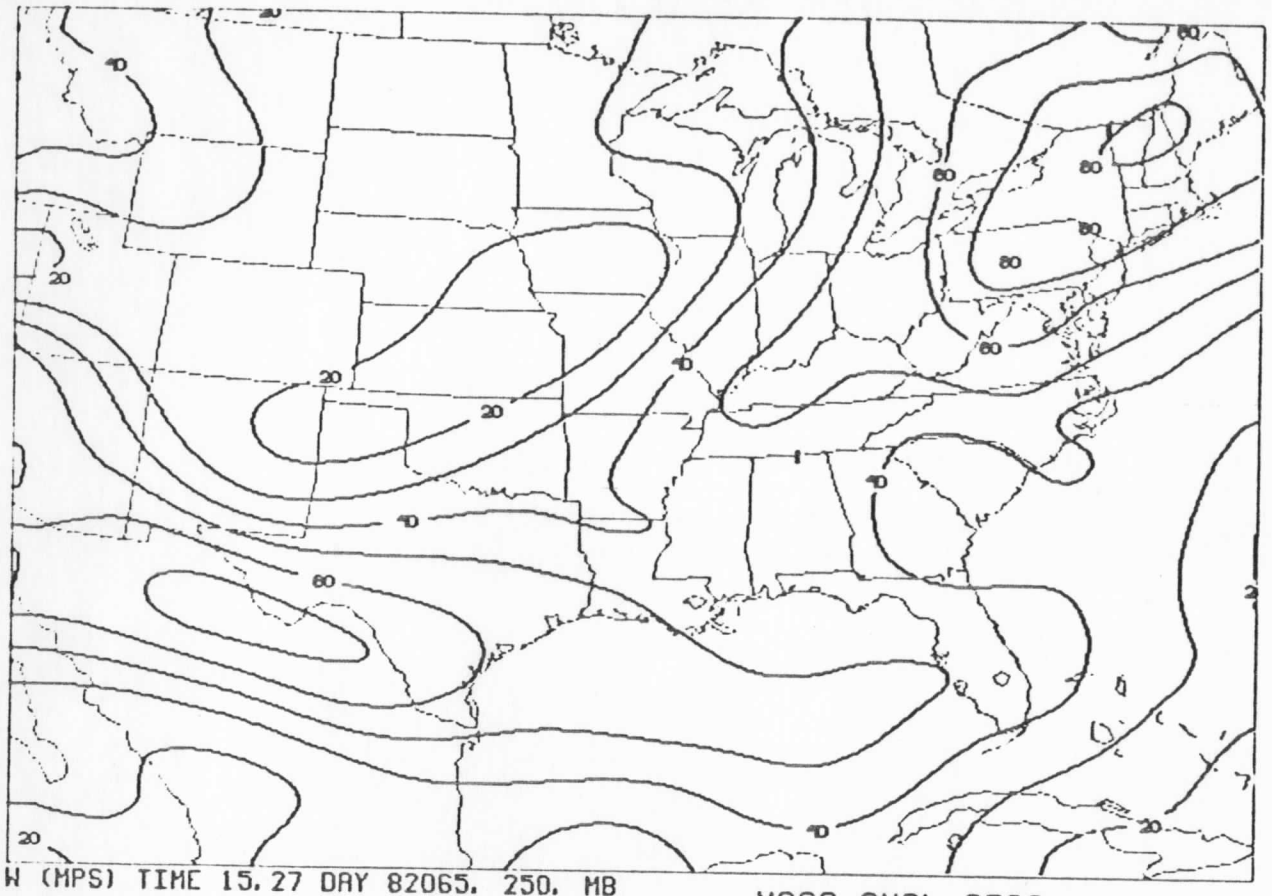
W (MPS) TIME 15.27 DAY 82065. 250. MB
VASG ANAL SEQ2

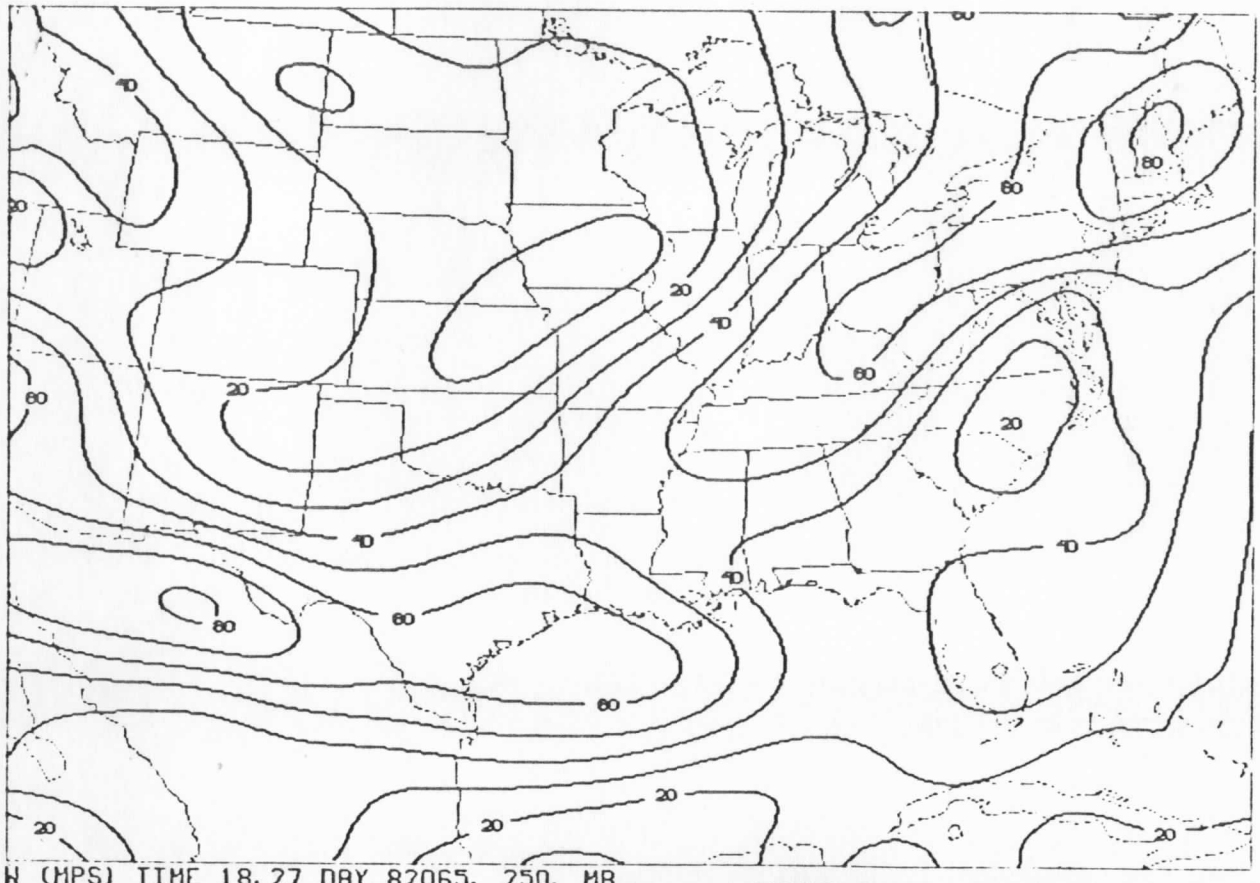
W (MPS) TIME 18.27 DAY 82065. 250. MB
VASG ANAL SEQ2

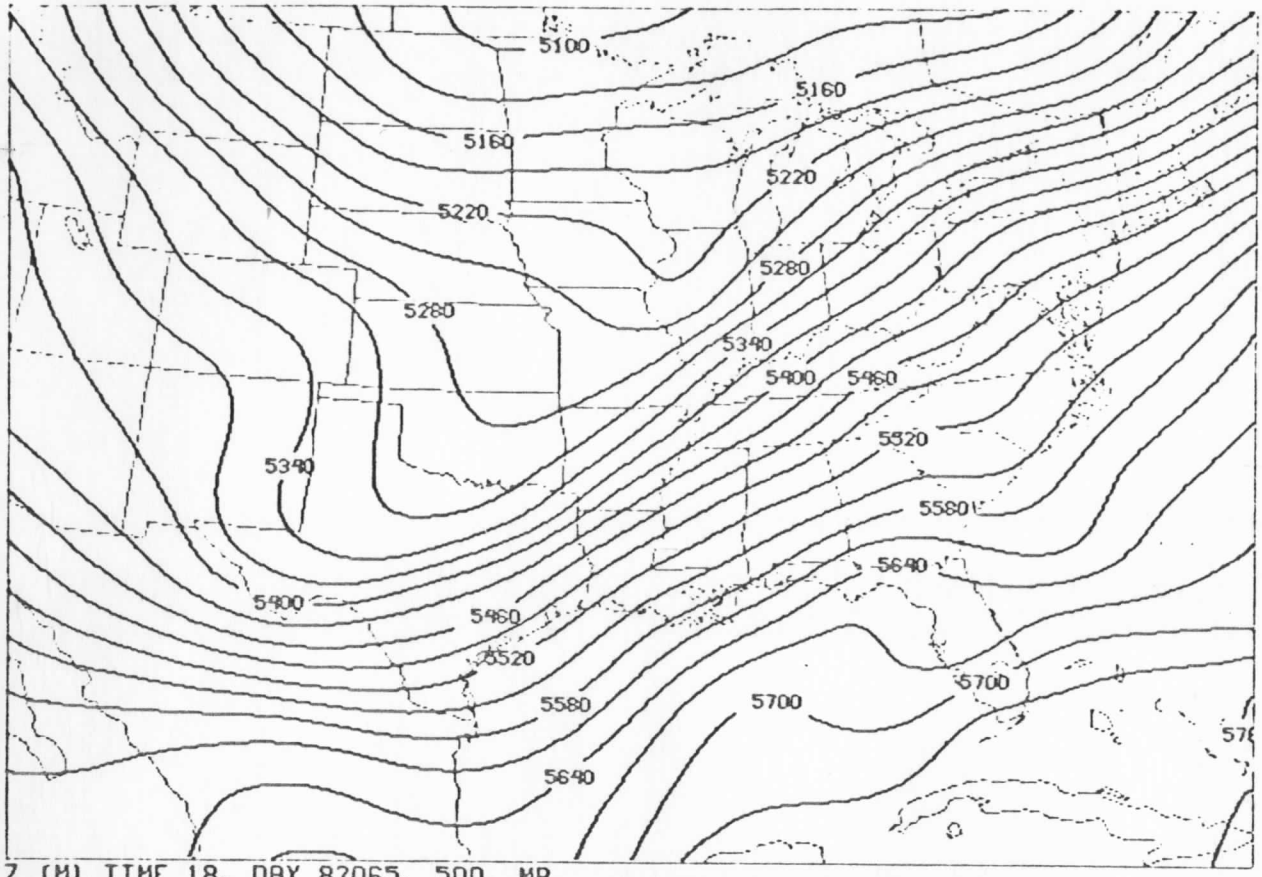

Z (M) TIME 18. DAY 82065. 500. MB THIK VAST ANAL SEQ3

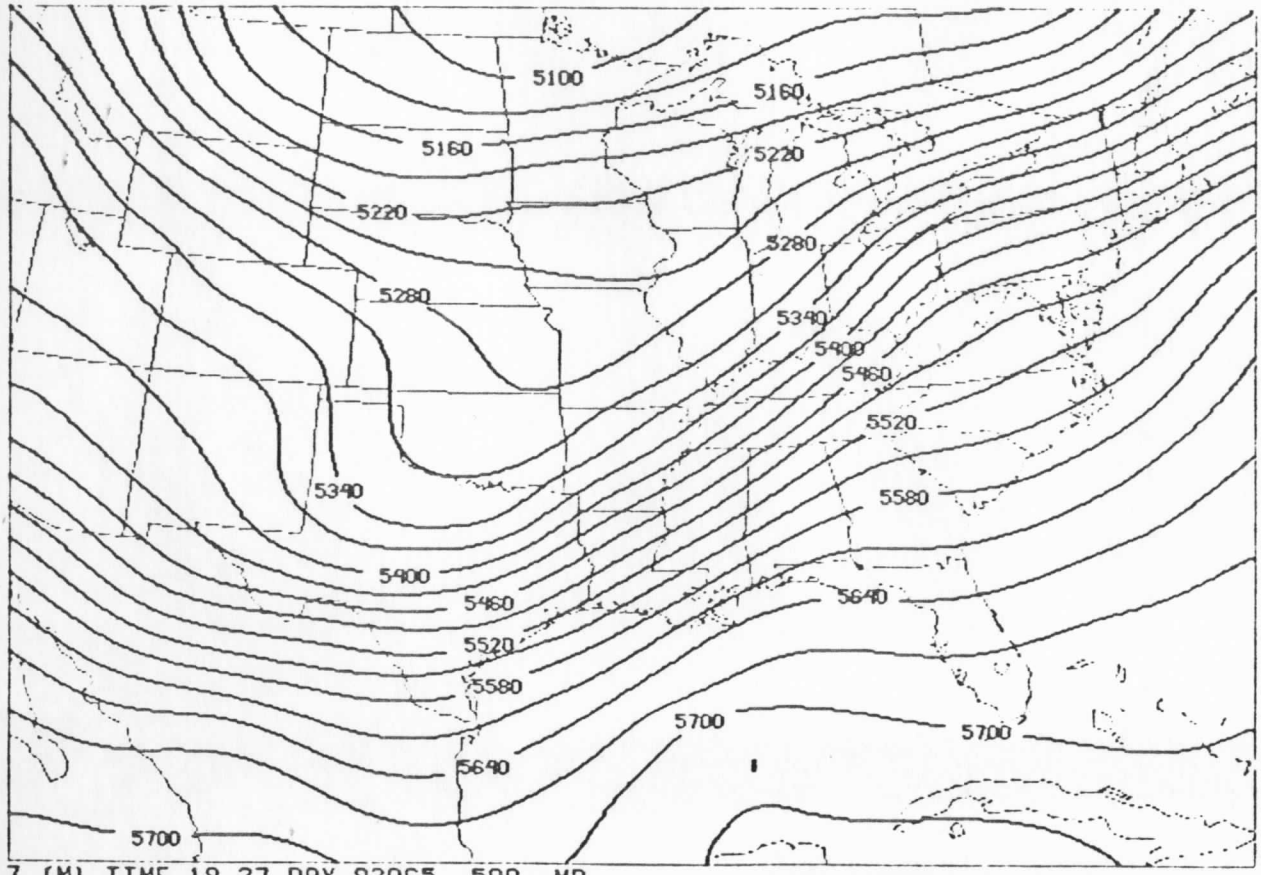

Z (M) TIME 18.27 DAY 82065. 500. MB VASG ANAL SEQ3

THIK

Fig 2.10

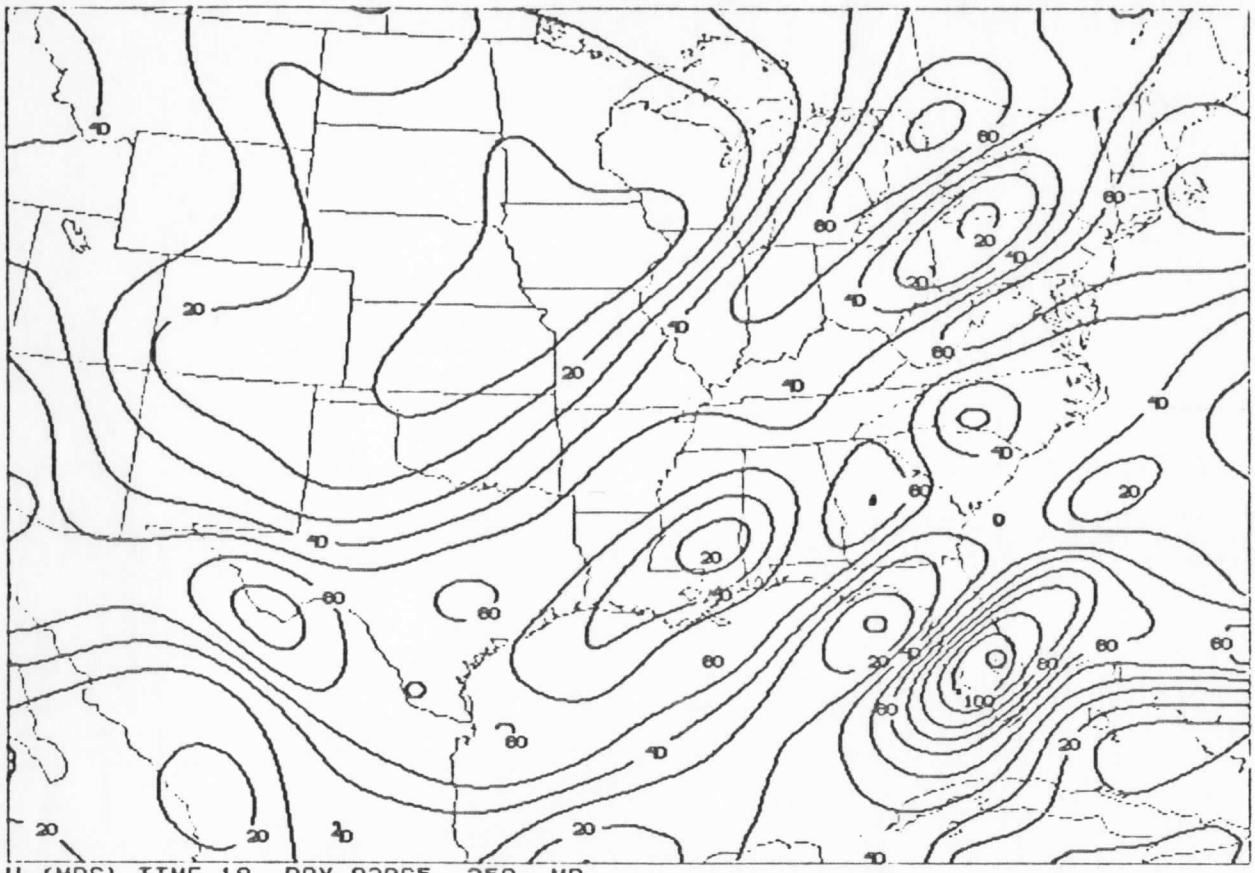
W (MPS) TIME 18. DAY 82065. 250. MB
VAST ANAL SEQ3

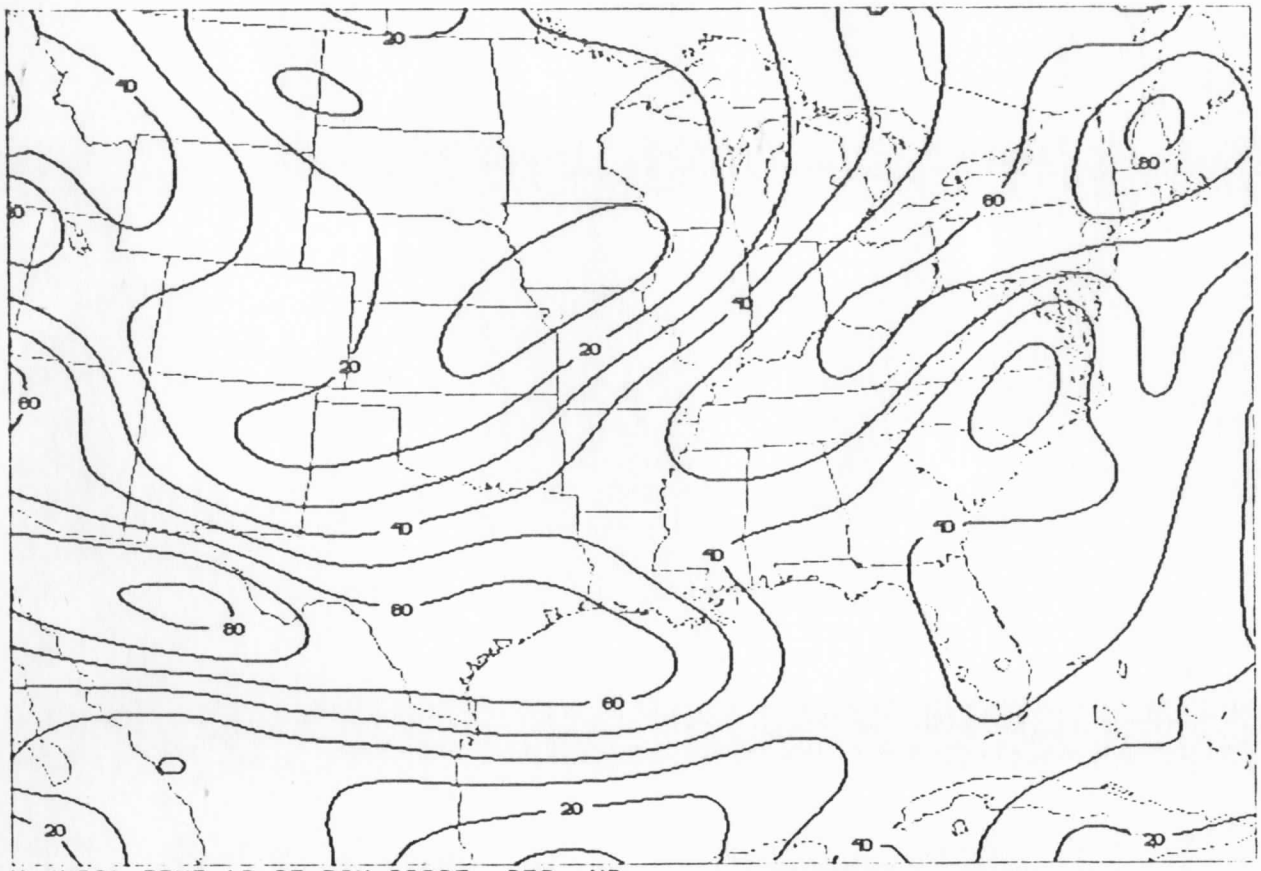
W (MPS) TIME 18.27 DAY 82065. 250. MB
VASG ANAL SEQ3

Fig. 3.1

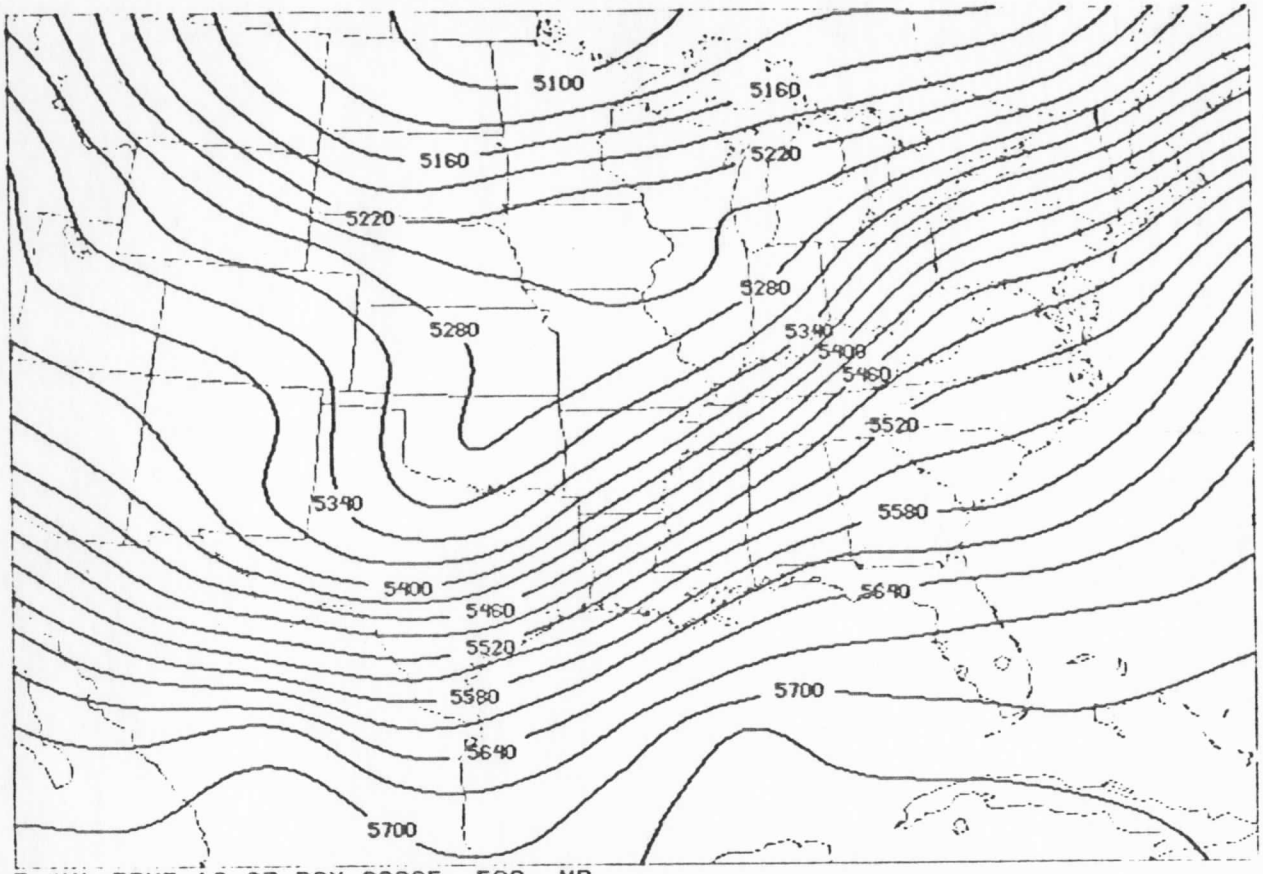

Z (M) TIME 18.27 DAY 82065. 500. MB

THIK VASG ANAL SEQ4

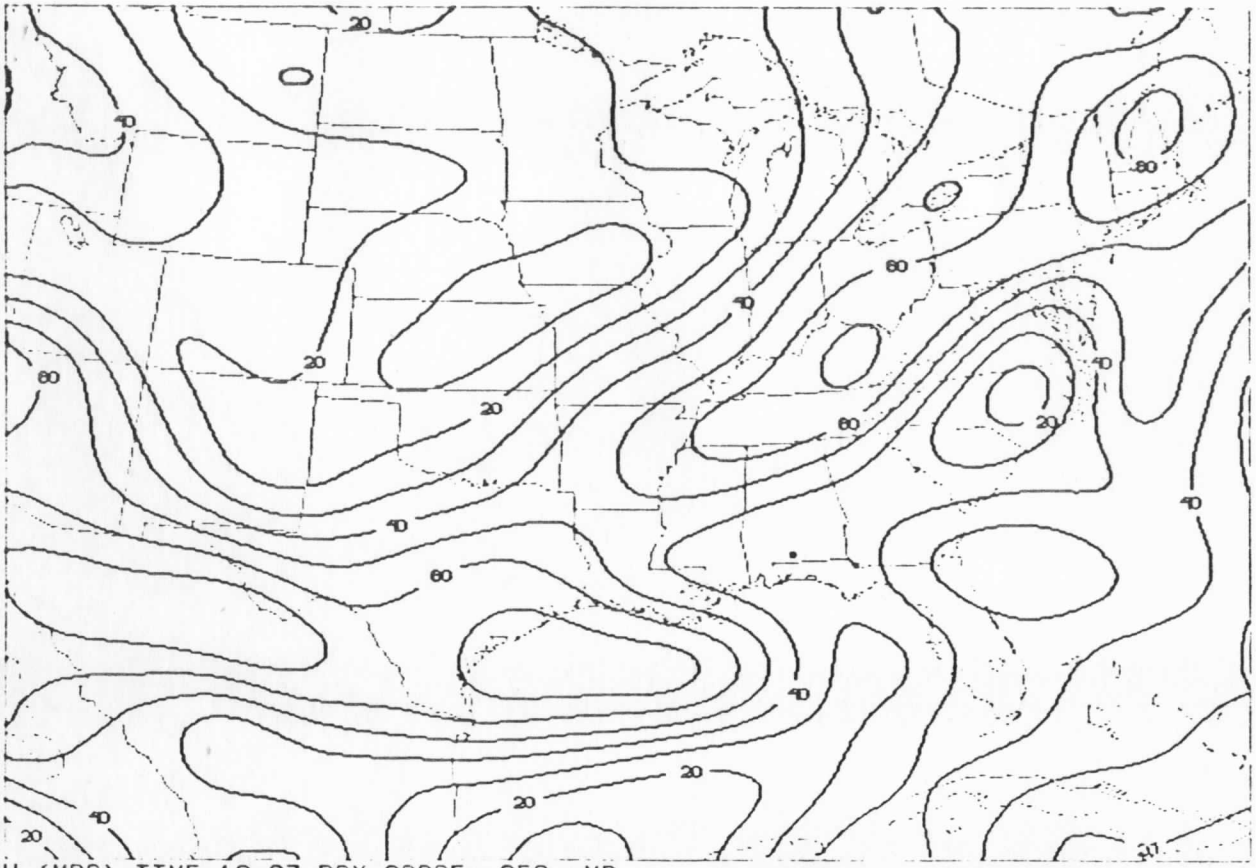

W (MPS) TIME 18.27 DAY 82065. 250. MB

VASG ANAL SEQ4

FIG 2.13

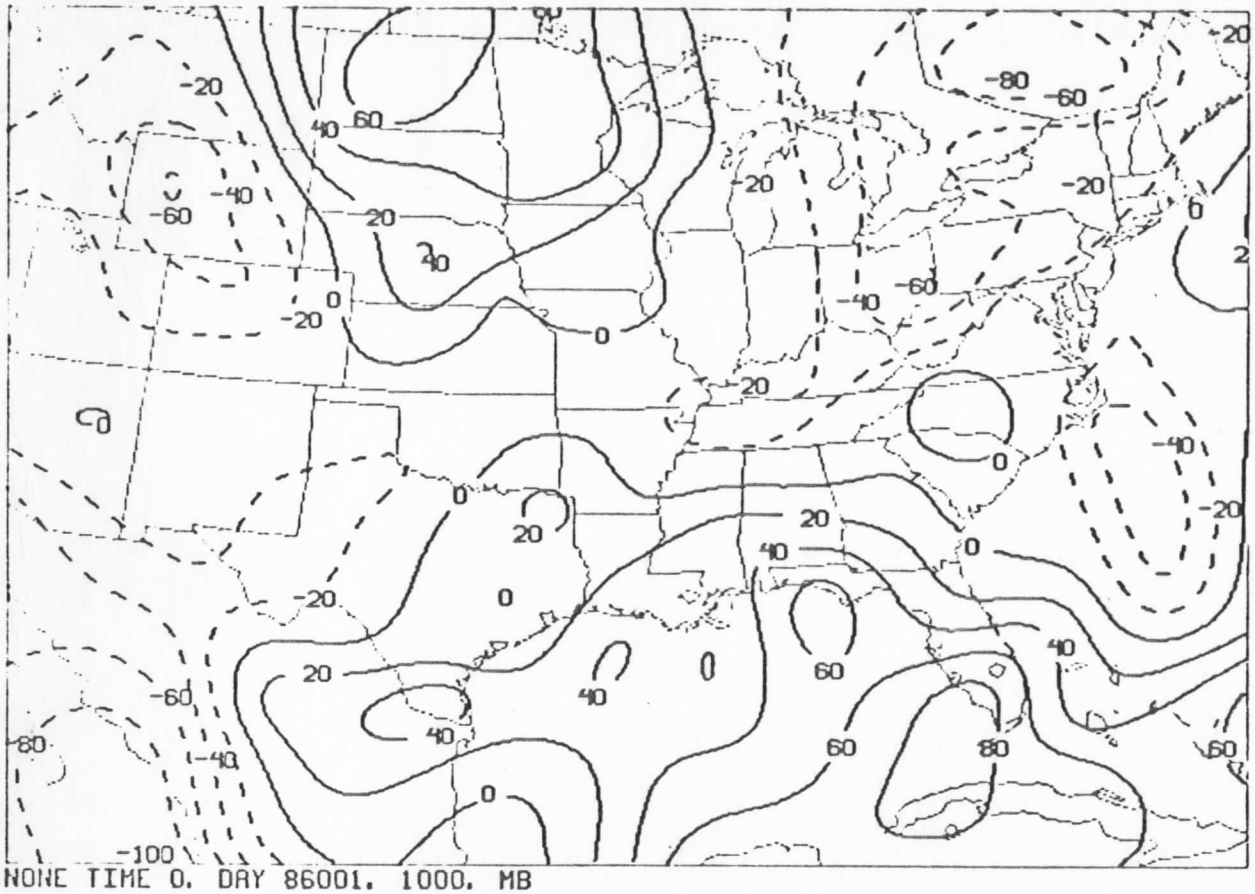

VAST SEQ3

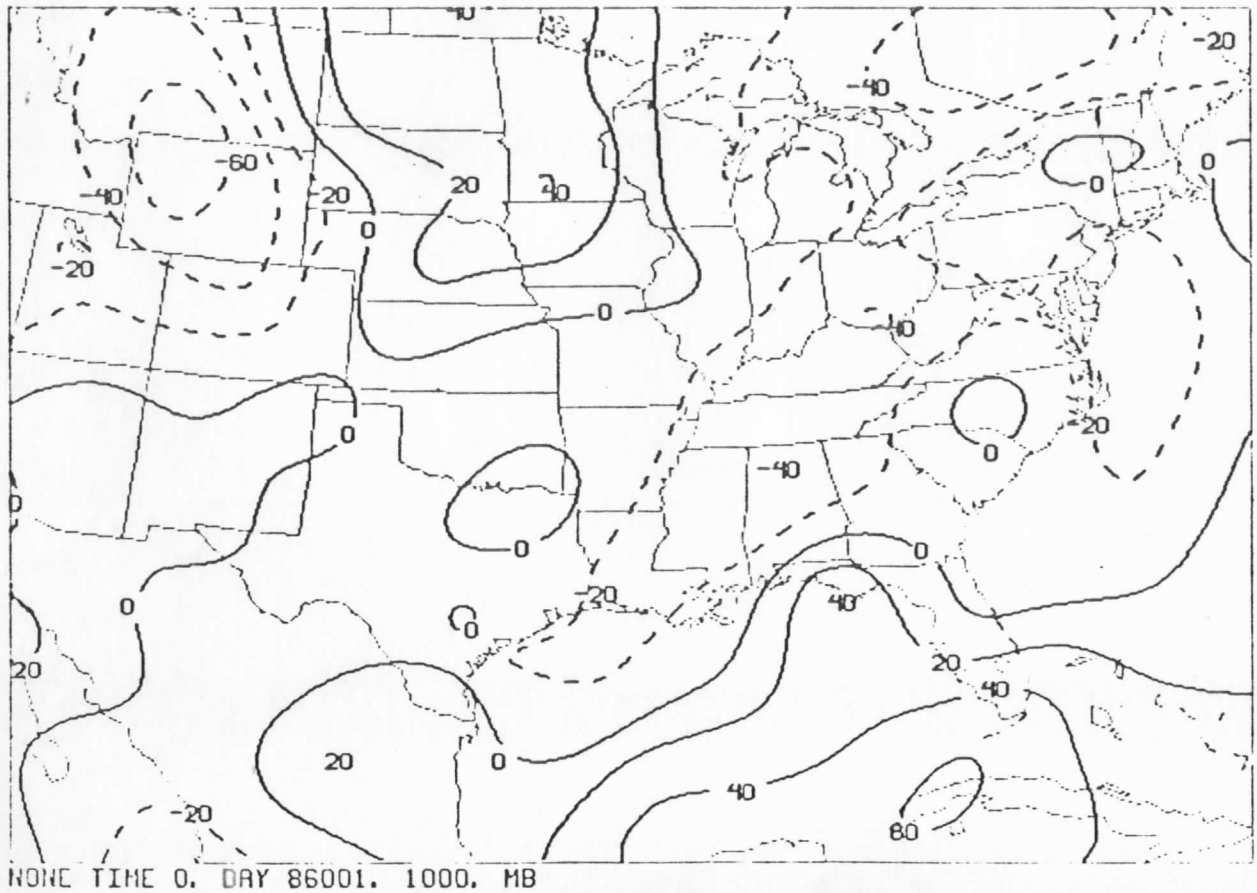

VASG SEQ3

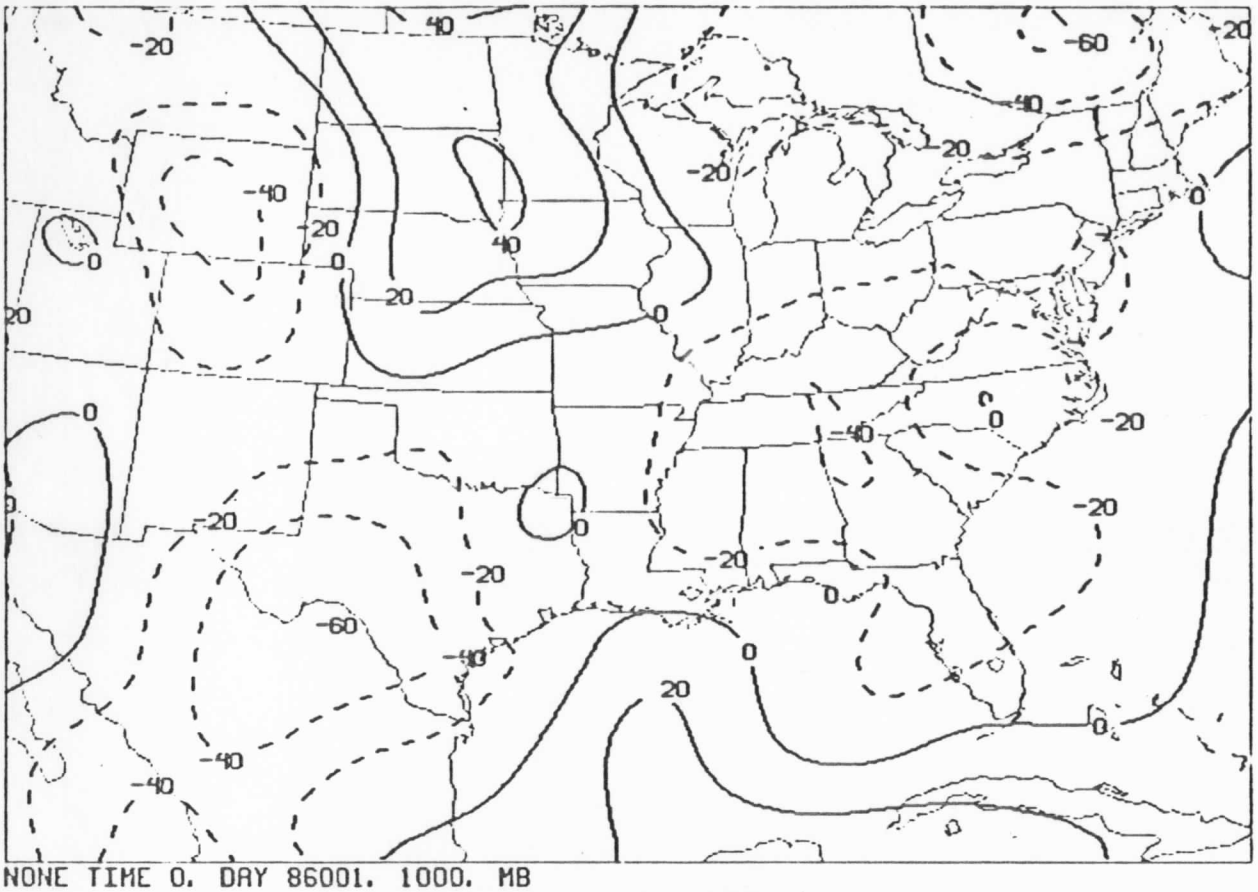

CONTROL

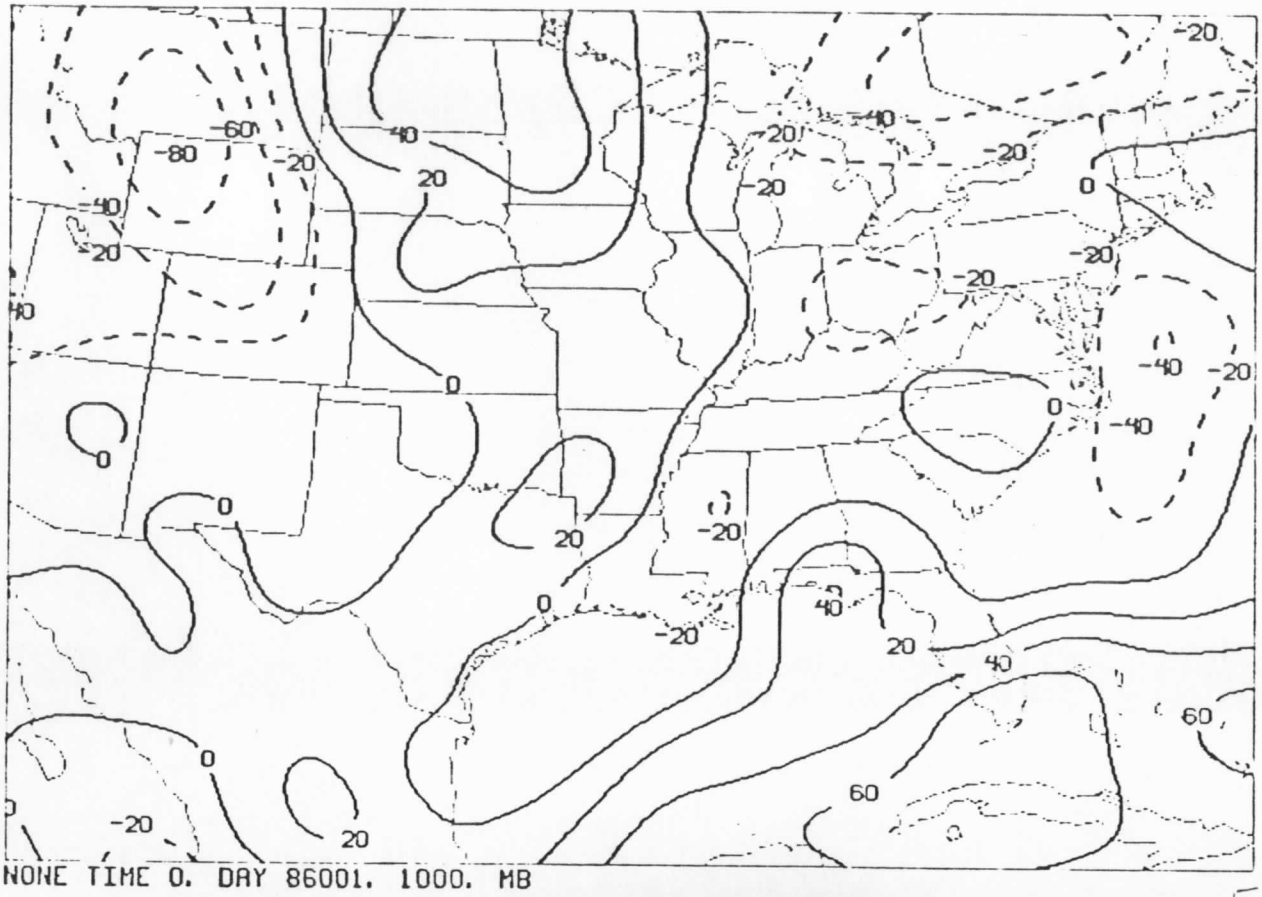

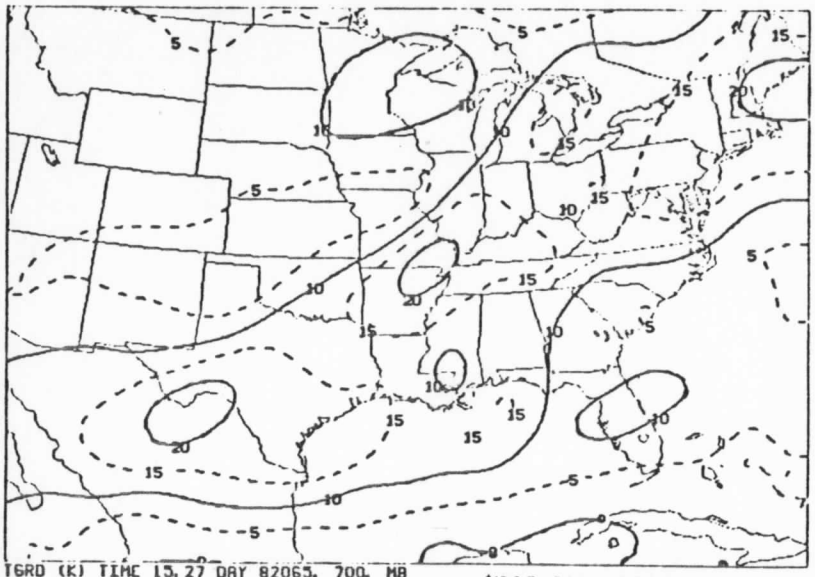
TGRD (K) TIME 15.27 DAY 82065. 700. MB
VAST ANAL SEQ2

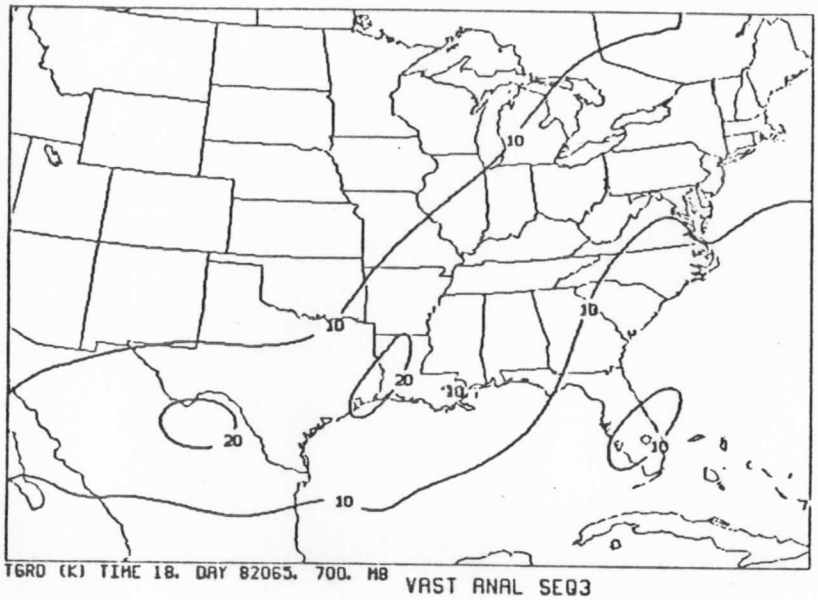
TGRD (K) TIME 18. DAY 82065. 700. MB
VAST ANAL SEQ3

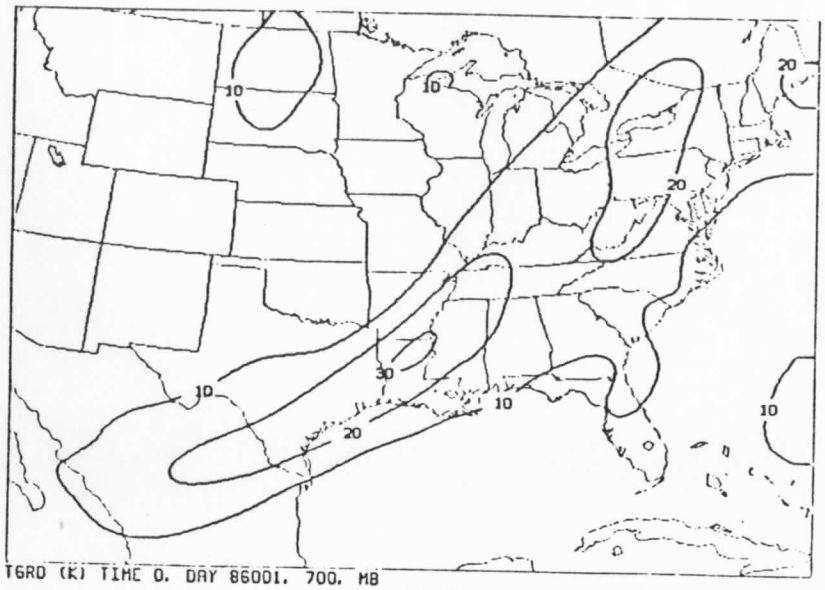
TGRD (K) TIME 0. DAY 86001. 700. MB
VAST 6HR PROG VTOOZ SEQ3

Fig 2.15

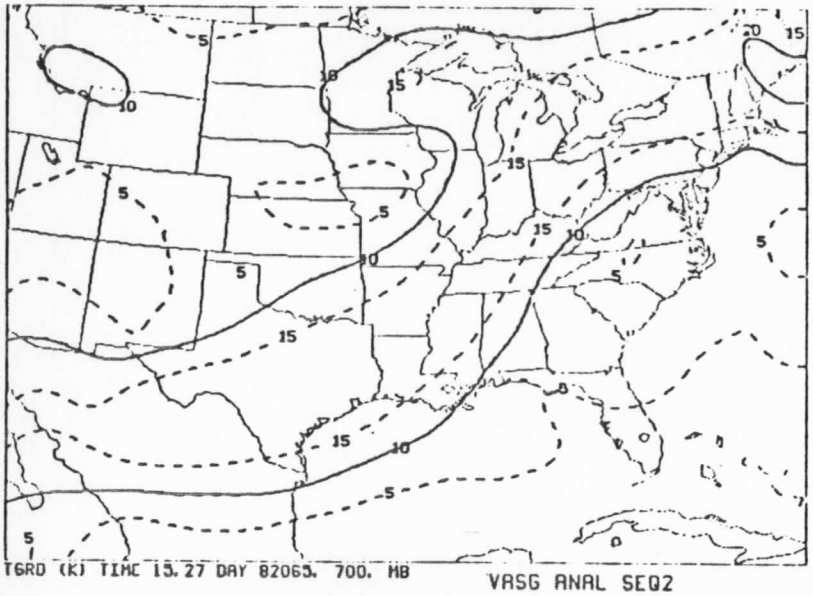

VASG ANAL SEQ2

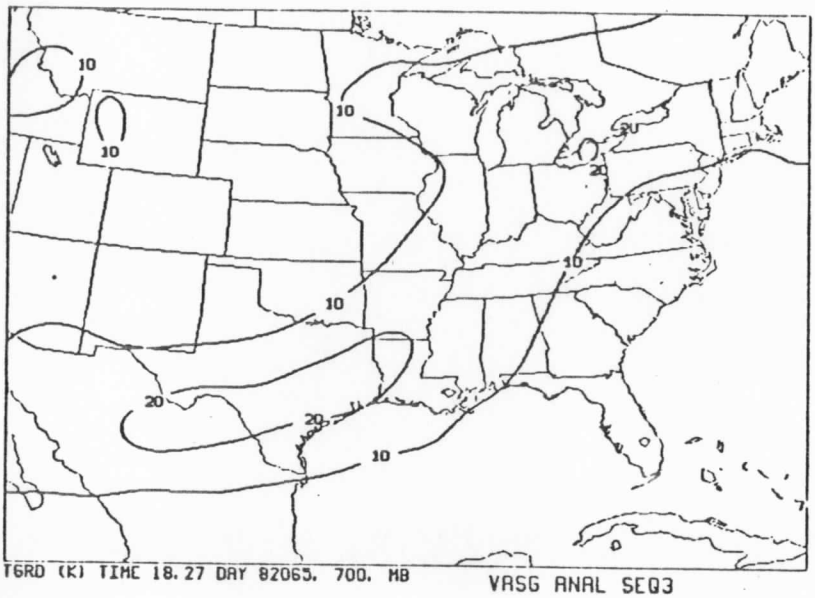

VASG ANAL SEQ3

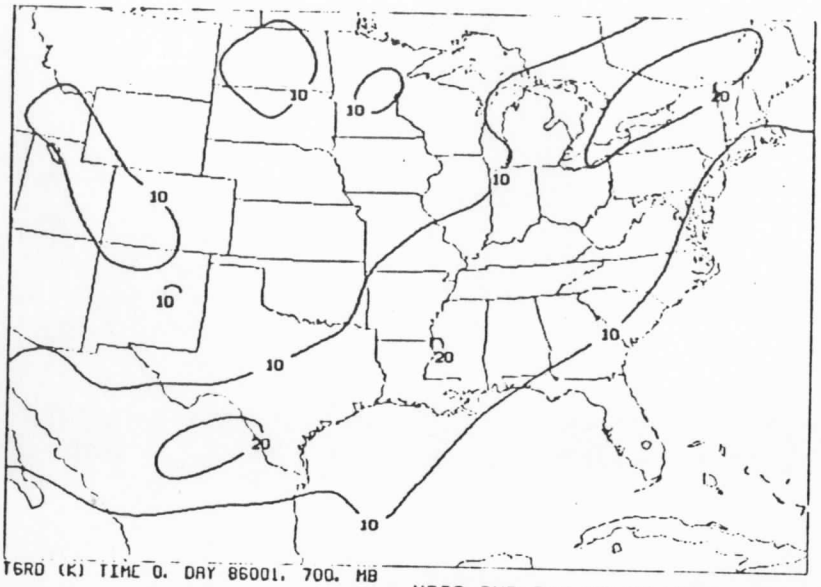

VASG 6HR INC VTOOZ SEQ3

Fig. 16

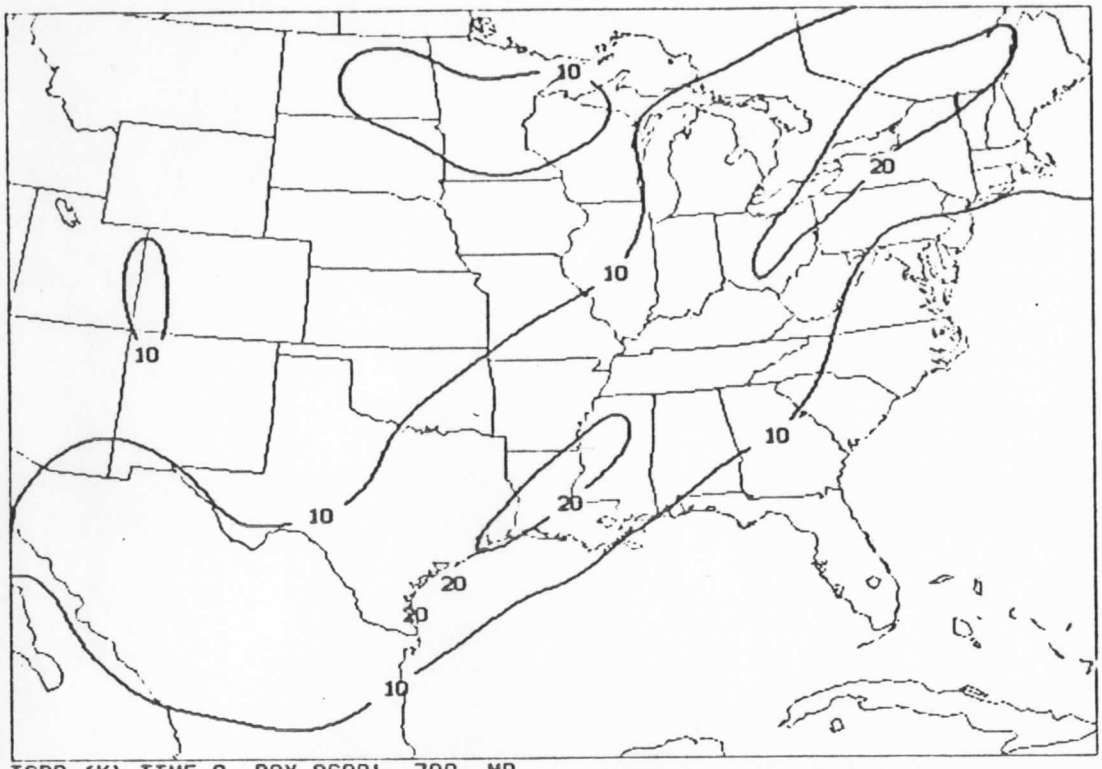

TGRD (K) TIME 0. DAY 86001. 700. MB

CONTROL 12HR PROG VALID 00Z

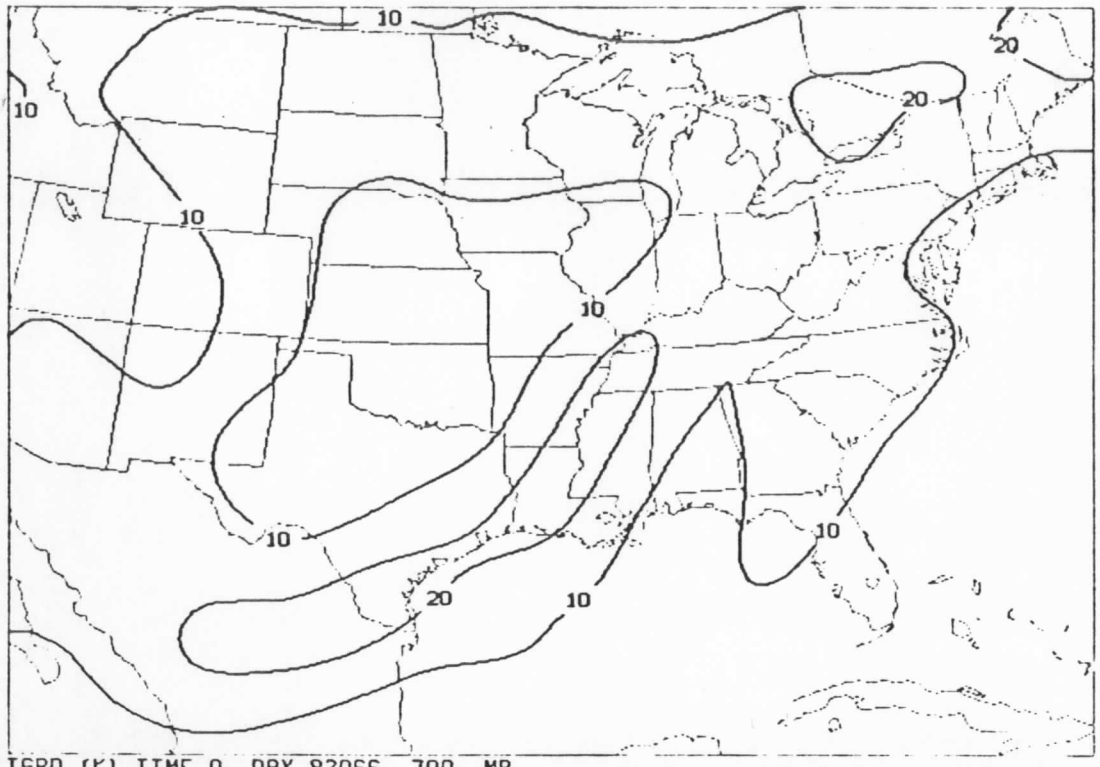

TGRD (K) TIME 0. DAY 82066. 700. MB

00Z RS VERIF ANALYSIS

Fig. 17

Mean Sea Level Pressure

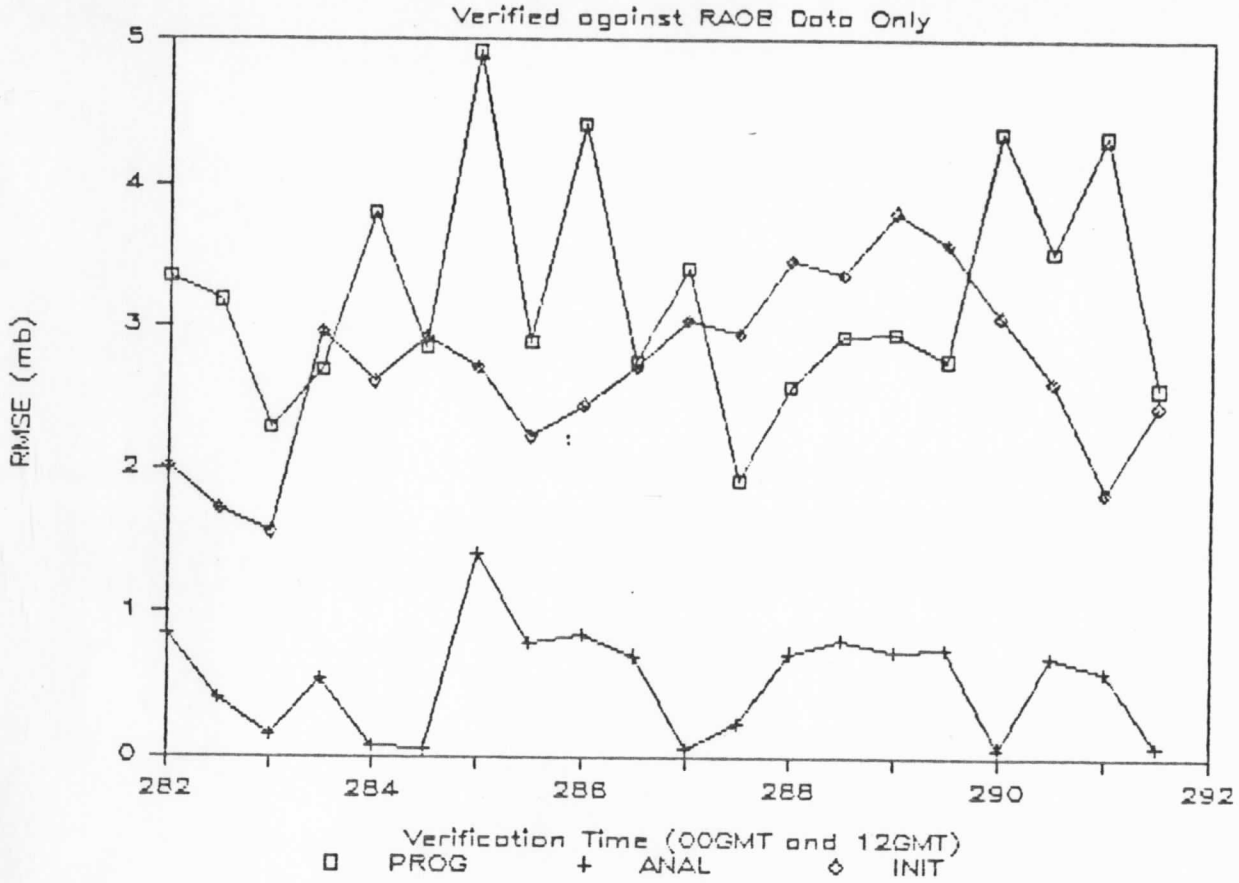

1000–500 mb Thickness

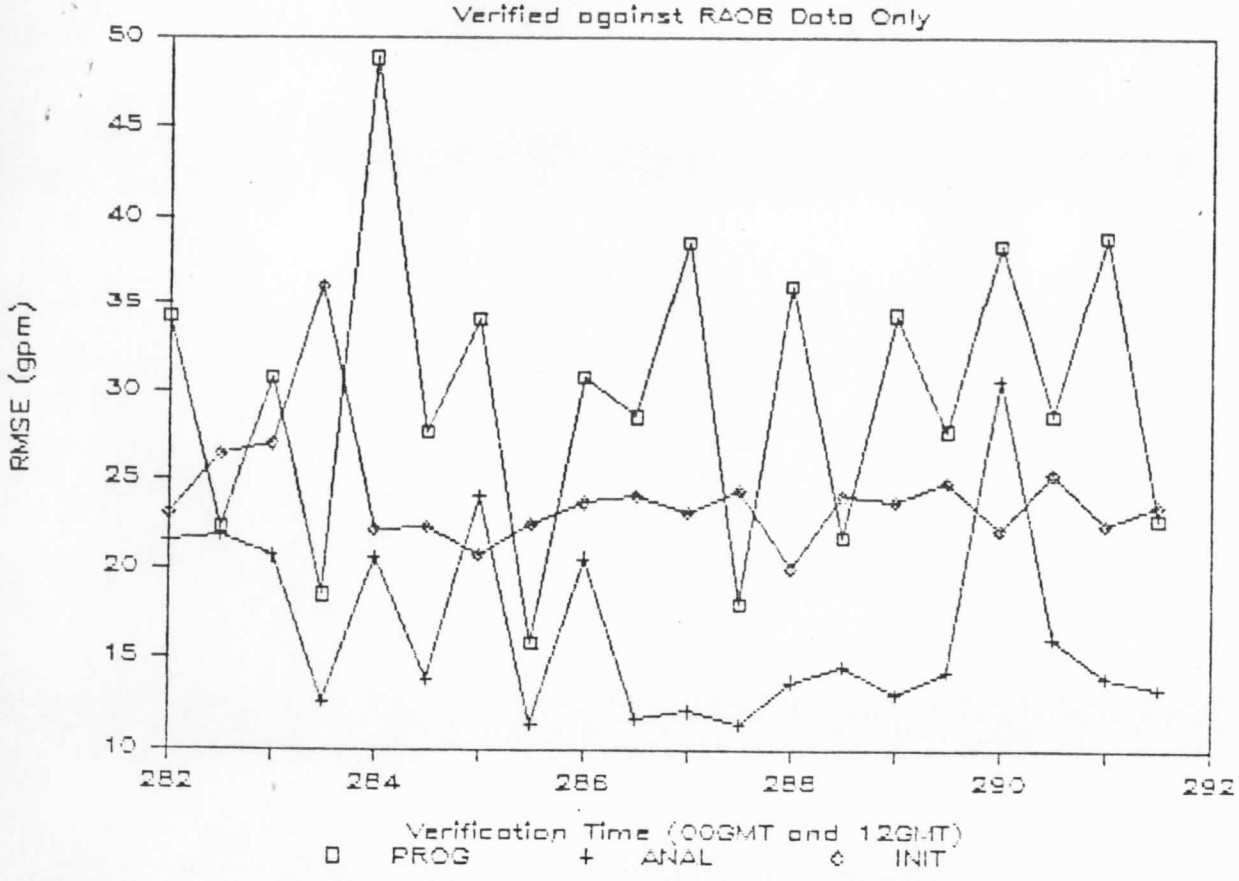

Fig. 9

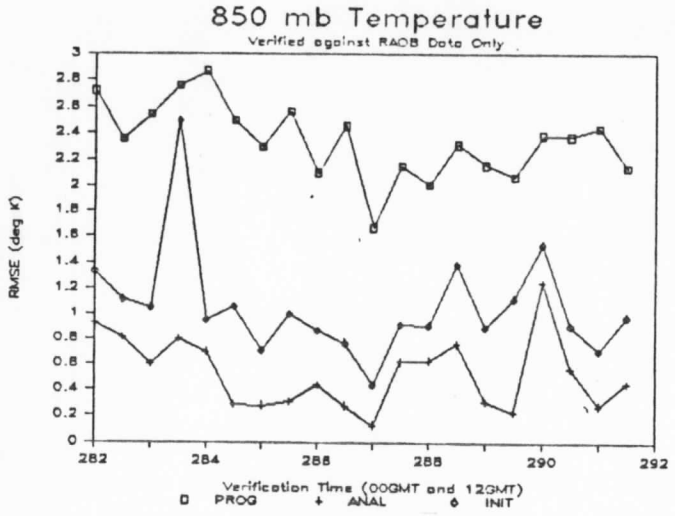
850 mb Temperature
Verified against RAOB Data Only
RMSE (deg K)
Verification Time (00GMT and 12GMT)
PROG
ANAL
INIT

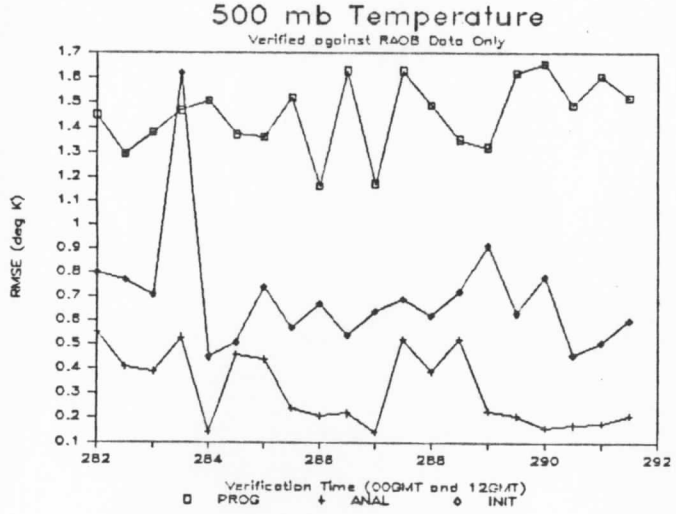
500 mb Temperature
Verified against RAOB Data Only
RMSE (deg K)
Verification Time (00GMT and 12GMT)
PROG
ANAL
INIT

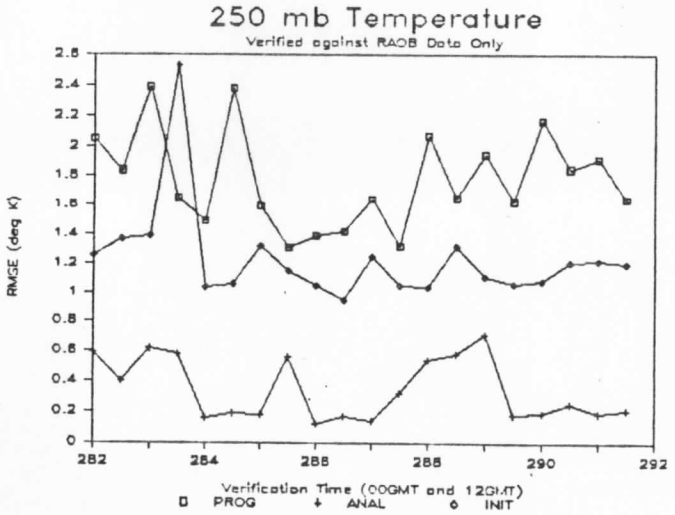
250 mb Temperature
Verified against RAOB Data Only
RMSE (deg K)
Verification Time (00GMT and 12GMT)
PROG
ANAL
INIT

Fig 2.19

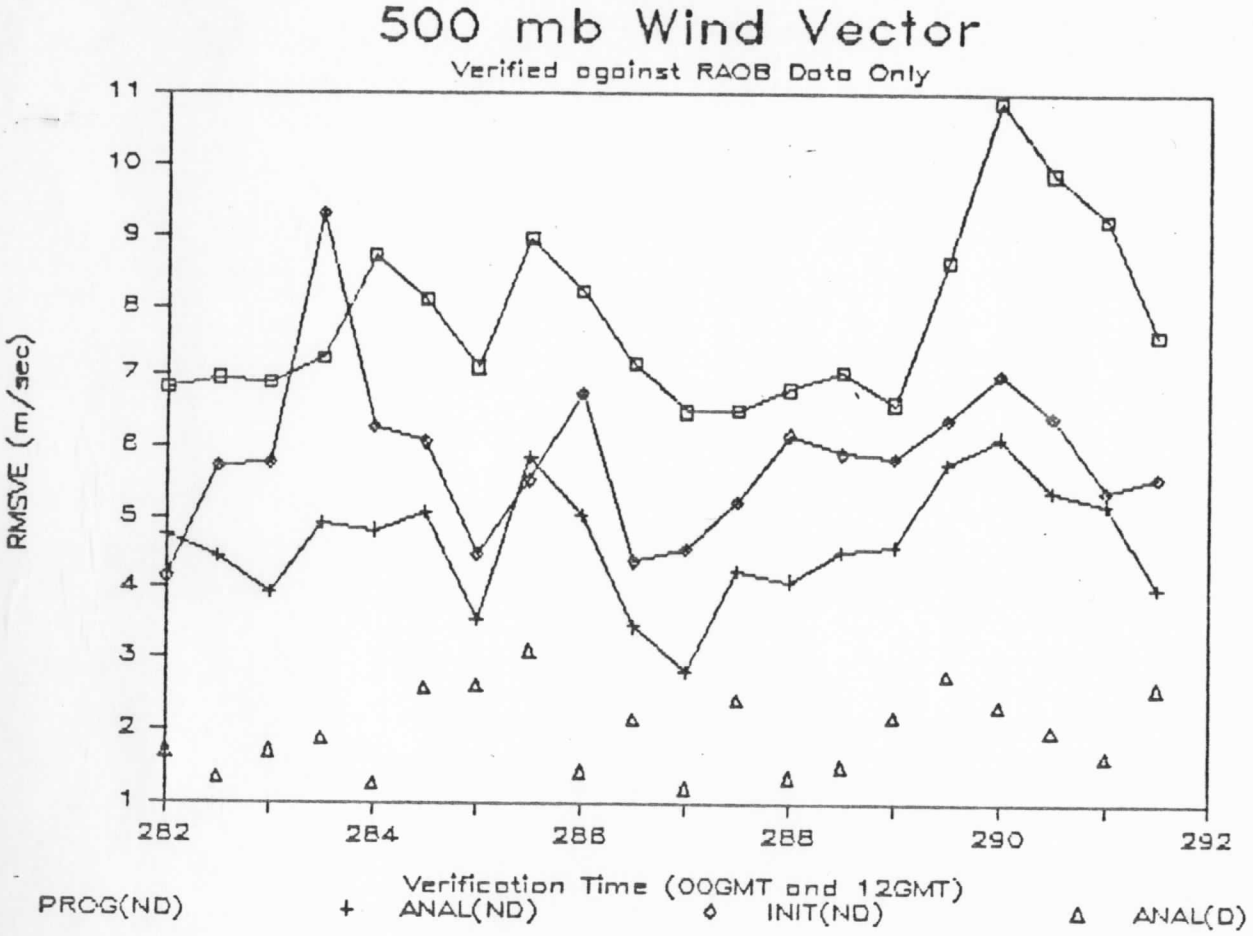
500 mb Wind Vector
Verified against RAOB Data Only
RMSVE (m/sec)
11
10
9
8
7
6
5
4
3
2
1
282
284
286
288
290
292
Verification Time (00GMT and 12GMT)
PROG(ND)
ANAL(ND)
INIT(ND)
ANAL(D)

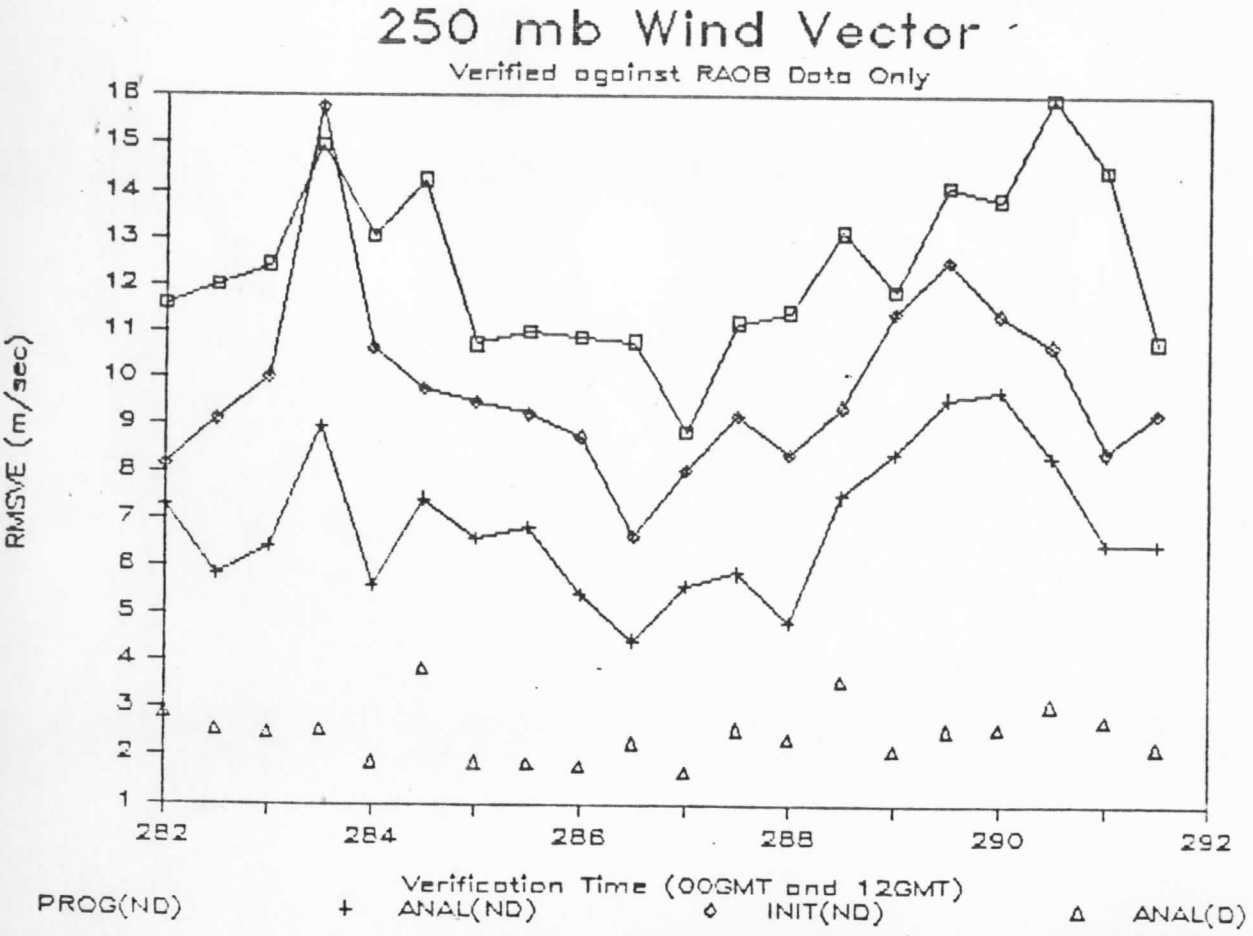
250 mb Wind Vector
Verified against RAOB Data Only
RMSVE (m/sec)
16
15
14
13
12
11
10
9
8
7
6
5
4
3
2
1
282
284
286
288
290
292
Verification Time (00GMT and 12GMT)
PROG(ND)
ANAL(ND)
INIT(ND)
ANAL(D)

FIG 2.2b

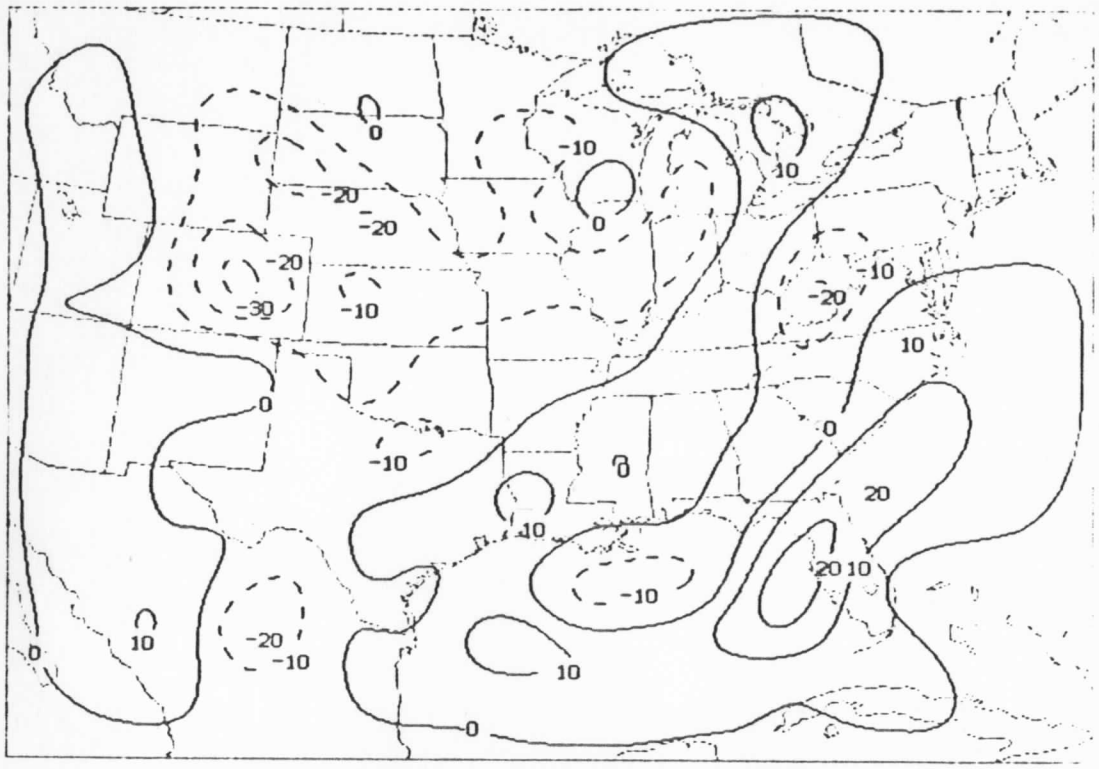

500MB PROG OMEGA VT 00GMT 10 OCT 11985

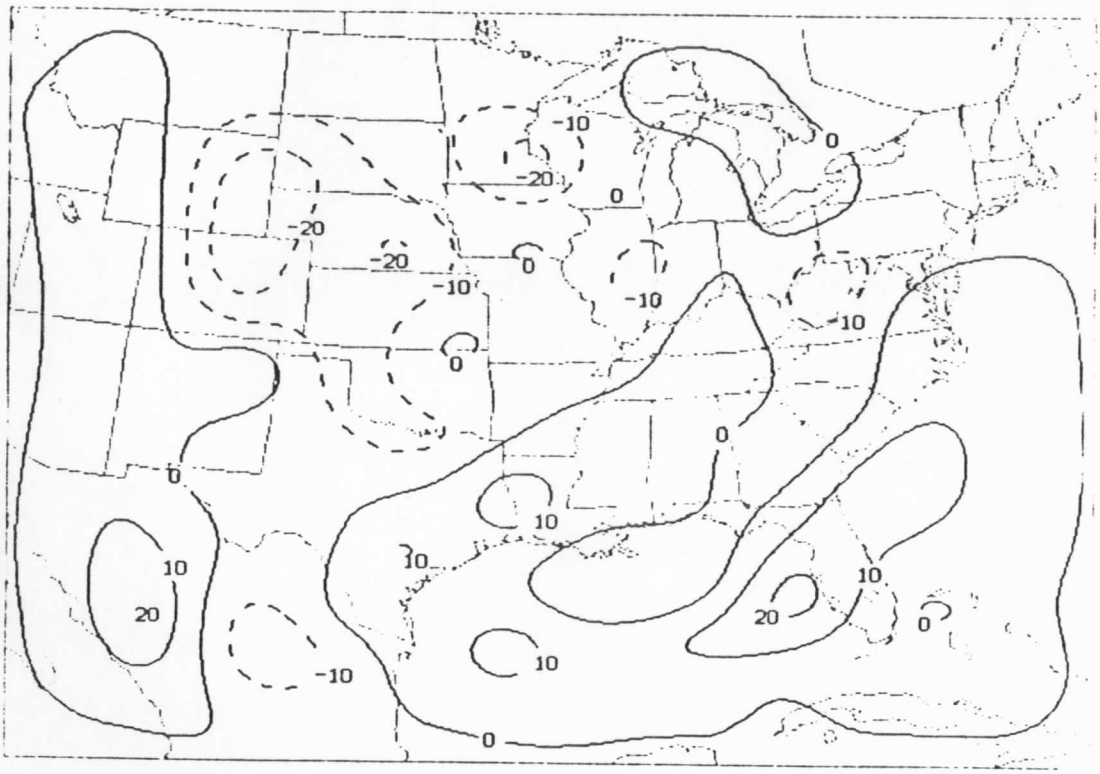

500MB INIT OMEGA VT 00GMT 10 OCT 1985

Fig 2.2

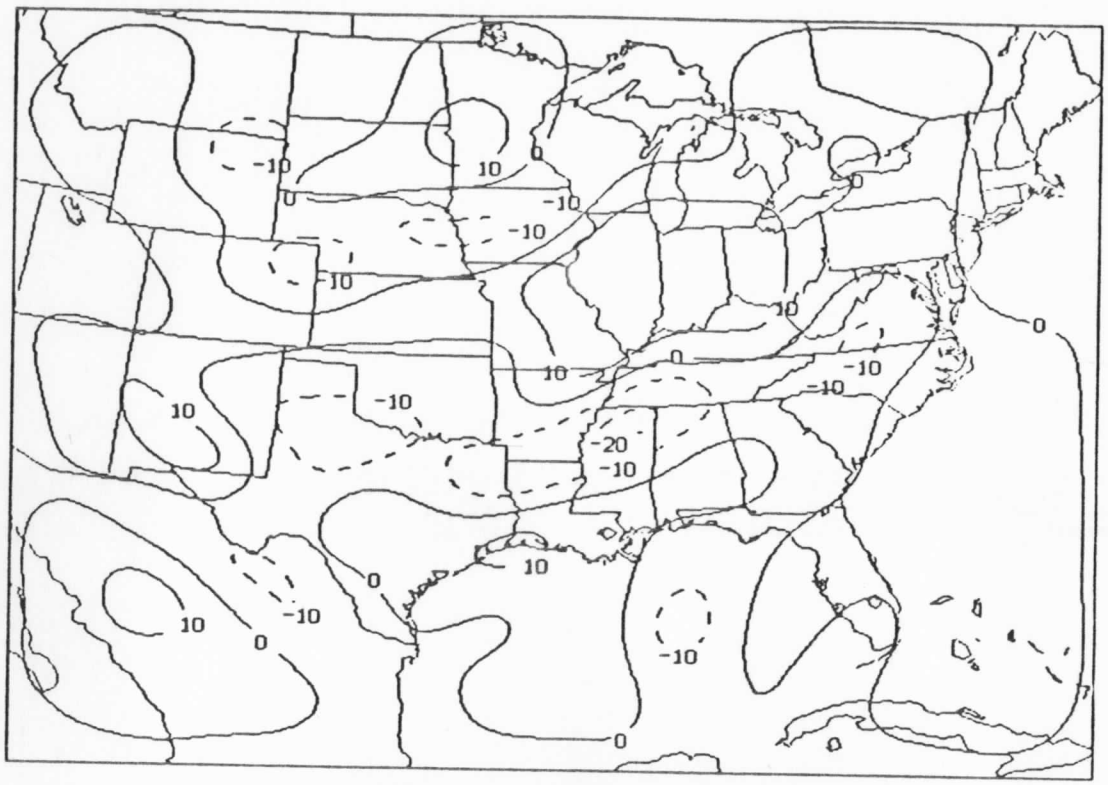

500MB PROG OMEGA VT 00GMT 16 OCT 1985

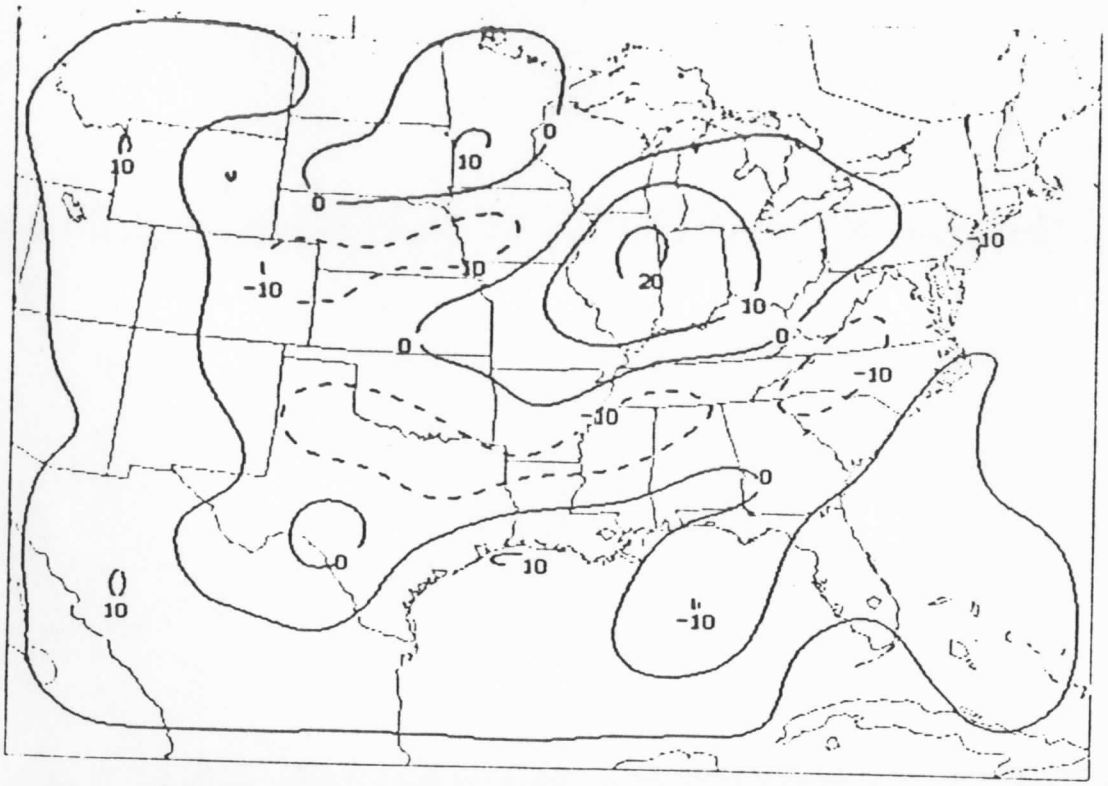

500MB INIT OMEGA VT 00GMT 16 OCT 1985

Fig. 1.22

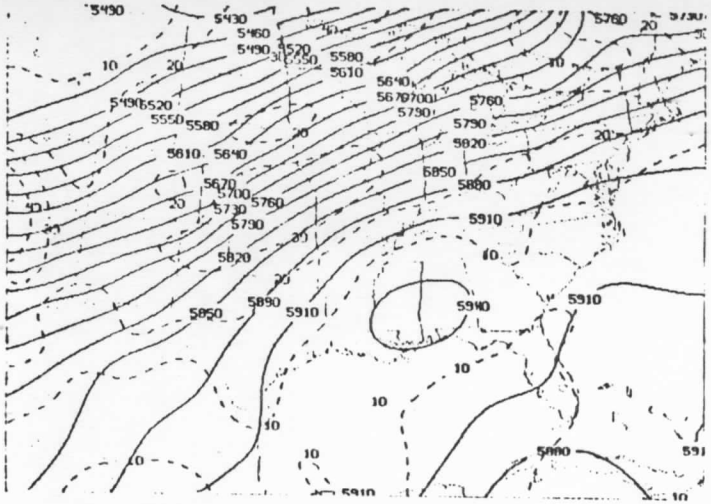

500MB HGHT/WIND ANAL 00GMT 09 OCT 1985

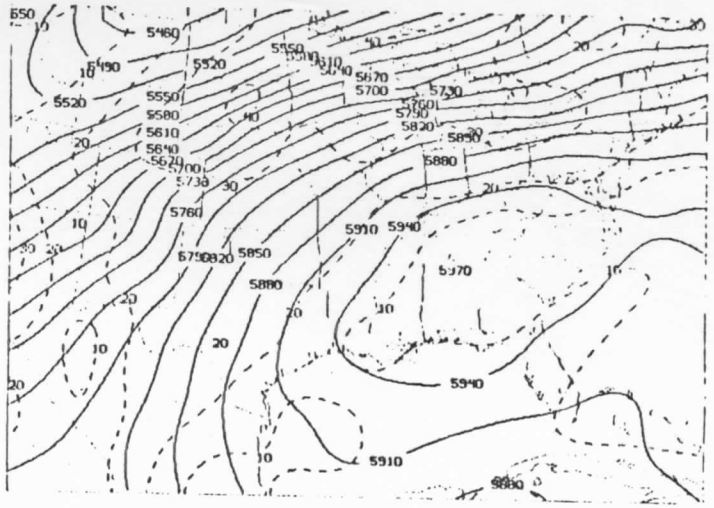

500MB HGHT/WIND ANAL 12GMT 09 OCT 1985

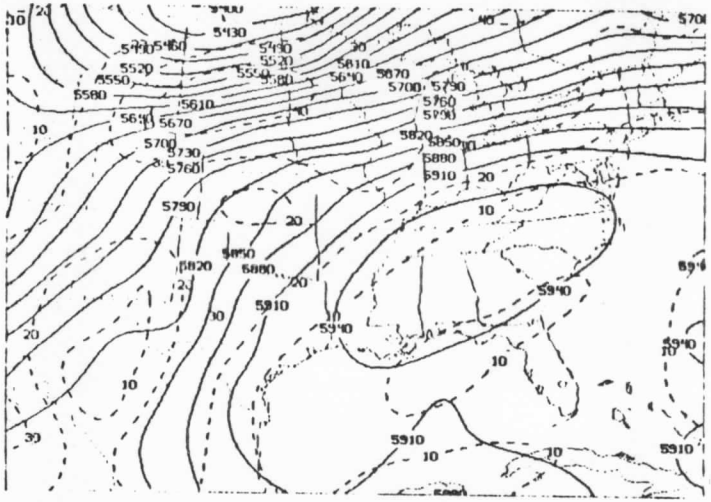

500MB ANAL HGHT/WIND 00GMT 10 OCT 1985

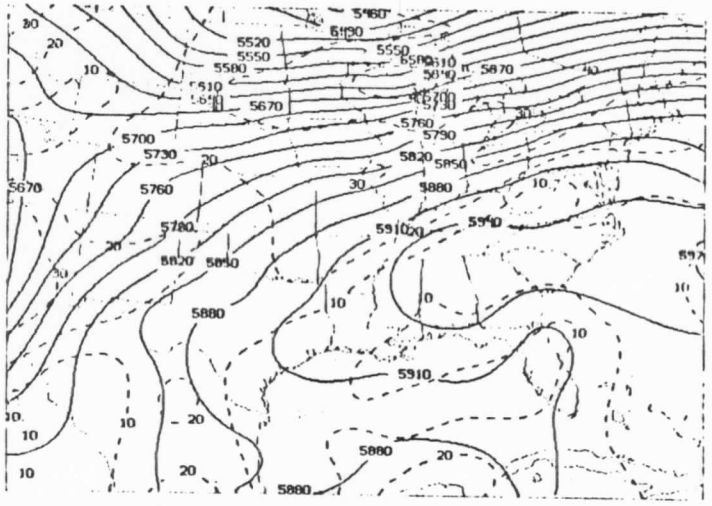

500MB HGHT/WIND ANAL 12GMT 10 OCT 1985

FIG 2.23(1)

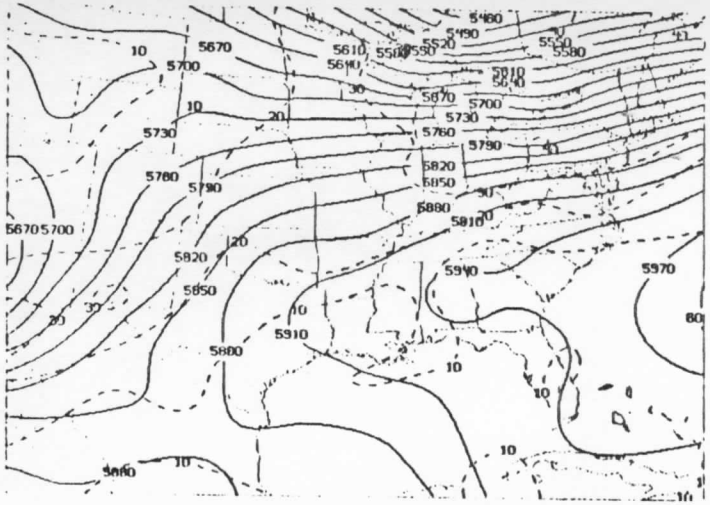

500MB HGHT/WIND ANAL 00GMT 11 OCT 1985

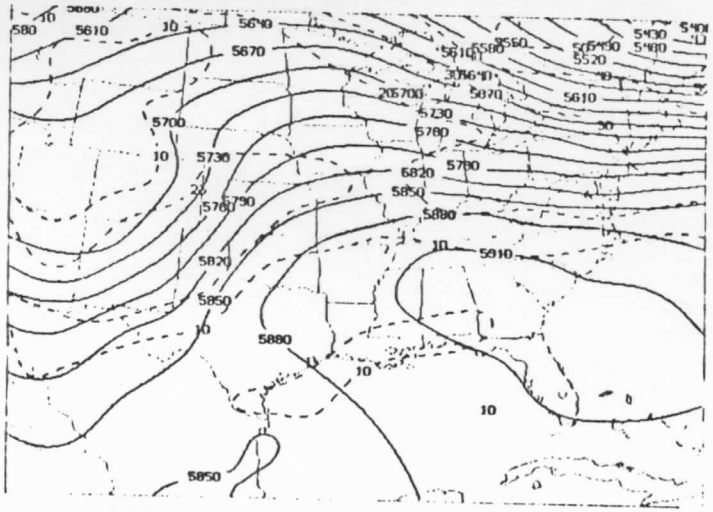

500MB HGHT/WIND ANAL 12GMT 11 OCT 1985

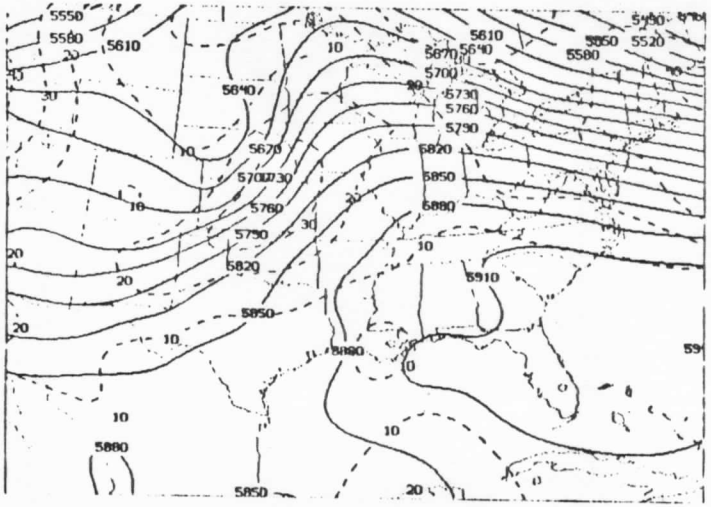

500MB HGHT/WIND ANAL 00GMT 12 OCT 1985

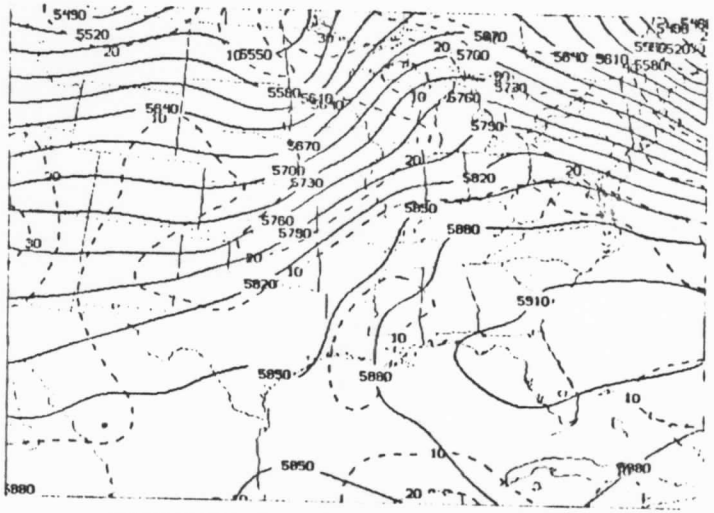

500MB HGHT/WIND ANAL 12GMT 12 OCT 1985

FIG 2.23 (a)

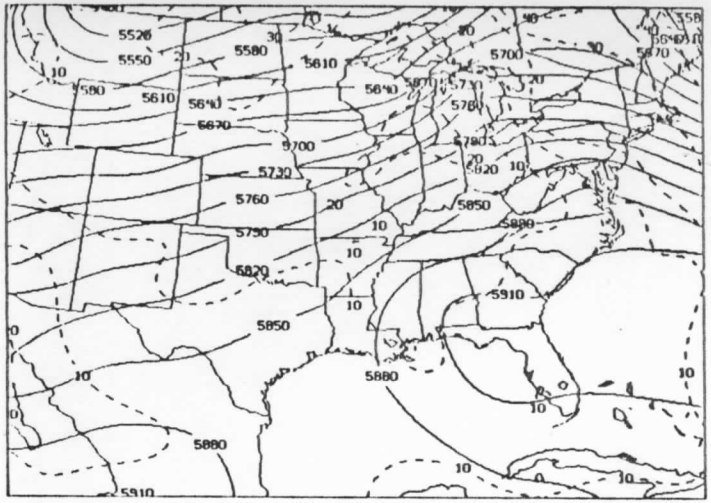

500MB HGHT/WIND ANAL 00GMT 13 OCT 1985

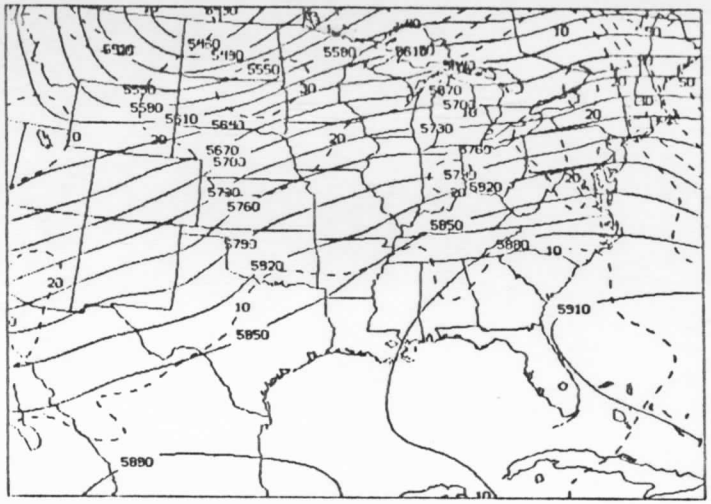

500MB HGHT/WIND ANAL 12GMT 13 OCT 1985

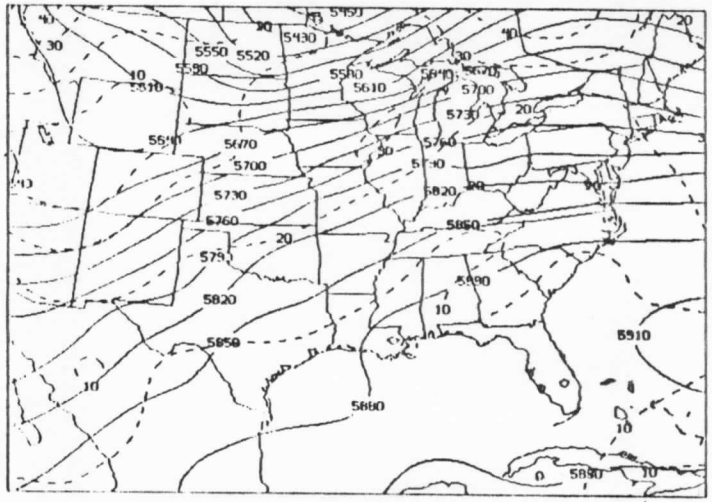

500MB HGHT/WIND ANAL 00GMT 14 OCT 1985

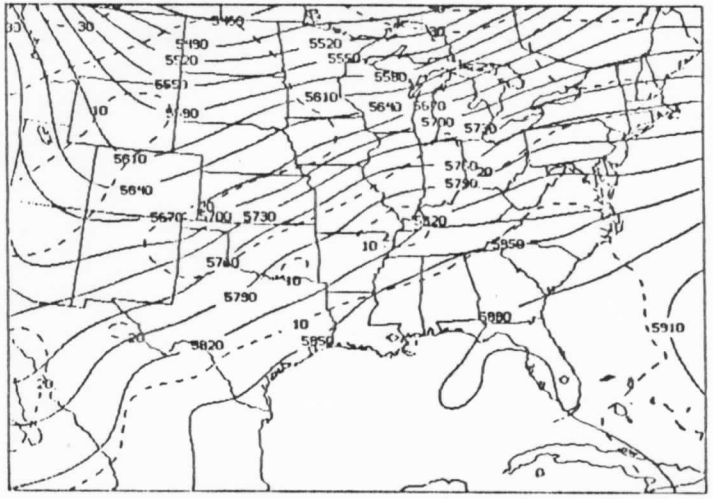

500MB HGHT/WIND ANAL 12GMT 14 OCT 1985

Fig 2.2 (3)

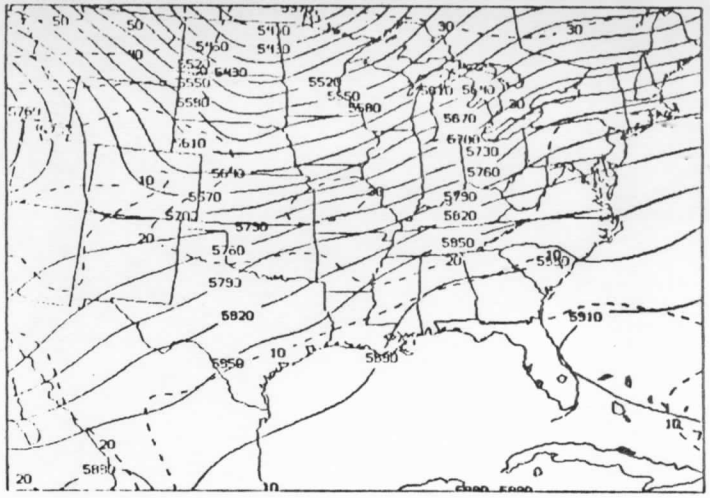

500MB HGHT/WIND ANAL 00GMT 15 OCT 1985

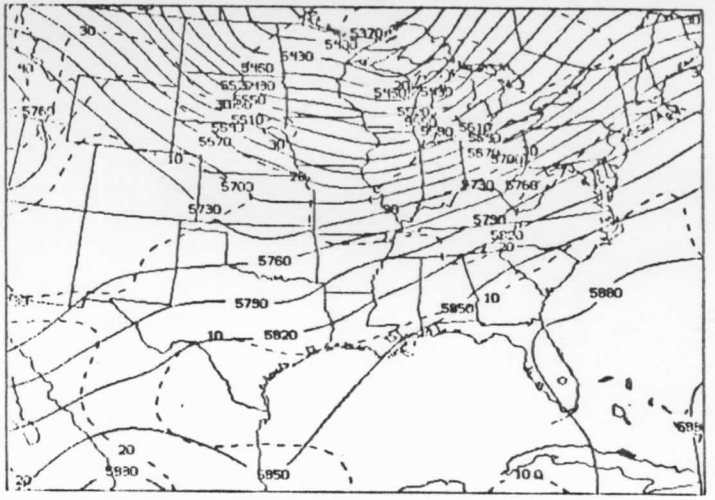

500MB HGHT/WIND ANAL 12GMT 15 OCT 1985

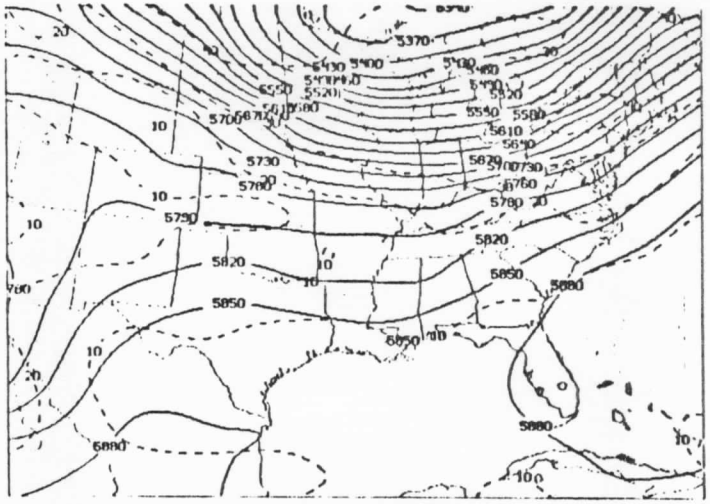

500MB HGHT/WIND ANAL 00GMT 16 OCT 1985

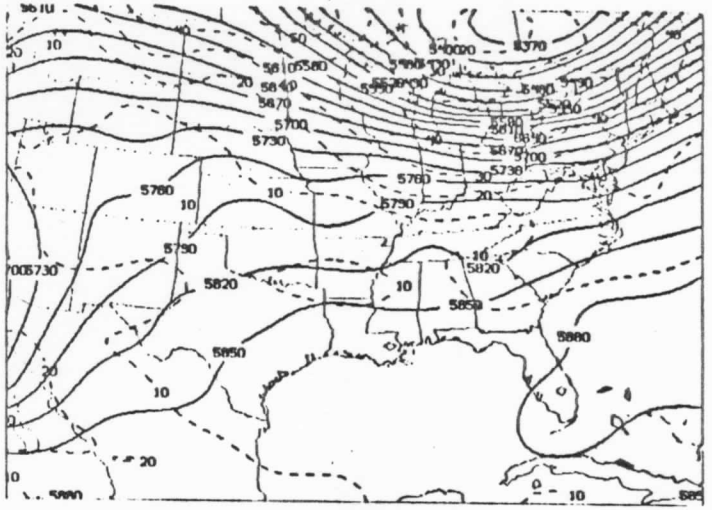

500MB HGHT/WIND ANAL 12GMT 16 OCT 1985

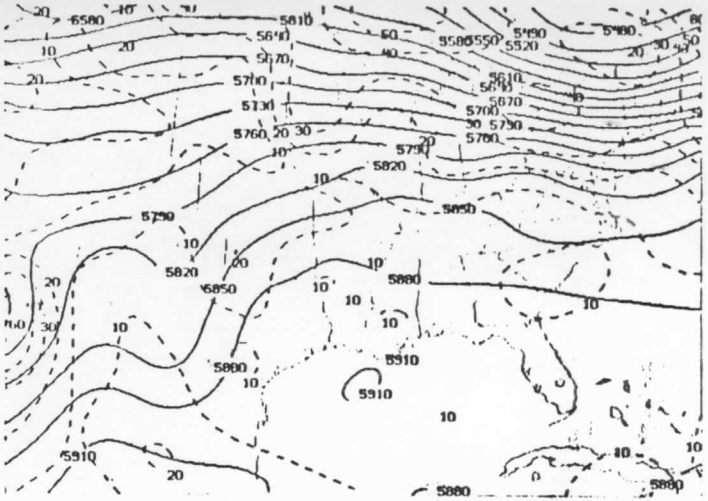

500MB HGHT/WIND ANAL 00GMT 17 OCT 1985

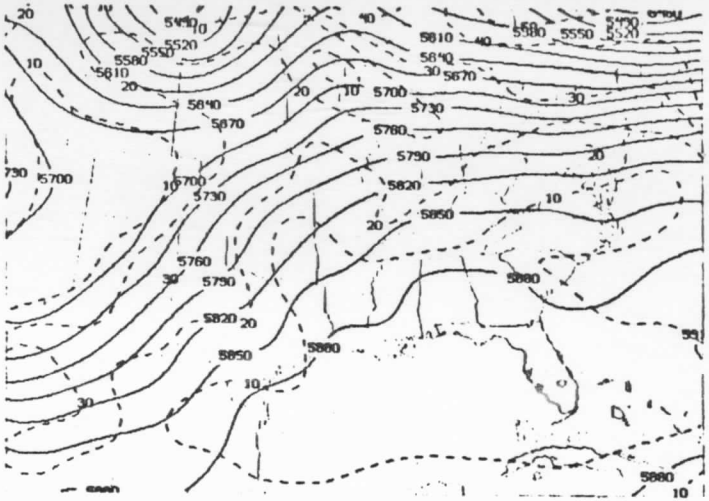

500MB HGHT/WIND ANAL 12GMT 17 OCT 1985

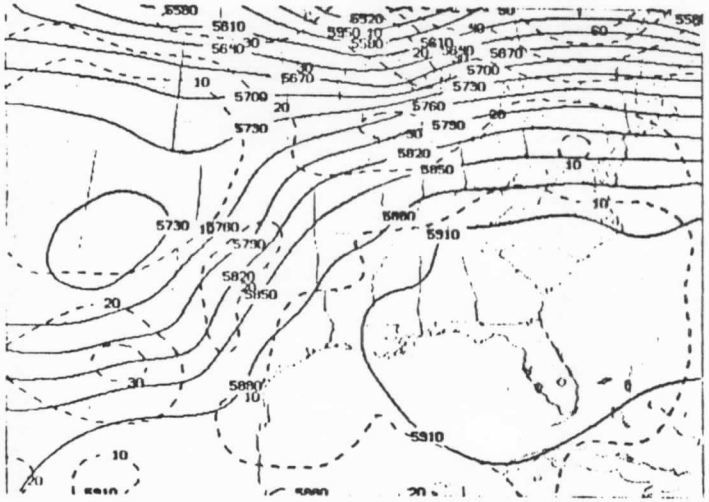

500MB HGHT/WIND ANAL 00GMT 18 OCT 1985

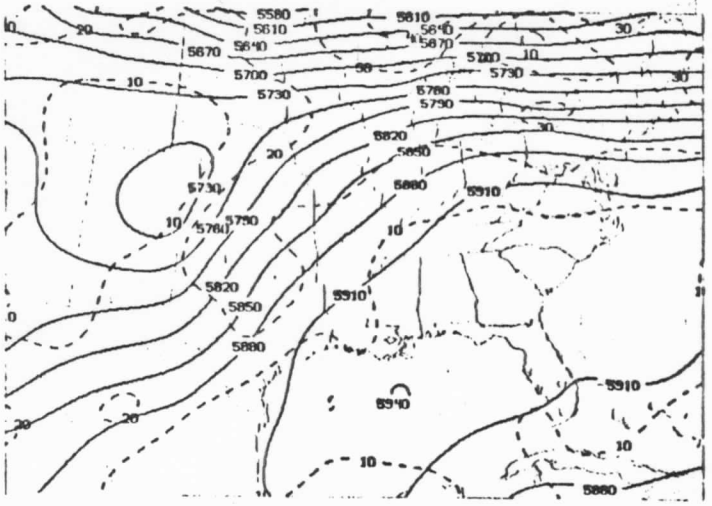

500MB HGHT/WIND ANAL 12GMT 18 OCT 1985

Fig. 2.23

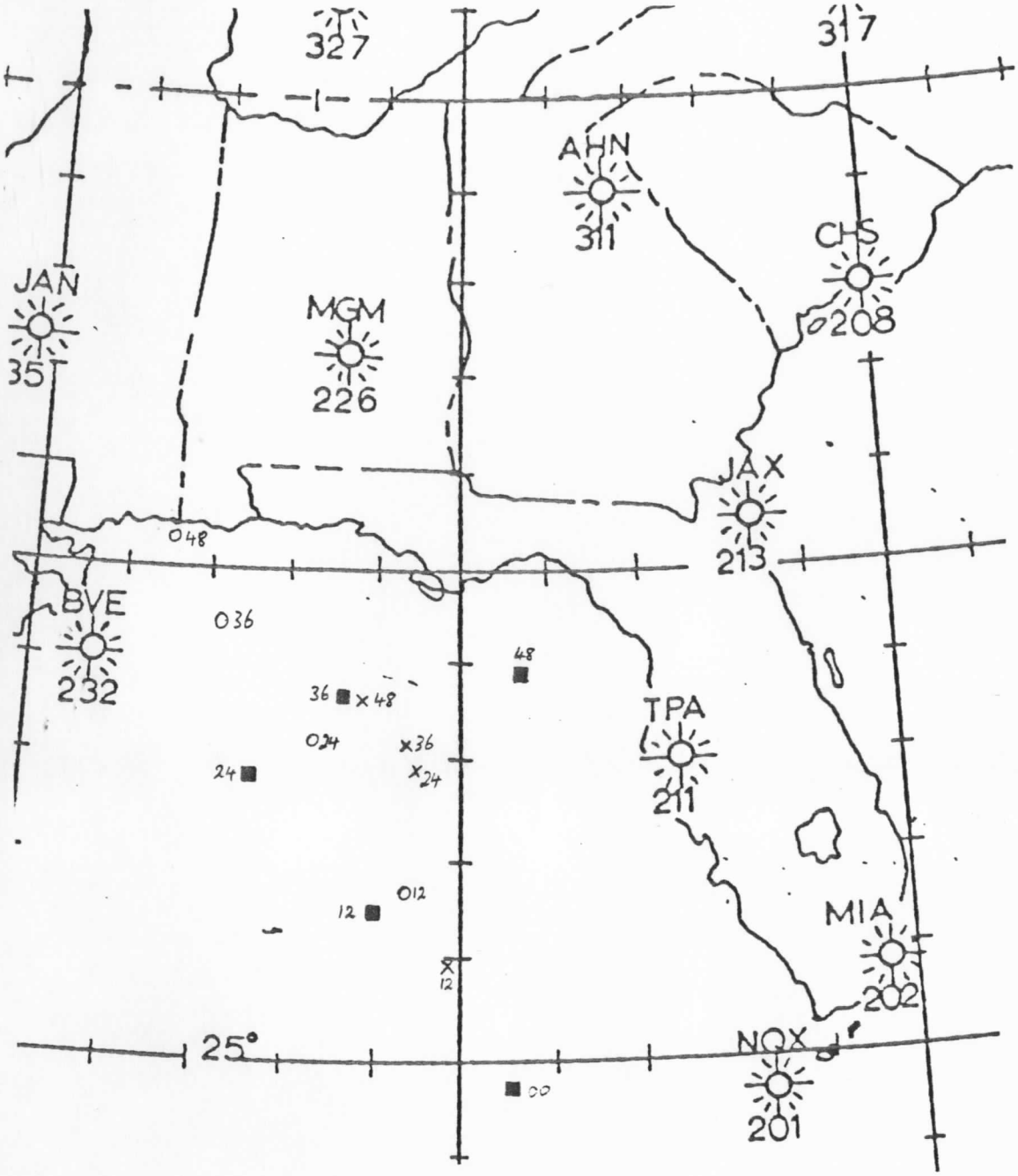
327
317
AHN
311
CHS
208
JAN
35
MGM
226
JAX
213
048
BVE
232
036
48
36 x 48
024
x36
x24
24
TPA
211
012
12
MIA
202
X
12
25°
NQX
201
00

Fig. 2

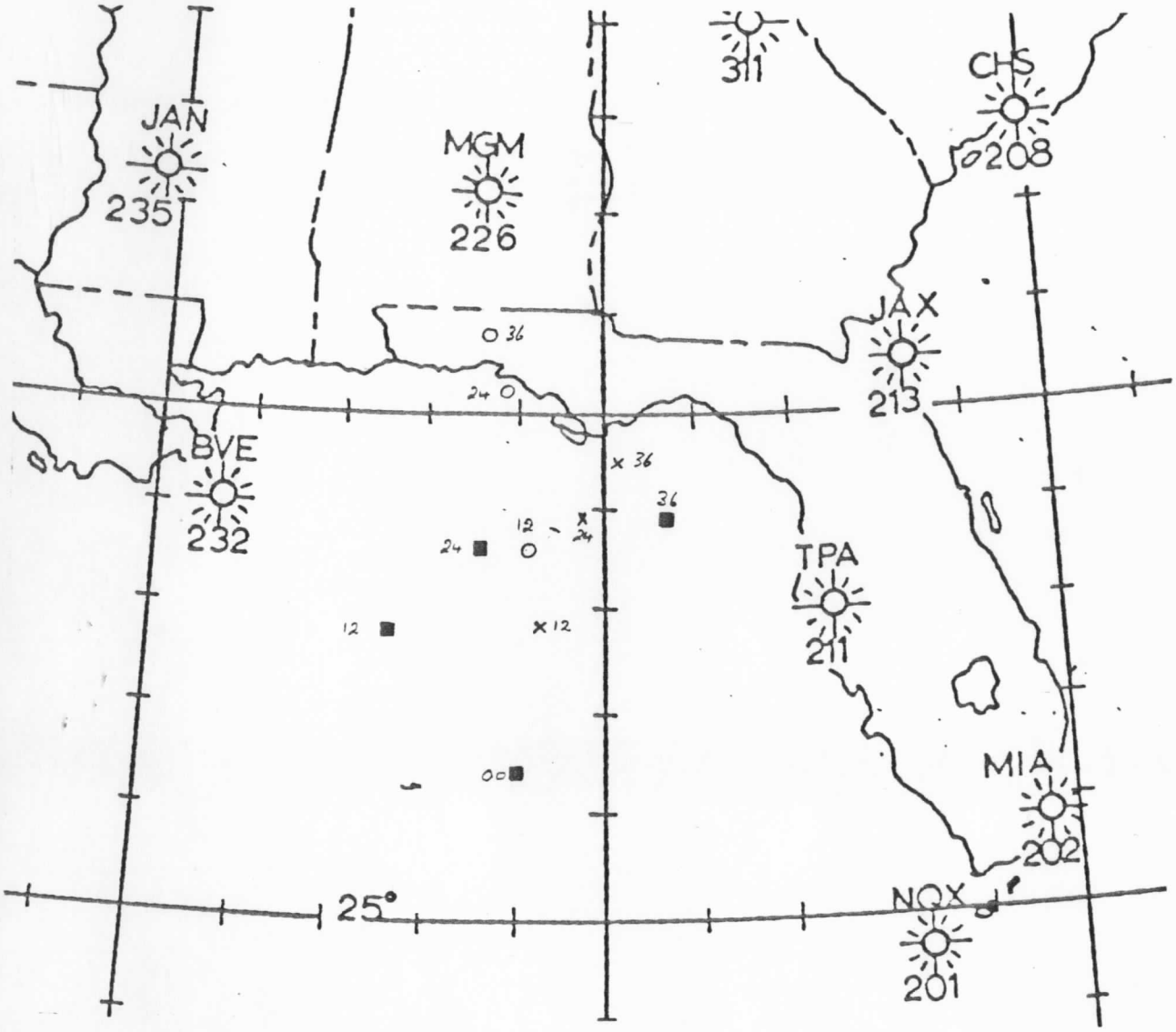
JAN
235
MGM
226
311
CHS
208
JAX
213
BVE
232
TPA
211
MIA
202
NQX
201
25°

Fig 2

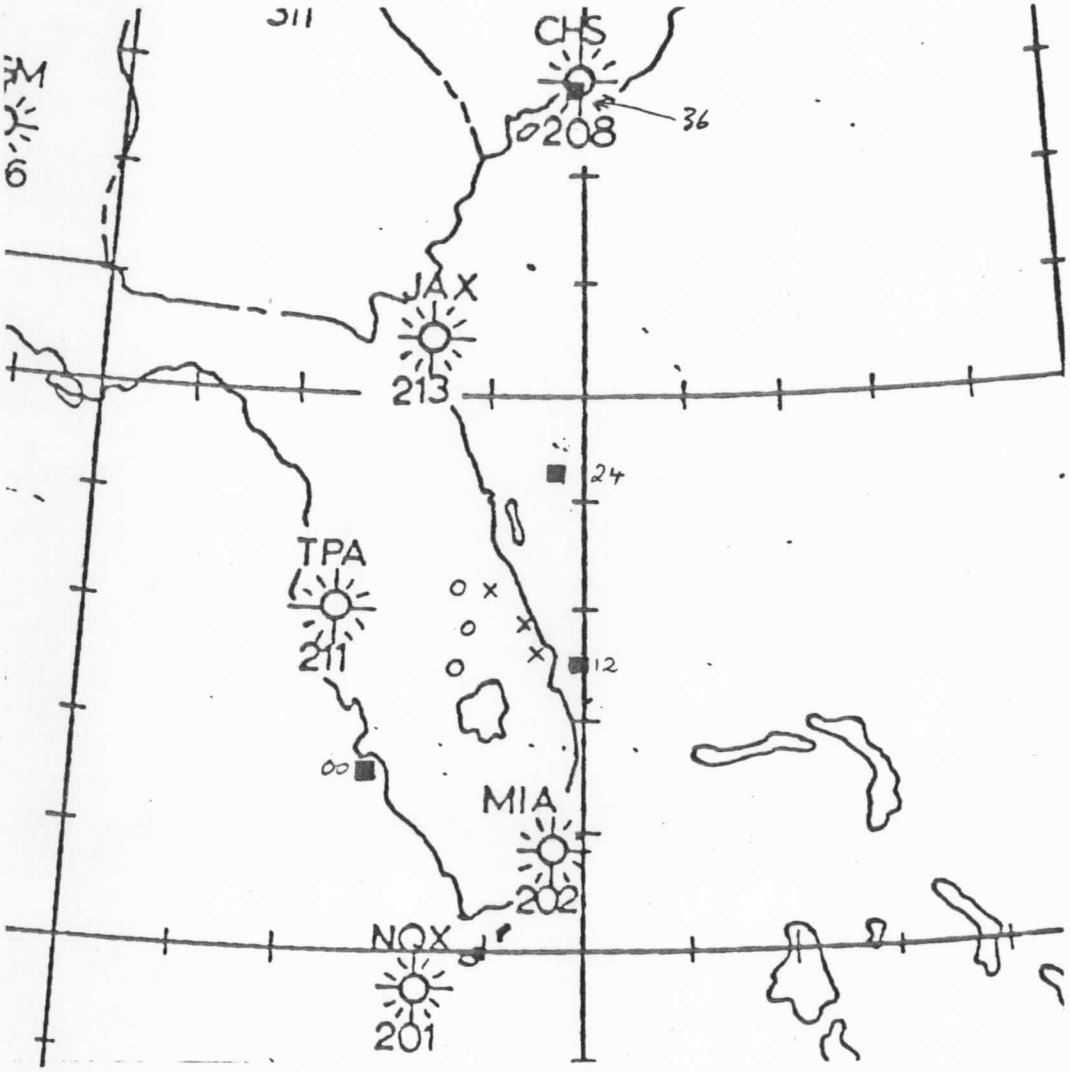
311
CHS
36
208
6
JAX
213
24
TPA
211
12
MIA
202
NOX
201

200 MB VAS GRAD AND CLOUD/WV WINDS

200 MB RADIOSONDE WINDS

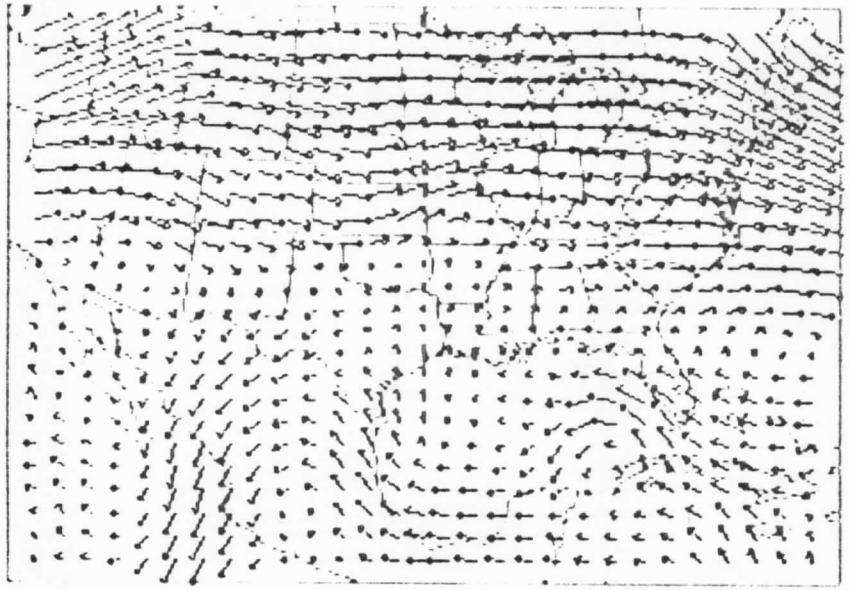

SATELLITE

INITIAL DLM VALID 12 GMT 29 AUG 85

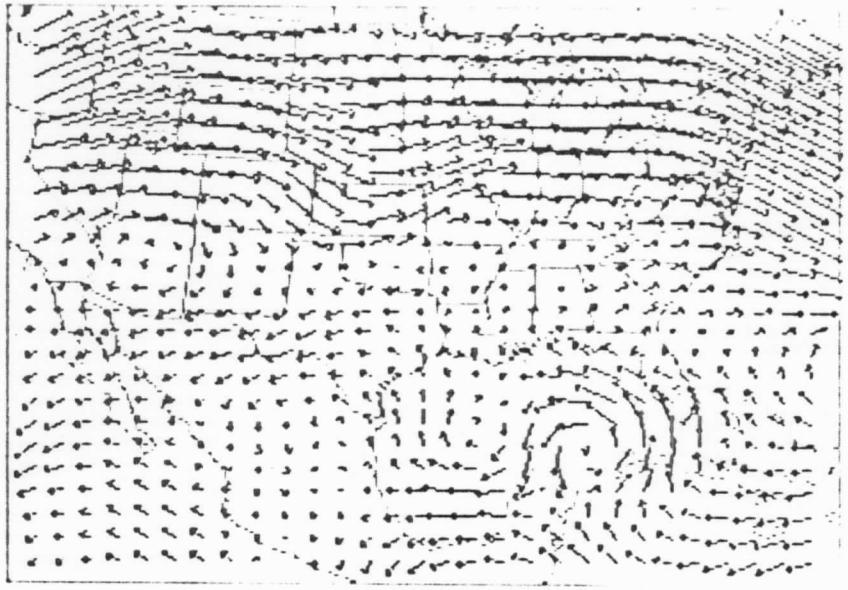

RADIOSONDE

Fig. 2.11 (a)

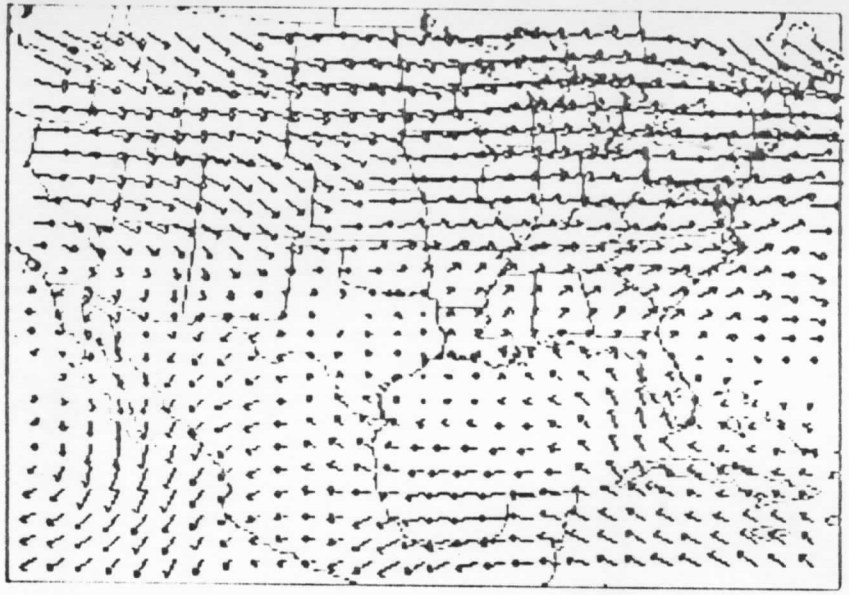

SATELLITE

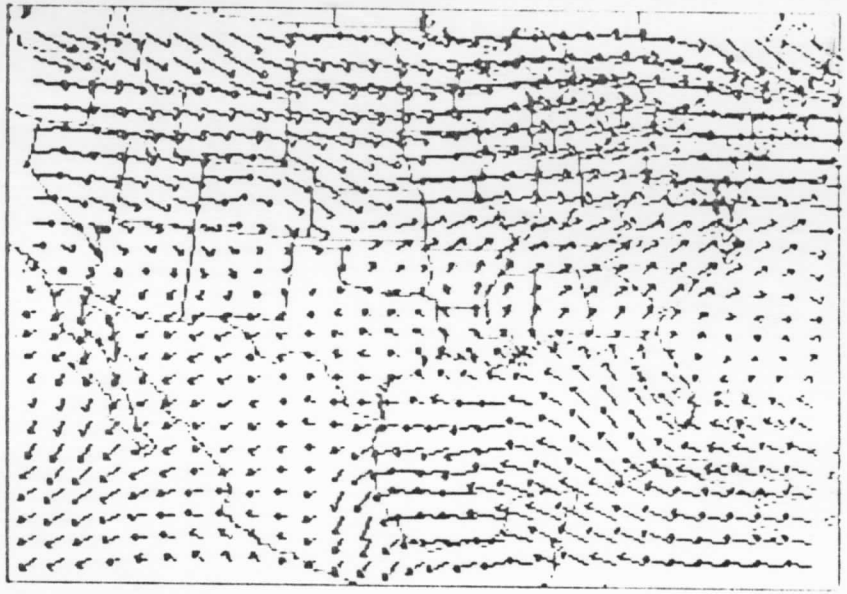

12 HR FCST DLM VALID 00 GMT 30 AUG 85

RADIOSONDE

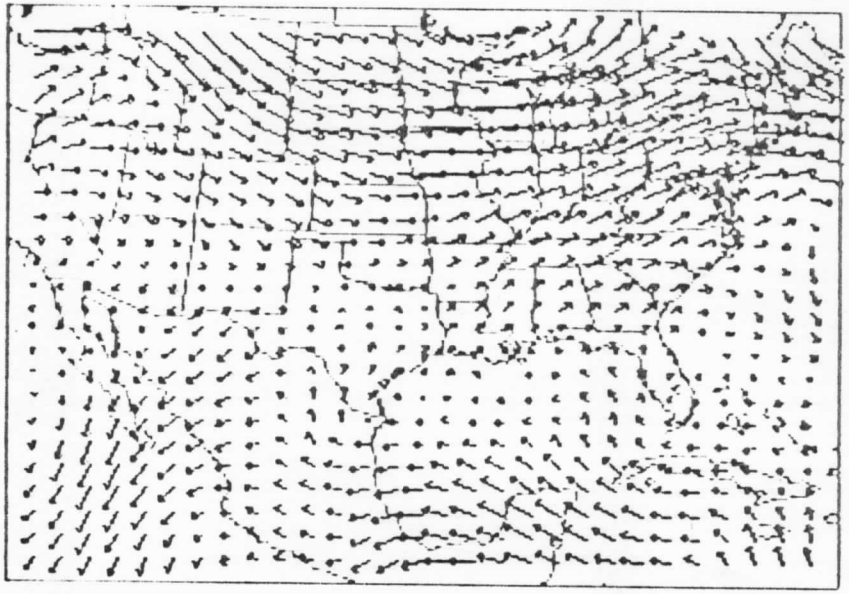

SATELLITE

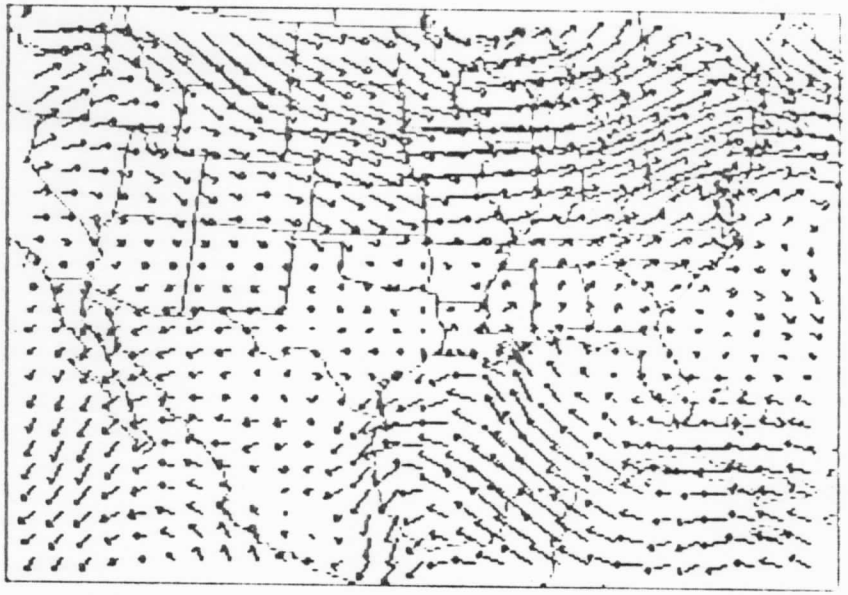

24 HR FCST DLM VALID 12 GMT 30 AUG 85

RADIOSONDE

Fig. 2.7a(2)

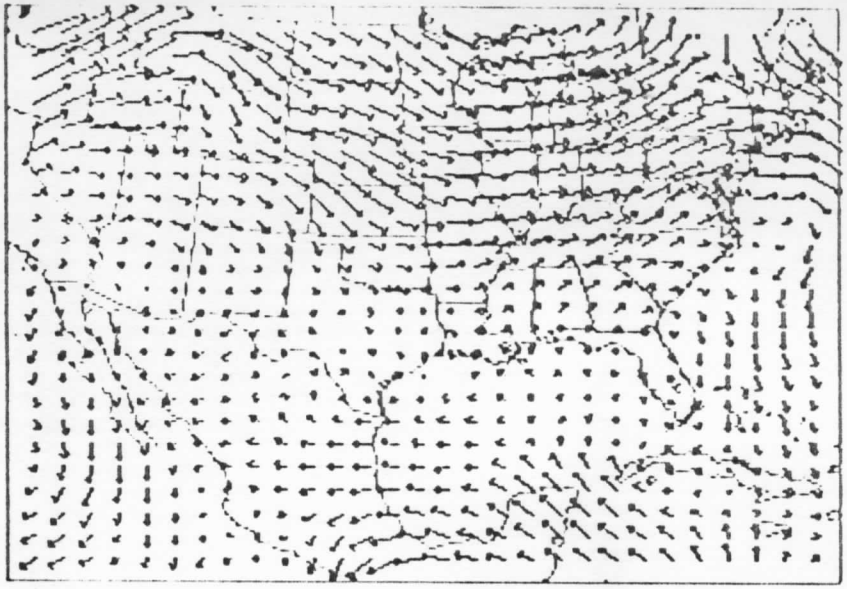

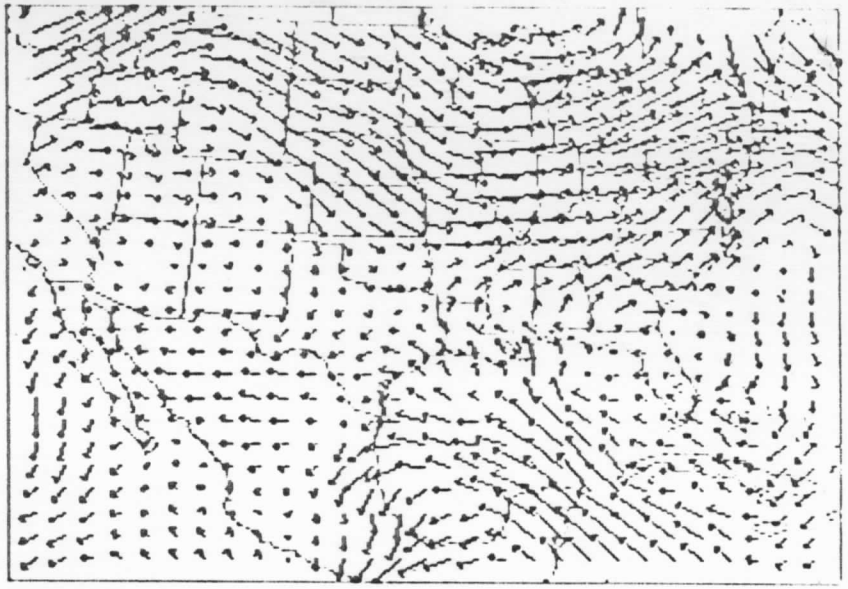

SATELLITE 36 HR FCST DLM VALID 00 GMT 31 AUG 85 RADIOSONDE

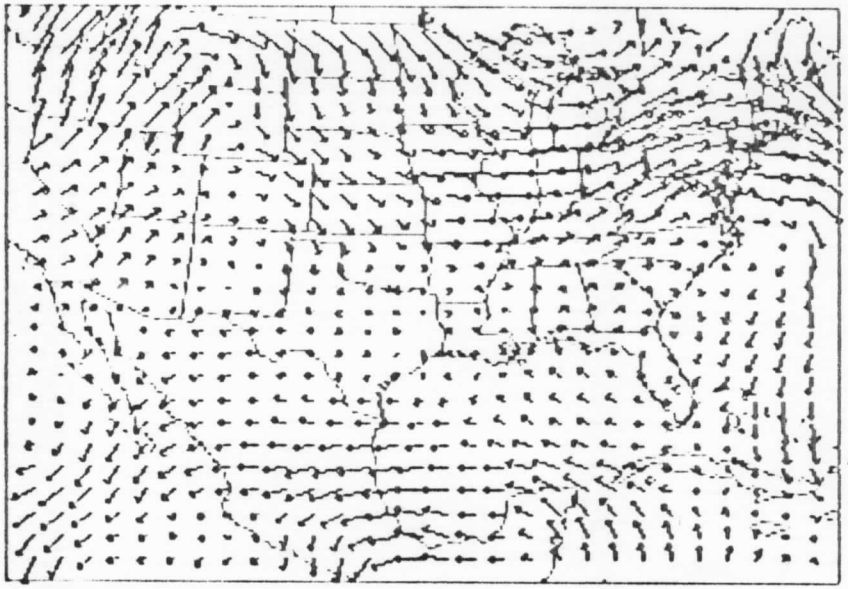

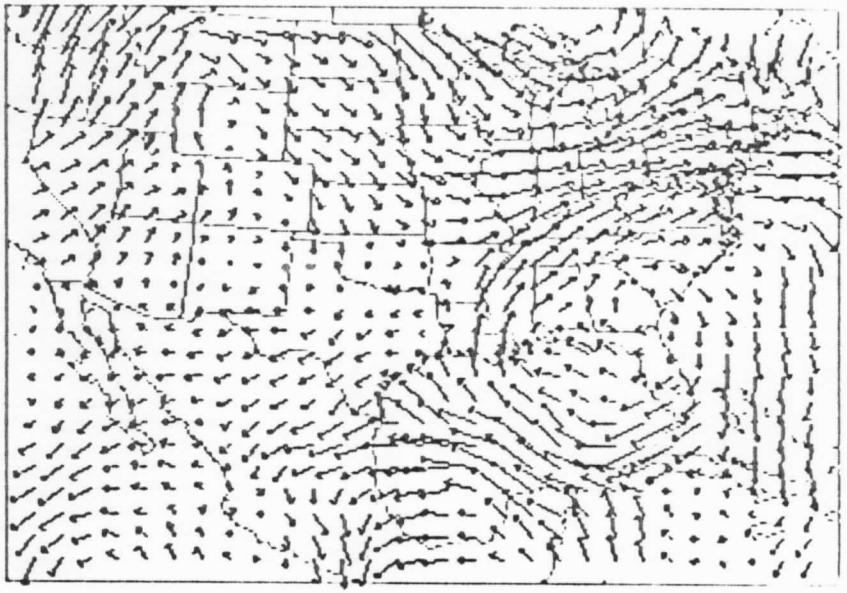

SATELLITE 48 HR FCST DLM VALID 12 GMT 31 AUG 85 RADIOSONDE

Fig 2.mgf

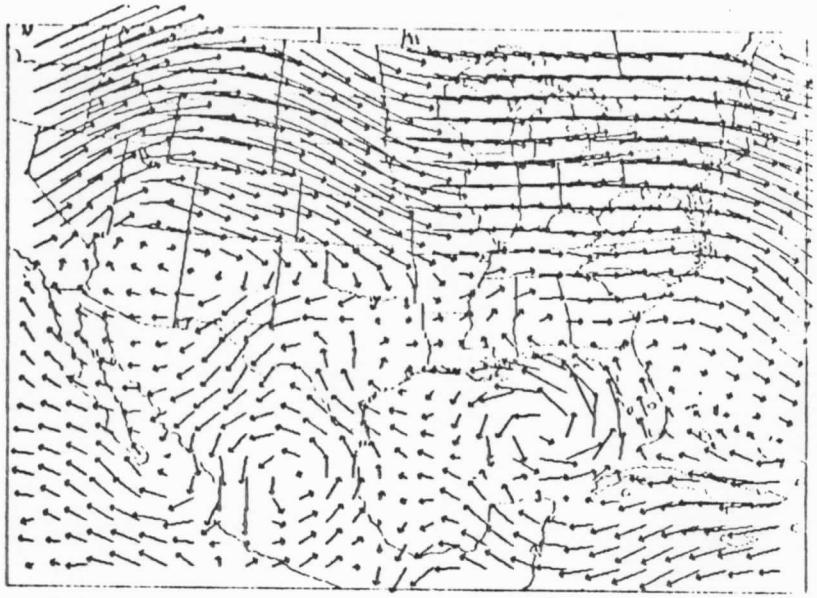

ELENA 00Z 30 AUG 00HRS DLM SAT

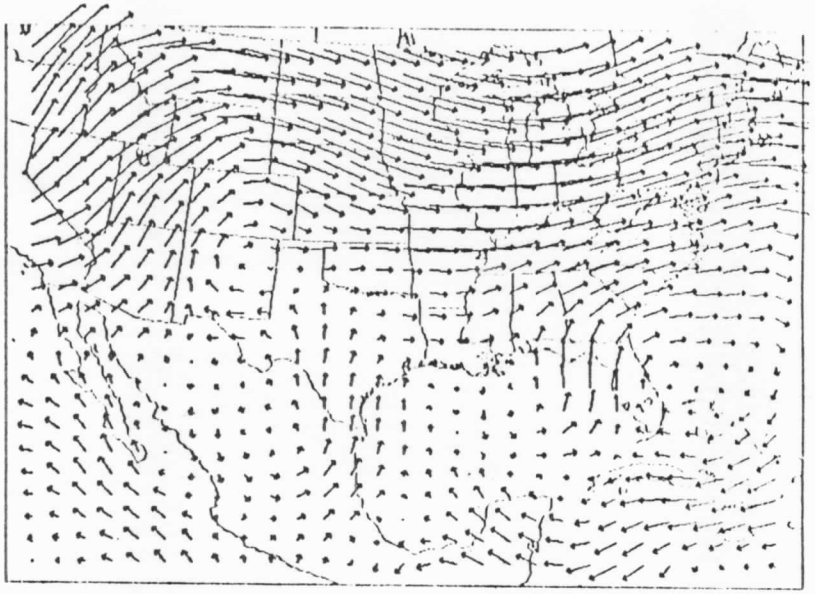

ELENA 00Z 30 AUG 12HRS DLM SAT

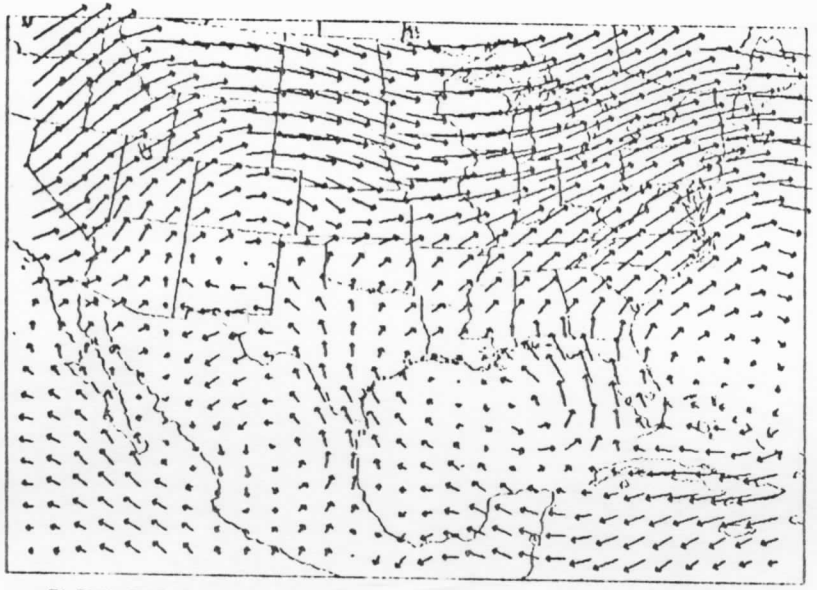

ELENA 00Z 30 AUG 06HRS DLM SAT

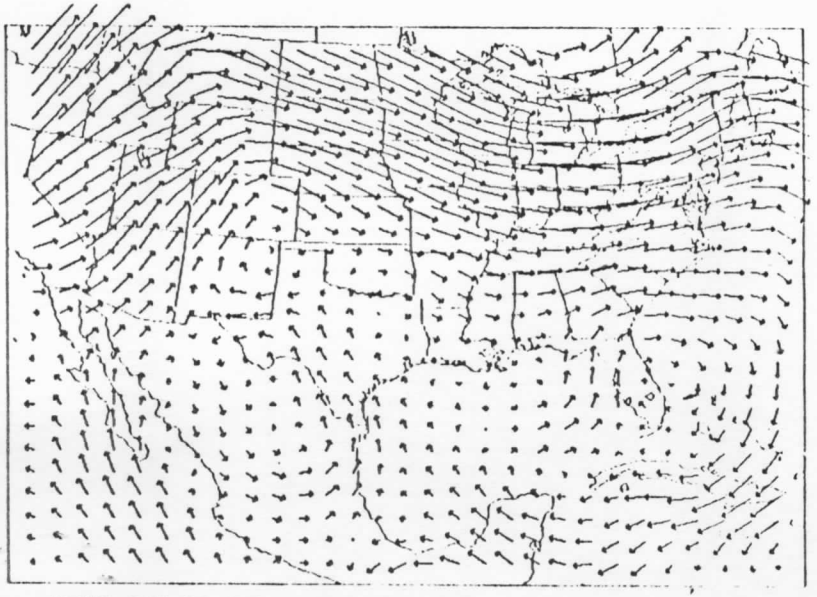

ELENA 00Z 30 AUG 18HRS DLM SAT

FIG 2.11(c)

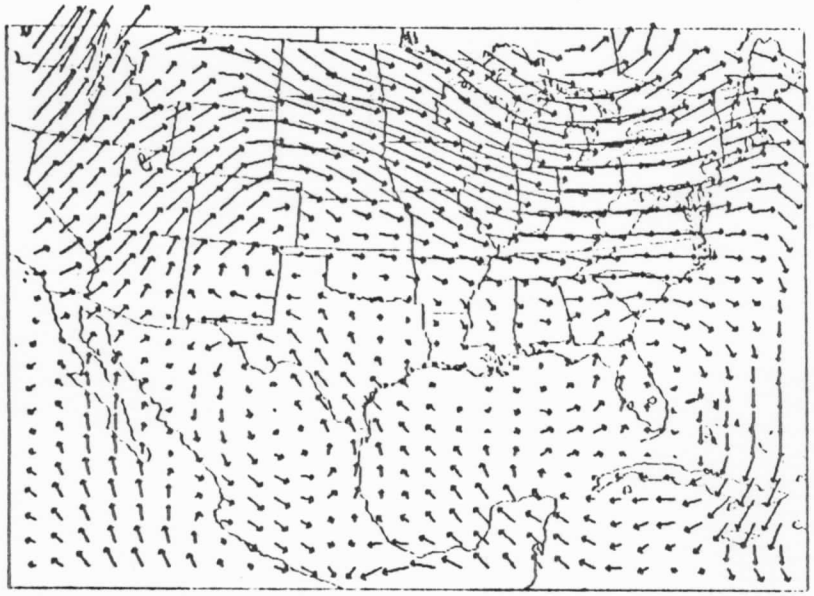

ELENA 00Z 30 AUG 24HRS DLM SAT

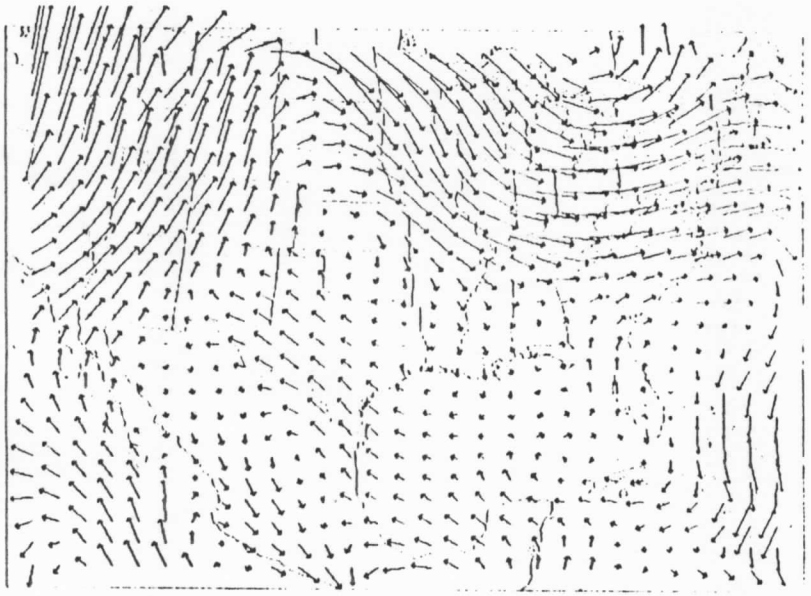

ELENA 00Z 30 AUG 36HRS DLM SAT

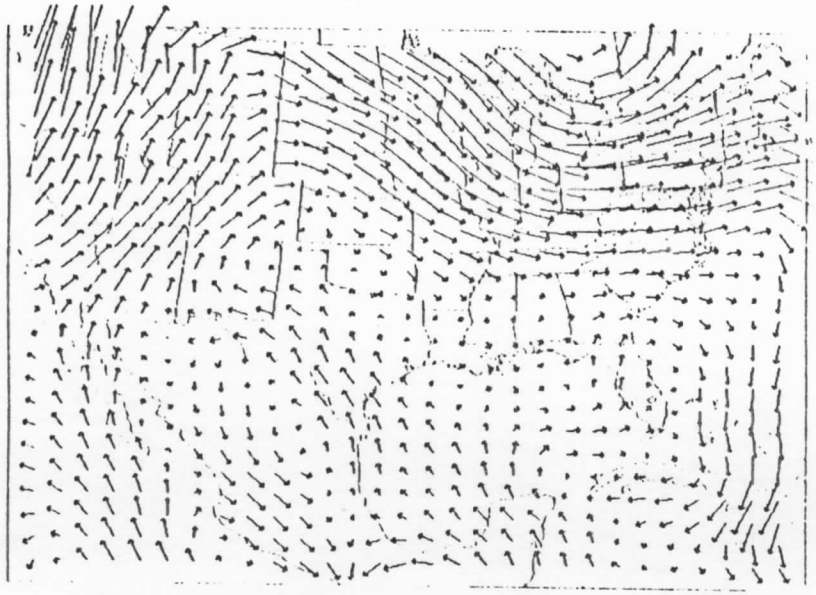

ELENA 00Z 30 AUG 30HRS DLM SAT

FIG 2.n56

References

Bourke, W. P. and J. L. McGregor, 1983: A non-linear vertical mode initialization scheme for a limited area prediction model. Mon. Wea. Rev. 111, 1749-1771.

Earl, P. L., 1985: Impact of the initial specification of moisture and vertical motion on precipitation forecasts with a mesoscale model. M.Sc. Thesis, University of Wisconsin-Madison, Dept. of Meteorology Publication 85.00.E1, 87 pp.

Hayden, C. M., 1985: Estimating the wind field from VAS temperature soundings. Submitted to J. Clim. Appl. Meteor.

Hill, C. K. and R. E. Turner, 1983: NASA's AVE/VAS program. Bull. Amer. Meteor. Soc., 64, 796-797.

Hovermale, J. B. and R. E. Livezey, 1977: Three-year performance characteristics of the NMC hurricane model. Preprints 11th Tech. Conf. Hurricanes and Tropical Meteorology. Miami. Amer. Meteor. Soc., 122-124.

Leslie, L. M., G. A. Mills, L. W. Logan, D. J. Gauntlett, G. A. Kelly, J. L. McGregor and M. J. Manton, 1985: A high resolution primitive equations MWP model for operations and research. Aust. Meteor. Mag., V33, No.1.

LeMarshall, J. F., W. L. Smith and G. M. Callan, 1985: Hurricane Debby--an illustration of the complementary nature of VAS soundings and cloud and water vapour motion winds. Bull. Amer. Meteor. Soc., 66, 258-263.

Lewis, J. M. and J. C. Derber, 1985: The use of adjoint equations to solve a variational adjustment problem with advective constraints. Tellus 37A 309-322.

Lewis, J. M., C. M. Hayden, C. S. Velden, T. R. Stewart, R. J. Lord, S. B. Goldenberg and S. D. Aberson, 1985: The use of VAS winds and temperatures as input to barotropic hurricane track forecasting. Preprints, 16th Conf. on Hurricanes and Tropical Meteorology, Houston. Amer. Meteor. Soc., pp. 42-43.

Menzel, W. P., G. A. Mills, A. J. Schreiner, C. M. Hayden and W. L. Smith, 1985: Multivariate analyses of ALPEX satellite retrievals. Scientific Results of the Alpine Experiment, Venice Oct/Nov 1985.

Mills, G. A. and L. M. Leslie, 1985: The use of NWP model output in the prediction of significant weather events. Aust. Meteor. Mag., V33, No. 3, Sept. 1985.

Smith, W. L., 1983: The retrieval of atmospheric profiles from VAS geostationary radiance observations. J. Atmos. Sci., 40, 2025-2035.

Stewart, T. R., C. M. Hayden and W. L. Smith, 1985: A note on water-vapour wind tracking using VAS data on McIDAS. Bull. Amer. Meteor. Soc., 66, 1111-1115.

Velden, C. S., W. L. Smith and M. Mayfield, 1984: Application of VAS and TOVS to tropical cyclones. Bull. Amer. Meteor. Soc., 65, 1059-1067.

Velden, C. S., 1985: Hurricane Elena--a formal account. CIMSS View. Vol I, No. 2, Fall, 1985.

PART 3

APPENDICES

APPENDIX 1

DATA ASPECTS

The analysis and forecast system acquires data via catalogued data sets. When these data files, grids or observations, are to be viewed on the McIDAS interactive system they must be put into 'LW' or large word arrays. When data is sent to McIDAS from NMC it is in compressed transmission format (CTF) stored on LW files. Routines to process these data types will be described below.

The analysis and forecast routines themselves are run as IBM steps, as opposed to McIDAS steps, and therefore can use only regular IBM datasets for input/output. Presently, these datasets can be catalogued on a special disk pack. Input to the analysis are grids and observations; grids are stored on direct access devices in what is known as field storage (FS) format, observations are stored on sequential files in what is known as 'ANMRC' format. The analysis FS format and forecast FS format do not match; the analysis FS files contain only 95 grids and are stored by column (column,row) the forecast FS files contain 124 grids and are stored by row (row,column). Since these two FS files are not compatible, there are two sets of routines to handle FS file - LW file interfacing; use 'DOALLP' to handle analysis FS files as well as 'ANMRC' observation files, use 'FSDISP' and 'FSRETV' to handle forecast FS files.

The NMC data system is rather complicated, it involves running batch jobs on the NOAA computer, a NAS 9000 series, at Suitland Maryland. Usually the data requested from this system is the NMC global or LFM analysis or forecast fields, and these four data sets are brought over routinely every day. These four files are saved in a CTF type LW file when they arrive from Suitland, the

grids are in their respective file until overwritten twelve hours later by the next day's grids. To check the contents of a CTF file and to process the grids in a CTF file use McIDAS foreground keyin NMCU. Table 1 relates the data types to the CTF type LW file name and the approximate time that the request for data is sent to Suitland. Use command XMIT to send a job to the NOAA computer, when the job comes back use command NMCG to unspool it and put it in a LW file.

MD files and grid files are used for two functions; displaying data and saving intermediate results. All of the McIDAS commands for displaying and processing data use MD files and grid files, IBM type catalogued data sets cannot be accessed in McIDAS foreground. Some of the routines which do data conversion or regridding were written to use MD files or grid files for storage of results; however, they may later be converted to write directly to a catalogued data set.

Table 1 NMC batch jobs for grids.

Grid Type	Cut-off Time	McIDAS Module Name	McIDAS CFT-LW File Name	Approximate Release Time
LFM	00Z	NMNLFM00	LFM00Z	03Z
LFM	12Z	NMNLFM12	LFM12Z	15Z
GLOBAL	00Z	NMNGBL00	GBL00Z	04Z
GLOBAL	12Z	NMNGBL12	GBL12Z	16Z

APPENDIX 2

LINK LIBRARY SYSTEM

For almost all of the analysis-forecast routines the grid dimensions are hard wired into the code. This presents a problem when the dimensions change or several versions are to be used concurrently. A solution to this problem is to use a private link library on a catalogued data set and to use INCLUDE statements in the source code for defining grid dimensions. An INCLUDE statement will be replaced by the designated PARAMETER card at compile time. All source members in this category must use a special execute step procedure called MCANMR. This procedure uses a particular catalogued link library that was predefined by a user. The user also modifies source member VRINO1 by redefining new grid dimensions, JL is the number of rows; and IL is the number of columns. Procedure MCANMR is found in member SUMCANMR, the link library is defined by the LKED.SYSLIN statement.

Link library members exist for all functions, and are tabulated in Table A.2.1, separated by job-step. Several of the jobsteps require more than one linklib member, and sometimes code has been split into more than one member for logistical or line-limit reasons. Sample JCL jobs for a cold-start analysis/forecast and an incremental analysis forecast cycle are held in editor members VBCOLD and VBASSM.

It should be noted that should the grid resolution or the geographical domain be changed, then as well as any necessary changes to the parameter card (VRINO1), a separate compilation of the projection parameter routine must be made, using application- specific projection parameters.

Table A.2.1 List of LINKLIB members for each major jobstep.

PREFORMAT FILES:	VRDAPFMT	
McIDAS FILES TO DISK:	VRDOALLP VRANMRDF	
DATA VALIDATION:	VRUSVALP VRSCINEX VRWRITMS	
PREANALYSIS:	VRPREANAL VRBLKDAT VRSCOMP VRRDVWRD VRDTIO VRREADMS VRWRITMS VRMOVLEV VRTIMDAT	
ANALYSIS:	COLD START	INCREMENTAL
	VRANALUSV VRGMACCV VRMSLANP VRGMSCNV VRGMANL VRGMAN1 VRDTIO VRREADMS VRWRITMS VRMOVLEV	VRANALUSV VRGMACCV VRMSLANP VRGMSCNI VRGMANL VRGMAI1 VRDTIO VRREADMS VRWRITMS VRMOVLEV
TOPOGRAPHY GENERATION:	VRPPTOPO	
NESTING TENDENCY GENERATION:	VRARPE7	
PREPROCESSOR:	VRARPE1	
INCREMENTAL PREPROCESSOR:	VRARPE1D	
PROGNOSIS MODEL:	VRARPE2 VRARPE3	
POSTPROCESSOR:	VRARPE5A	

* NB: All jobsteps use either the analysis or prognosis field storage files FSOPNP or FSOPEN, and all also use the projection routine, an example for EPAC case studies is available in editor member VREPSETP.

APPENDIX 3

A NOTE ON THE GRIDS

The map projection used is the Lambert Conformal Conic Projection. The following parameters define the grid:

GU - grid-length in nautical miles

NML - normal longitude: the longitude (°E) which is parallel to the N-S grid-lines

DU - E-W grid coordinate at the normal longitude (defines offset of grid relative to NML)

TANL - tangent latitude: the latitude at which NML intersects the poleward grid row

STL1 - standard latitudes

STL2 - standard latitudes

These are shown diagrammatically in Figure A.III.1

For unfortunate reasons shrouded in history, the grid conventions are different in the analysis and the prognosis model segments of the system. The analysis system has its origin at the northwest corner of the grid, with the first dimensions increasing southwards, and the second dimension increasing eastwards. The program's model and interface codes have a conventional right-handed system, with the origin in the southwest corner of the grid, and with the first (second) index increasing eastwards (northwards).

For this reason, separate field storage library members are used for the two parts of the code. (FSOPNP for analysis convention, FSOPEN for model convention). This results in the interfaces between grid-files and the internal marking of the codes being transparent to the user.

FIG A.3.1

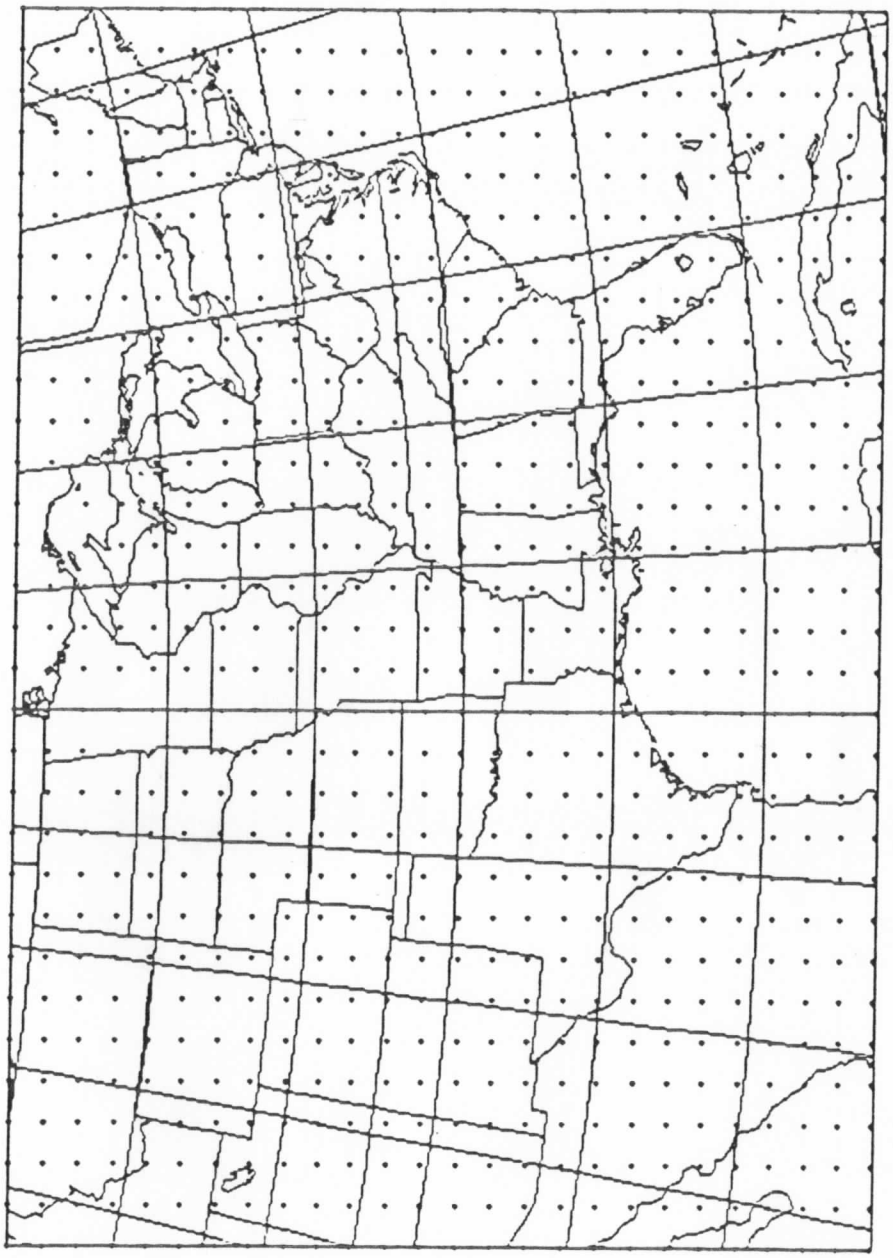

APPENDIX 4: PARAMETER CARDS AND FILES

A.4.1 SAMPLE JCL STRUCTURE

Examples of the data handling and analysis and nested model integration job are in the McIDAS edition in members VBCOLD & VBASSM for the version #2 and incremental analysis codes respectively. In all cases there is a comment briefly describing each job-step, and where feasible the data cards have been individually commented.

A.4.2 THE OBJECTIVE ANALYSIS STEP - Version #2

Required data sets:

FT26 (direct access) - guess field in field storage form

FT25 (direct access) - analysis output data set (field storage form)

FT22 (direct access) - temporary data set, which can be used for restart purposes

FT32 (direct access) - data tables from preanalysis

Parameter Card No. 1

IL, IH, JL, JH . . . FØRMAT (3I4)

- the lower and upper grid dimensions in the I (north to south) and J (west to east) directions.

Parameter Cards No. 2-18

IND MINRPX SDFCTR . . . FØRMAT (2I5,F5.2)

IND - the field indicator (see below)

MINRPX - the starting radius used to compute the variable pass radius. Thus MINRPX is the minimum value of the radius of influence for the first correction pass.

SDFCTR - an amount by which the data rejection tolerance is multiplied. Thus if it is required to tighten the data rejection tolerances, then this factor should be reduced.

N.B. The "IND" parameter is used extensively as a switch in the analysis, and is associated with each type of SCM analysis as follows:

IND = 1 - analysis of geopotential thickness

IND = 2 - analysis of geopotential height ϕ (dummy)

IND = 3 - analysis of $\partial\phi/\partial I$

IND = 4 - analysis of $\partial\phi/\partial J$

IND = 5 - analysis of isotachs (dummy)

IND = 6 - analysis of temperatures

IND = 7 - analysis of 500-250 thickness

IND = 8 - analysis of dewpoint depression

IND = 9 - analysis of 1000mb height

IND = 10 - analysis of MSLP (dummy)

IND = 11 - analysis of 1000-500 thickness (dummy)

IND = 12 - analysis of 1000-500 thickness

IND = 13 - analysis of MSLP

IND = 14 - analysis of u-component of wind

IND = 15 - analysis of v-component of wind

IND = 16 - surface temperature analysis

IND = 17 - surface dewpoint analysis

Parameter card No. 19

ISTART IEND ISTRM IGCOR ITOPT IMOPT FØRMAT (6I2)

ISTART - first of the analysis modules to be executed

IEND - last of the analysis modules to be executed

ISTRM - stream function switch (0=no, 1=yes)

IGCOR - geostrophic wind correction option (0=no, 1=yes)

ITOPT - temperature analysis module switch (0=no, 1=yes)

IMOPT - dewpoint depression analysis module switch (0=no, 1=yes)

N.B. The six analysis modules are:

1 - reference level and gross thickness specification (GROSAN)

2 - specification of layer thickness below 250 mb (ANBL25)

3 - specification of layer thickness above 250 mb (ANAB25)

4 - analysis of temperatures (TANAL)

5 - analysis of dewpoints (MANAL)

6 - analysis of wind (WANAL)

A.4.3 INCREMENTAL ANALYSIS VERSION

The required files and the parameter cards are the same in this version as they are in the preceding section, with this ONE EXCEPTION:

IGCOR can now range from 0-9, and represents the weight of the geostrophic to the gradient wind. The weight given to the geostrophic (gradient) wind varies linearly from 0(1) when IGCOR=0 to 1(0) when IGCOR=9.

A.4.4 THE PREPROCESSOR

Required data sets:

FT10 - (direct access): analysis data set on pressure surfaces in field storage format

FT11 - (sequential) : topography data set

FT12 - (direct access): output data set for model initiation in field storage format

Parameter Card No. 1

ISURF IWIND TOPF IHGHT
(unformatted read)

ISURF = 1: surface temperature and dewpoint analyses are available
= 0: derive surface temperature and moisture from lowest sigma surface values

IWIND = 0: use divergent winds
= 1: use non-divergent winds

TOPF: factor to multiply grid-point topography (can be used to enhance or reduce the topography, after smoothing, depending on the application)

IHGHT = 0: reads analysis temperatures
= 1: calculates temperatures from geopotentials using the method of J.C. Derber

Parameter Card No. 2

This card is a dummy.

Parameter Card No. 3

NSIG, SIGMAS (kz)
(unformatted read)

NSIG - number of sigma levels required (the program tests for a match of this number with the number of levels specified in the PARAMETER statement)

SIGMAS-the NSIG sigma level values, with the lowest value (highest level) first

A.4.5. THE INCREMENTAL PRE-PROCESSOR

Required files:

FT10 - input analysis data set (field storage)

FT12 - output data set (the forecast model input field storage)

FT15 - input program's data set (field storage). This was the guess field for the analysis of FT10

FT16 - the model restart file which is to be updated by the interpolated analysis increments

Parameter Card No. 1

KTPRG, IWIND - unformatted

KTPRG is the timestep of the model restart which is being updated by the analysis increments

IWIND = 0 divergent winds variants
=1 non-divergent wind variants

Parameter Card No. 2

NSIG, SIGMAS (unformatted)

NSIG - the number of sigma levels

SIGMAS - the NSIG sigma level values, with the lowest numerical value (higher level) first

A.4.6 THE NESTING CODE:

Required data sets:

FT10 - topography data set

FT11 - FT15

FT12 - up to five field storage data sets containing external system data, interpolated to the model grid, commencing at time zero and finishing at required forecast time. Time internal between these data sets must be constant.

FT30 - output tendency data set

Parameter Card No. 1

IOFF JOFF --: FØRMAT(2I5)

Offset of inner fine mesh from coarse mesh origin, in coarse mesh units. If doing a coarse mesh (outer) forecast, then (1,1).

Parameter Card No. 2

IRATIO TOPF --: FØRMAT(I5,F5.1)

IRATIO - ratio of fine mesh to coarse mesh grid units

TOPF - factor to multiply grid-point topography (see section III.2.4)

Parameter Card No. 3

NSIG, SIGMAS (I2,1X, or F6.3)

NSIG - number of sigma levels

SIGMAS - sigma level disposition. This must be the same as used in the model, or the program will stop.

A.4.7 THE PROGNOSIS MODEL

Required data sets:

FT10 - input file (output from preprocessor)

FT11 - land/sea mask file

FT20 - model output data set, known as the restart file

FT31 - boundary tendency file (from nesting step)

FT41 - output of model data to be used to provide inner fine mesh forecast

FT31 - temporary data set for use during vertical mode initialization

Parameter Card No. 1

KTFRST KTLAST IRST JRST (unformatted)

KTFRST - first timestep of integration (if KTFRST is not 1, then the model restart file is used as input, and must thus exist)

KTLAST - last timestep of integration
IRST - frequency (in timesteps) of output of model variables to restart file
JRST - special timestep for writing to restart file

Parameter Card No. 2

DT TFILT (unformatted)

DT - timestep in seconds

TFILT - Asselin filter coefficient (normally 0.8)

Parameter Card No. 3 (Initialization parameters)

MINDS(I),I=1,3 KVMI MODES (unformatted)

MINDS(1)=0 full initialization
=1 surface pressure constrained initialization

MINDS(2)=1 vorticity included (this is the preferred option)
=2 resets tangential velocities to zero

MINDS(3)=0 scheme A
=1 scheme B (preferred option)

KVMI - number of iterations of VMI initialization (=0, no VMI; =3, usual no. of iterations)

MODES- number of vertical modes to be initialized (usually 2)

Parameter Card No. 4 - nesting options

NEST NESTWR NESTRD NSTINT (unformatted)

NEST =0 fixed boundaries
=1 updated lateral boundaries (nesting "on")

NESTWR interval in timesteps between writing to internal fine mesh nesting file FT41

NESTRD =0 not reading fine mesh boundary data
=1 reading fine mesh boundary data

NSTINT =0 input data is in field storage form, as output by preprocessor
=1 input data has been interpolated from coarse mesh input data (only applicable to inner fine mesh model run)

Parameter Card No. 5

IOFF JOFF ILC JLC NB IRATIO (unformatted)

IOFF - Offset of fine mesh on coarse mesh grid
JOFF (i.e. coarse mesh coordinates of pt(1,1) on fine mesh grid)

ILC - Grid dimensions of coarse mesh
JLC

NB - Number of boundary rows used in boundary updating (see section 2.2 of Leslie et. al. 1985)

IRATIO - Ratio of coarse mesh to fine mesh grid-length

Parameter Card No. 6

ILAPS (unformatted)

ILAPS the lapse rate in tenths of degrees K per Km used for calculating geopotentials below the lowest sigma surface. If set to 99, log-linear extrapolation from the lowest two sigma surfaces is used.

Parameter Card No. 7 Physics options

LPHYS LSURF LCONLS LCONCU LVERDF LHDIF

These are each switches, 1=on, 0=off.

LPHYS - switch to call the physics routine. This will over-ride all other switches if set off.

LSURF - surface temperature and moisture prediction scheme

LCONLS - large scale convective adjustment scheme

LCONCV - convective parameterization scheme

LVERDF - vertical diffusion code

LHDIFF - switches on horizontal diffusion of convective heating and moistening profiles

Parameter Cards 8-17

IPRT(KK) JPRT(KK) (unformatted)

Up to 10 gridpoints at which full profiles of all model variables can be printed each timestep for diagnostic purposes.

A.4.8. THE POST-PROCESSOR

Required files:

FT20 - input. This is the model restart file.

FT10-FT19 - up to 10 field storage data sets for output of required timestep data on pressure surfaces

FT30-FT39 - up to 10 field storage data sets for output of required timestep data on sigma surfaces

Parameter Card No. 1

NSTEP1 NSTEP2 NSTEP3 (FORMAT 3I3)

NSTEP1 - first timestep required to be post-processed

NSTEP2 - last timestep required to be post-processed

NSTEP3 - frequency of timesteps to be post-processed. (i.e. post-process from NSTEP1 to NSTEP2 at intervals of NSTEP3)

Note that there can be a maximum of 10 timesteps postprocessed, and that the requested timestep data must exist on the restart file.

Parameter Card No. 2

IFILT ISOUT FØRMAT(I2,1X,I2)

IFILT = 1 - spatially filter all fields after interpolation
= 0 - no spatial filter applied

ISOUT = 1 - required sigma surface fields
= 0 - no sigma surface fields output

Parameter Card No. 3

LEVS(K), K=1,NPLEVS FØRMAT(12I5)

The pressure levels to which the sigma surface fields are to be interpolated, in decreasing numerical value.

APPENDIX 5: DIAGNOSTIC ROUTINES